Acta morphologica et anthropologica 25 (1–2)

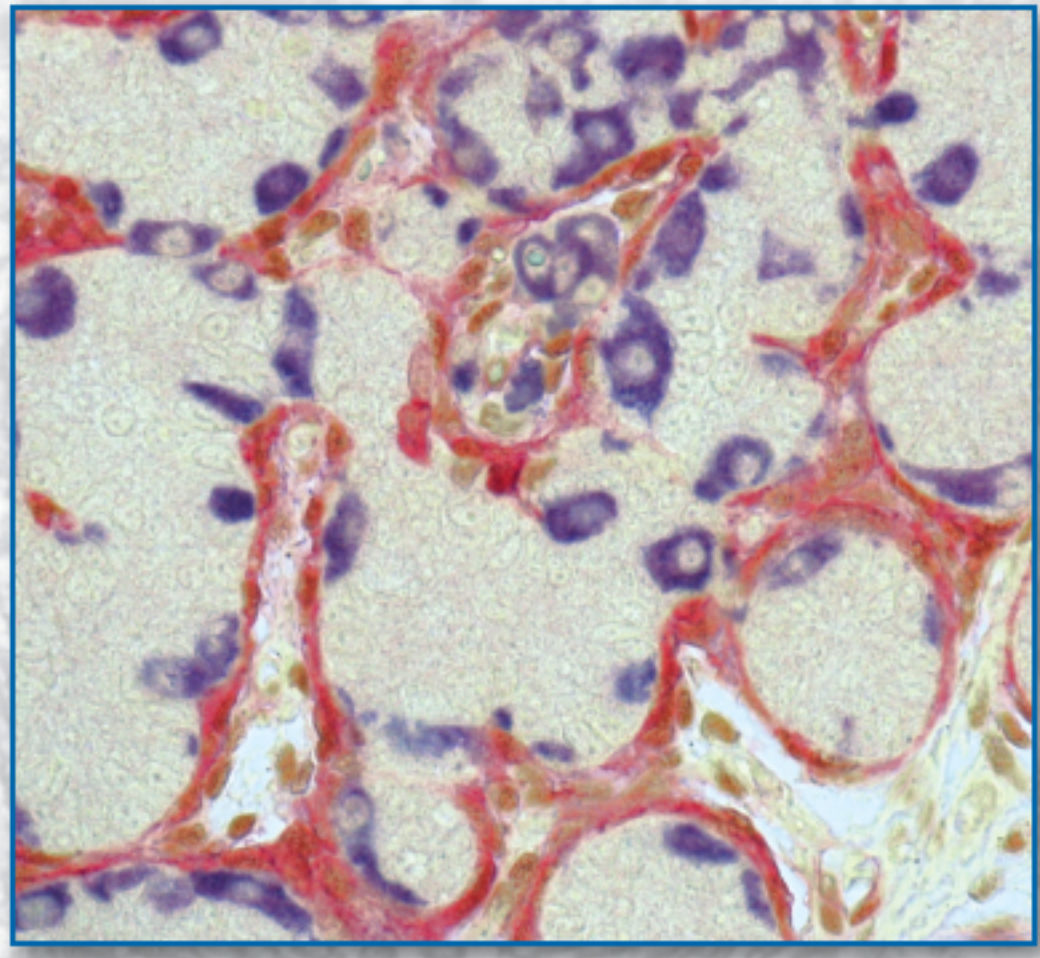

Prof. Marin Drinov Publishing House
of Bulgarian Academy of Sciences

Acta morphologica et anthropologica

is the continuation of
Acta cytobiologica et morphologica

Editor-in-Chief: Prof. Nina Atanassova
e-mail: ninaatanassova@yahoo.com
+359 2 979 2342
Deputy Editor-in-Chief: Prof. Dimitar Kadiysky
e-mail: dkadiysky@yahoo.com; dimkad@bas.bg
+359 2 979 2311
Executive Secretary: Assoc. Prof. Y. Gluhcheva
e-mail: ygluhcheva@hotmail.com
+359 2 979 2344

Editorial Correspondence
Institute of Experimental Morphology, Pathology and Anthropology with Museum
Bulgarian Academy of Sciences
Acta morphologica et anthropologica
Acad. Georgi Bonchev Str., Bl. 25
1113 Sofia
Bulgaria
Email:iempam@bas.bg
Tel.: +359 2 979 2311

Издаването на настоящия том 25, книжки 1 и 2 е осъществено с финансовата подкрепа на Фонд „Научни изследвания“

Prof. Marin Drinov Publishing House of Bulgarian Academy of Sciences
Bulgaria, 1113 Sofia, Acad. Georgi BonchevStr., Bl. 6

Graphic designer Veronika Tomcheva
Format 70×100/16 Printed sheets 8.00
Printing Office of Prof. Marin Drinov Publishing House of Bulgarian Academy of Sciences
Bulgaria, 1113 Sofia, Acad. Georgi Bonchev Str., Bl. 5

ISSN 1311-8773 (print)
ISSN 2535-0811 (online)

Acta morphologica et anthropologica

25 (1-2)

25 (1-2) ● Sofia ● 2018
Institute of Experimental Morphology, Pathology and Anthropology with Museum
Bulgarian Anatomical Society

Contents

Review Articles

Institute of Experimental Morphology, Pathology and Anthropology with Museum
Bulgarian Anatomical Society

Acta morphologica et anthropologica, 25 (1-2)
Sofia ● 2018

Morphology

Effect of Nickel (II) Complexes with Mannich Bases on Viability and Proliferation of Human Cancer Cells

Radostina Alexandrova[1], Tanya Zhivkova[1], Lora Dyakova[2], Reni Kalfin[2], Ramona Tudose[3], Elena-Maria Mosoarca[3], Osama Azmy[4], Otilia Costisor[3]*

[1] *Institute of Experimental Morphology, Pathology and Anthropology with Museum, Bulgarian Academy of Sciences, Sofia, Bulgaria*
[2] *Institute of Neurobiology, Bulgarian Academy of Sciences, Sofia, Bulgaria*
[3] *Institute of Chemistry Timisoara of the Romanian Academy, Timisoara, Romania*
[4] *Medical Research Division, National Research Centre, Cairo, Egypt*

* Corresponding author e-mail: rialexandrova@hotmail.com

The aim of our study was to evaluate the influence of four nickel (II) complexes with ligands containing the antipyrine moiety N,N'-bis(4-antipyrylmethyl)-piperazine (BAMP) or N,N'-tetra-(antipyryl-1-methyl)-1,2-diaminoethane (TAMEN) on viability and proliferation of cultured human cancer cells. The following permanent cell lines were used as model systems: MCF-7 (luminal A type breast cancer), SK-BR-3 (Her2 - positive breast cancer), Caco-2 (colorectal adenocarcinoma), HepG2 (hepatocellular cancer), 8MGBA (glioblastoma multiforme). The investigations were performed by MTT test and neutral red uptake cytotoxicity assay (in short-term experiments, 24-72h, with monolayer cultures) and colony-forming method (in long-term experiments, 20 days, with 3D cancer cell colonies). The results obtained reveal that applied at a concentration range of 1 - 200 μg/ml $Ni_2(BAMP)(CH_3COO)_4$ and $Ni_2(BAMP)(Cl)_4$ are more pronounced cytotoxic agents as compared to $Ni(TAMEN)(ClO_4)_2$ and $Ni(TAMEN)(NCS)_2$. Both ligands (BAMP, TAMEN) do not significantly decrease viability and proliferation of the treated cells

Key words: mannich bases, nickel, polynuclear complexes, cytotoxic activity, human cancer cell lines

Introduction

The discovery of antitumor activity of cisplatin and its successful application in clinical oncology stimulated scientists to search for other metal compounds with promising anticancer potential [9, 19].

Nickel (Ni) is important for proper functioning of the immune system, influences hormonal activity and has been considered as an essential micronutrient for humans. In animals, nickel deficiency has been associated with decreased growth, reduced re-

production, changes in glucose and lipid metabolism [2, 6, 28]. Ni(II) complexes with various ligands have been reported to possess antitumor properties in vitro and / or in vivo [3, 7, 15, 16, 27].

Mannich bases, a structurally heterogeneous class of chemical compounds, are products of a condensation reaction (Mannich reaction) of a compound with active hydrogen(s) with an amine (primary or secondary) and formaldehyde (any aldehyde) [5, 17, 24]. Mannich bases express a wide variety of biological activities including antineoplastic potential [5, 24].

It has been found in our previous investigations that Ni(II) complexes with Mannich base N,N'-bis(4-antipyrylmethyl)-piperazine (BAMP) significantly reduced viability and proliferation of retrovirus transformed rat sarcoma (LSR-SF-SR) and chicken hepatoma (LSCC-SF-Mc29) cells [3].

The aim of our study was to evaluate the cytotoxic activity of four nickel (II) complexes with ligands containing BAMP or TAMEN (N,N'-tetra-(antipyryl-1-methyl)-1,2-diaminoethane) on viability and proliferation of cultured human cancer cells.

Materials and Methods

Materials. Dulbecco's modified Eagle's medium (D-MEM) and fetal bovine serum (FBS) were purchased from Gibco-Invitrogen (UK). Dimethyl sulfoxide (DMSO), neutral red and trypsin were obtained from AppliChem (Germany); purified agar and thiazolyl blue tetrazolium bromide (MTT) were from Sigma-Aldrich Chemie GmbH (Germany). All other chemicals of the highest purity commercially available were purchased from local agents and distributors. All sterile plastic ware was from Orange Scientific (Belgium).

Compounds. Four Ni(II) complexes with ligands containing the antipyrine moiety N,N'-bis(4-antipyrylmethyl)-piperazine (BAMP) and N,N'-tetra-(antipyryl-1-methyl)-1,2-diaminoethane (TAMEN) - $Ni_2(BAMP)(CHCOO_3)_4$, $Ni_2(BAMP)(Cl)_4$, $Ni(TAMEN)(ClO_4)_2$, $Ni(TAMEN)(NCS)_2$, as well as both ligands were investigated. The synthesis as well as the physical and chemical characteristics of the compounds were already published [10, 11].

Nickel(II) complexes as well as their ligands BAMP and TAMEN were dissolved in dimethylsulfoxide (the concentration of the compound in the stock solution was 1 mg/ml containing 1-2% DMSO) and then diluted in culture medium.

Cell lines and cultivation. The following human permanent cell lines were used as model systems in our investigations: MCF-7 (luminal A type breast cancer), SK-BR-3 (Her2 - positive breast cancer), Caco-2 (colon adenocarcinoma), HepG2 (hepatocellular cancer) and 8MGBA (glioblastoma multiforme).

The cells were grown as monolayer cultures in a D-MEM medium, supplemented with 5-10% fetal bovine serum, 100 U/ml penicillin and 100 mg/ml streptomycin. The cultures were maintained at 37°C in a humidified CO_2 incubator (Thermo Scientific, HEPA Class 100). For routine passages the cells were detached using a mixture of 0.05% trypsin – 0.02% ethylendiaminotetraacetic acid (EDTA). The experiments were performed during the exponential phase of cell growth.

Cytotoxicity assays. The cells were seeded in 96-well flat-botommed microplates at a concentration of 1×10^4 cells/well. After the cells were grown for 24 h to a subconfluent state (~ 60-70%), the culture medium was removed and changed by media modified with different concentrations (1, 10, 50, 100 and 200 mg/ml) of the compounds tested. Each concentration was applied into 4 to 8 wells. Samples of cells grown in non-modified medium served as controls. After 24, 48 and 72 h of incubation, the effect of

the compounds on cell viability and proliferation was examined by neutral red uptake cytotoxicity (NR) assay [8] and thiazolyl blue tetrazolium bromide (MTT) test [18].

Optical density was measured at 540 nm using an automatic microplate reader (TECAN, Sunrise™, Austria). Relative cell viability, expressed as a percentage of the untreated control (100% viability), was calculated for each concentration. Concentration–response curves were prepared and the effective cytotoxic concentration 50 (CC_{50}) of the compounds causing 50% reduction of cell viability was estimated from these curves. All data points represent an average of three independent assays.

Colony forming method. Tumor cells (10^3 cells/well) suspended in 0.45% purified agar in D-MEM medium containing different concentrations of the compounds examined (ranging from 1 to 250 mg/mL) were layered in 24 well microplates. The presence/absence of colonies was registered using an inverted microscope (Carl Zeiss, Germany) during period of 18-20 days. Colony inhibitory concentration (CIC) at which the compounds tested suppress completely the ability of tumor cells for 3D growth in semi-solid medium was determined.

Statistical analysis was performed using one-way analysis of variance (ANOVA) followed by Dunnett post-hoc test and Origin 6.1™.

Results and Discussion

Short-term experiments (24 – 72 h duration) with monolayer cell cultures have been performed by two methods with different molecular/cellular targets and mechanisms of action: MTT test (based on the ability of mitochondrial dehydrogenases to reduce the yellow water-soluble tetrazolium dye MTT to purple coloured formazan crystals) [25] and neutral red uptake cytotoxicity assay (relies on the accumulation of neutral red into lysosomes of viable cells [23]. The "concentration – response" curves showing the ability of Ni(II) complexes (applied at a concentration range of 1 – 200 μg/ml) to reduce viability and proliferation of the treated cells in a time-and concentration-dependent manner are presented in **Figs. 1-3.** Effective concentrations CC_{50} have been determined only for Ni(II) complexes with BAMP after 72 h incubation period **(Table 1)** because in all other cases cell viability was > 50% **(Figs. 1-3)**. The results obtained reveal that Ni(II) complexes with BAMP exhibit more pronounced cytotoxic activity as compared to Ni(II) complexes with TAMEN. Independently administered, the ligands (BAMP and TAMEN) do not significantly decrease viability / proliferation of the treated cells as compared to the control - the lowest viability has been found to be 94.3% +/- 5.4 (for MCF-7 cells, MTT test, 72 h, $p > 0.05$) and ≥ 91.7% +/- 4.6 (for 8MGBA cells, NR assay, 72h, $p > 0.05$).

Long-term influence (20 day treatment periods) of the compounds investigated on the ability of cancer cells to form 3D colonies in semi-solid medium has been studied. The results obtained demonstrate that among the compounds examined only Ni(II)-BAMP complexes can inhibit completely the 3D growth of the treated cancer cells **(Table 2**). Three dimensional (3D) cell culture systems have been recognized as more reliable models for cancer cell biology studies than 2D (monolayer) cell cultures and provide more realistic and predictable information on their drug sensitivity [14].

The cell lines used as model systems in our study exhibit different degree of sensitivity to the cytotoxic effect of the compounds investigated **(Table 3)** that can be a result of their specific biological characteristics. For example, SK-BR-3 cells are more resistant to the influence of the examined Ni(II) complexes than MCF-7 cells. Although both cell lines were established from human breast cancers, each one of them has its specific molecular profile: MCF-7 cells are estrogen receptor – positive, Her2 nega-

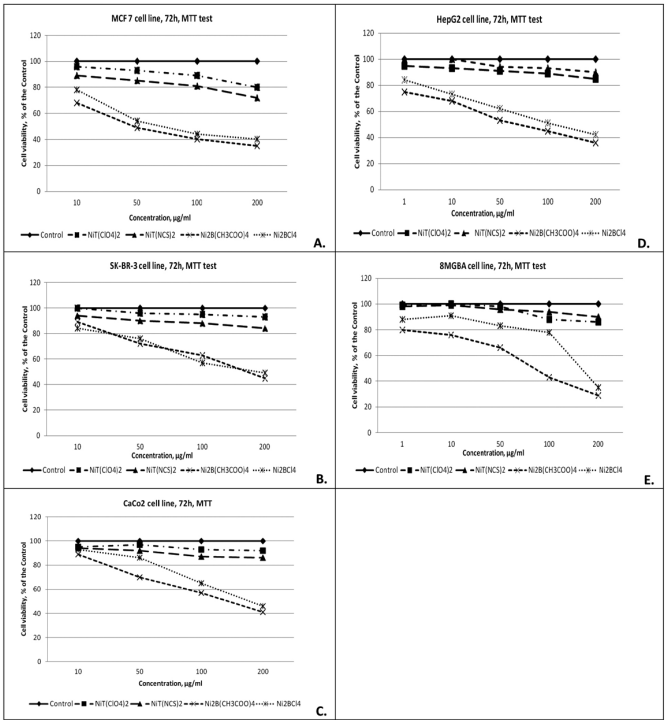

Fig. 1. Concentration-response curves of Ni(II) complexes with BAMP or TAMEN for human MCF-7 (**A**), SK-BR-3 (**B**), Caco-2 (**C**), HepG2 (**D**) and 8MGBA (**E**) cancer cells evaluated by MTT test after 72 h treatment period. B = BAMP, T = TAMEN.

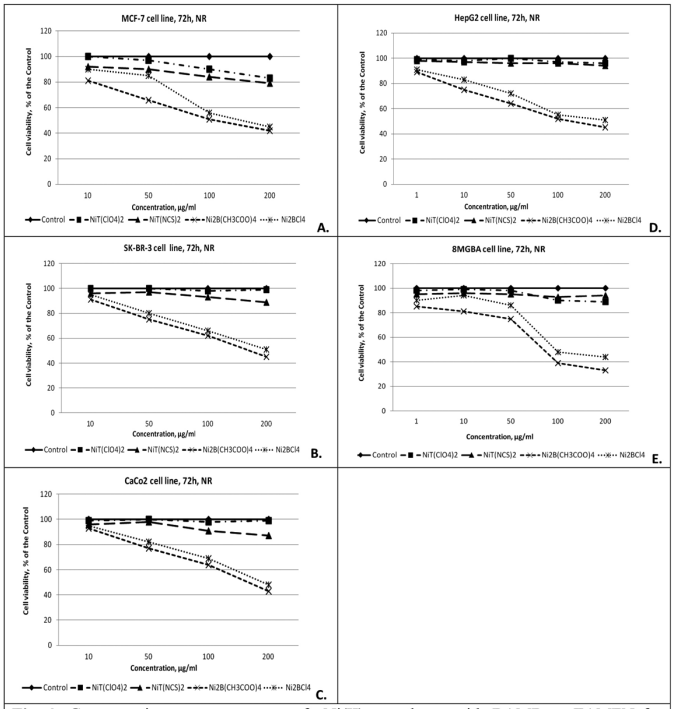

Fig. 2. Concentration-response curves of nickel(II) complexes with BAMP or TAMEN for human MCF-7 (**A**), SK-BR-3 (**B**), Caco-2 (**C**), HepG2 (**D**) and 8MGBA (**E**) cancer cells evaluated by neutral red uptake cytotoxicity assay (NR) after 72 h treatment period. B = BAMP, T = TAMEN.

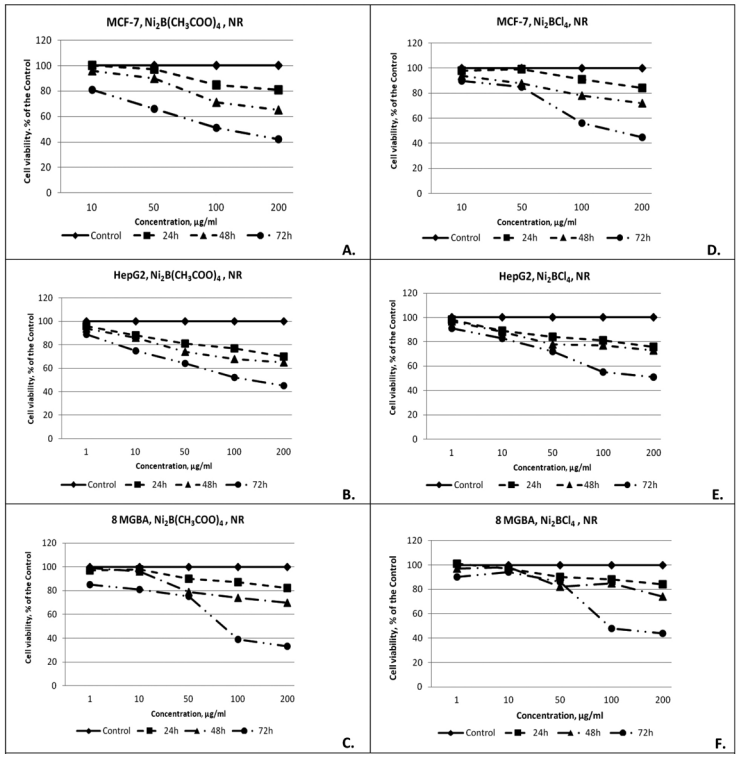

Fig. 3. Concentration-response curves of Ni(II) complexes with BAMP for human MCF-7 (**A, D**), HepG2 (**B, E**) and 8MGBA (**C, F**) cancer cells evaluated by neutral red uptake cytotoxicity assay (NR) after 24, 48 and 72 h treatment period. B = BAMP, T = TAMEN. MTT test after 72 h treatment periods. B = BAMP.

Table 1. Cytotoxicity (CC_{50}, μM, 72h) of Ni(II) complexes with BAMB (B) or TAMEN (T) in human MCF-7, SK-BR-3, Caco-2, HepG2 and 8MGBA cancer cell lines

Compound	Method	Cell line				
		MCF-7	SK-BR-3	Caco-2	HepG2	8MGBA
$NiT(ClO_4)_2$	MTT	n.d.	n.d.	n.d.	n.d.	n.d.
	NR	n.d.	n.d.	n.d.	n.d.	n.d.
$NiT(NCS)_2$	MTT	n.d.	n.d.	n.d.	n.d.	n.d.
	NR	n.d.	n.d.	n.d.	n.d.	n.d.
$Ni_2B(CH_3COO)_4$	MTT	57.2	206.1	172.3	81.8	100.8
	NR	131.0	202.2	198.8	151.7	100.8
Ni_2BCl_4	MTT	94.0	268.3	238.8	149.5	221.6
	NR	155.6 (208.8)	268.3	255.2	268.3	131.3

n.d. - CC_{50} was not determined at 72 h because at all examined concentrations the cell viability was > 50%.

Table 2. Effect of Ni(II) complexes with BAMB (B) or TAMEN (T) on 3D colony-forming ability of human MCF-7, SK-BR-3, Caco-2, HepG2 and 8MGBA tumor cells

	MCF-7	SK-BR-3	Caco-2	HepG2	8MGBA
$NiT(ClO_4)_2$	n.i.	n.i.	n.i.	n.i.	n.i.
$NiT(NCS)_2$	n.i.	n.i.	n.i.	n.i.	n.i.
$Ni_2B(CH_3COO)_4$	≥ 120	≥ 175	≥ 150	≥ 120	≥ 120
Ni_2BCl_4	≥ 135	≥ 235	≥ 200	≥ 135	≥ 135

Colony Inhibitory Concentration (CIC, μM) were determined after 18-20 day treatment period; n.i. = no inhibition

Table 3. Hierarchic orders of human cancer cell lines according to their sensitivity to the cytotoxic activity of Ni(II) complexes with BAMP (B)

Compound	Method	Hierarchic order
$Ni_2B(CH_3COO)_4$	MTT	MCF-7 > HepG2 > 8 MGBA > CaCo-2 > SK-BR-3
	NR	8 MGBA > MCF-7 > HepG2 > CaCo-2 ≥ SK-BR-3
	CFM	MCF-7 = 8MGBA = HepG2 > Caco-2 > SK-BR-3
Ni_2BCl_4	MTT	MCF-7 > HepG2 > 8 MGBA > CaCo-2 > SK-BR-3
	NR	8 MGBA > MCF-7 > CaCo-2 > HepG2 = SK-BR-3
	CFM	MCF-7 = 8MGBA = HepG2 > Caco-2 > SK-BR-3

All hierarchic orders start with the most sensitive cell line (with the lowest CC_{50} or CIC value); MTT = thiazolyl blue tetrazolium bromide test; NR = neutral red uptake cytotoxicity assay; CFM = colony-forming method.

tive, possess wild type p53 and mutant p110 (catalytic subunit of the phosphoinositide-3-kinase - PI3K) whereas SK-BR-3 cells are estrogen receptor - negative, Her2 positive, with mutant p53 and wild type p110 [1, 26]. Higher sensitivity of MCF-7 cells (in comparison to SK-BR-3 cells) to the inhibitory effect of xanafide (a DNA intercalatory agent and topoisomerase II inhibitor) has been reported [1]. In another study MCF-7 cells have been shown to be more sensitive to the cytotoxic effect of aloin (natural anthracycline from Aloe plant) than SK-BR-3 cells [12].

Mannich bases are heterogeneous group of chemical compounds that exhibit a wide range of biological activities including antiinflammatory, antiulcer, anticonvulsant, analgesic, antioxidant, antibacterial, antifungal, antiviral and antiparasitic properties. In addition, some Mannich bases have been proved to regulate blood pressure, to inhibit platelet aggregation or to express antiphyhotic effects. Anticancer potential of Mannich bases have also been reported [5, 24]. It has been found in our previous investigations that Cu(II) and Ni(II) complexes with BAMP and TAMEN decrease viability and prolif-

eration of cultured cancer cells [3, 4]. Cu(II), Co(II) and Ni(II) complexes with the same ligands express antimicrobial activities [20, 21, 22]. Similarly to the results obtained in the present study, Cu(II) complexes with BAMP are more pronounced cytotoxic agents for retrovirus-transformed rat sarcoma (LSR-SF-SR) and chicken hepatoma (LSCC-SF-Mc29) cells as well as human glioblastoma (8MGBA) cells than Cu(II) complexes with TAMEN [4]. The cytotoxic activity of $Ni_2(BAMP)(CH_3COO)_4$ and $Ni_2(BAMP)(Cl)_4$ is also significantly higher than those of $Ni(TAMEN)(ClO_4)_2$ and $Ni(TAMEN)(NCS)_2$, [4]. On the other hand, the same Ni(II) complexes with TAMEN are more effective antibacterial and antifungal agents than Ni(II) complexes with BAMP [20].
In this study we report for the first time the ability of Ni(II) complexes with BAMP ($Ni_2(BAMP)(CH_3COO)_4$ and $Ni_2(BAMP)(Cl)_4$) to suppress the 2D and 3D growth of human cell lines, established from cancers of the breast (luminal A type MCF-7 and Her2-positive SK-BR-3), colon (Caco-2), liver (HepG2) and brain (8MGBA). These are some of the most common and aggressive human malignancies [13] and searching for the effective new treatment modalities for them is among the major challenges of current biomedical sciences. Additional investigations are required to clarify better the antitumor potential of Ni(II) complexes with N,N'-bis(4-antipyrylmethyl)-piperazine (BAMP) as well as their molecular targets and mechanism(s) of action.

Acknowledgements: Supported by Grant № Б 02 30 / 12.12.2014, Fund "Scientific Research", Bulgarian Ministry of Education and Science; a bilateral project between Bulgarian Academy of Sciences and Romanian Academy; a bilateral project between Bulgarian Academy of Sciences and Medical Research Division, National Research Centre, Cairo, Egypt.

References

1. **Alami, N., J. Paterson, S. Belanger, S. Juste, C. K. Grieshaber, B. Leyland-Jones.** Comparative analysis of xanafide cytotoxicity in breast cancer cell lines. - *Br. J. Cancer,* **97**(1), 2007, 58-64.
2. **Alexandrova, R., O. Costisor, L. Patron.** Nickel. - *Exp. Pathol. Parasitol.,* **9**(1), 2006, 64-74.
3. **Alexandrova, R., G. Rashkova, T. Popova, R. Tudose, E. M. Mosoarca, S. Slavov, O. Costisor.** Preliminary investigations on cytotoxic activity of four nickel (II) complexes with Mannich type ligands on virus-induced tumor cell lines. - *Acta morphol. anthropol.,* **11,** 2006, 60-85.
4. **Alexandrova, R., G. Rashkova, T. Popova, S. Slavov, R. Tudose, E.-M. Mosoarca, O. Costisor.** Cytotoxic activity of three copper complexes with Mannich type ligands on tumour cell lines. - *Exp. Pathol. Parasitol.,* **8**/2, 2004, 93-98.
5. **Bala, S., N. Sharma, A. Kajal, S. Kamboj, V. Saini.** Mannich bases: an important pharmacophore in present scenario. - *Int. J. Med. Chem.* 2014, doi: 10.1155/2014/191072.
6. **Barceloux, D. G.** Nickel. - *J. Toxicol. Clin. Toxicol.,* **37,** 1999, 239-258.
7. **Beheshti, A., F. Hashemi, F. Behavndi, M. Zahedi, M. Kolahi, H. Motamedi, P. Mayer.** Synthesis, structural characterization, QSAR and docking studies of a new binuclear nickel (II) complex based on the flexible tetradentate N-donor ligand as a potent antibacterial and anticancer agent. - *Int. J. Biol. Macromol.,* **104**(Pt A), 2017, 1107-1123.
8. **Borenfreund, E., J. A. Puerner.** Toxicity determined in vitro by morphological alterations and neutral red absorption. - *Toxicol. Lett.,* **24**(2-3), 1985, 119-124.
9. **Chen, D., V. Milacic, M. Frezza, Q. P. Dou.** Metal complexes, their cellular targets and potential for cancer therapy. - *Curr. Pharm. Des.,* **15**(7), 2009, 777-91.
10. **Costisor, O., C. Stanescu, R. Tudose, I. Eremia, S. Policec.** New Pyrazolone Complex Compounds VII. N,N'-tetra(antipyryl-Methyl)-1,2-Ethanediamine A New Dinucleating Ligand. - *Bul. St. Teh. Inst. Politehnic "Traian Vuia" Timisoara, Ser. Chim.,* **39,** 1994, 79-84
11. **Costisor, O., W. Linert, S. Deusch, C. Stanescu.** Novel complexes of antipyrine ligands – dinuclrear copper(II), cobalt(II) and nickel(II) complexes of N,N'-tetra(antipyrylmethyl)-1,2-diaminoethane. - *J. Coord. Chem.,* **33,** 1994, 229-234.

12. **Esmat, A. Y., C. Tomasetto, M.-C. Rio.** Cytotoxicity of a natural anthraquinone (Aloin) against human breast cancer cell lines with and without ErbB-2: Topoisomerase II-alpha coamplification. - *Cancer Biology & Therapy,* **5**(1), 2006, 97-103.
13. **Europe PMC Funders Group.** The global burden of cancer 2013. - *JAMA Oncol.,* **1**(4), 2015, 505-527.
14. **Fitzgerald, K. A., M. Malhotra, C. M. Curtin, F. J. O' Brien, C. M. O' Driscoll.** Life in 3D is never flat: 3D models to optimise drug delivery. - *J. Control Release,* **215**, 2015, 39-54.
15. **Hegazy, W. H., M. H. Marzouk.** Cytotoxic activities of newly synthesized Co(II), Ni(II) and Cu(II) complexes with hexadentate hydrazonic ligands. - *Chem. Sci. Trans.,* **2**(4), 2013, 1482-1490.
16. **Li, D.-D., X.-M. Zhao, N. G., S. Zhi, Z.-W. Tao.** DNA binding, cleavage, and cytotoxicity of binuclear phenolate nickel(II) complexes. - *Journal of Coordination Chemistry,* **70**(12), 2017, 2113-2127.
17. **Mannich, C., B. Kather. Mannich, C., B. Kather.** About condensation products of amine salts, formaldehyde and antipyrine. - *Arch. Pharm.,* **257,** 1919, 18-33 [in German].
18. **Mosmann, T.** Rapid colorimetric assay for cellular growth and survival: application to proliferation and cytotoxicity assays. - *J. Immunol. Meth.,* **65**(1-2), 1983, 55-63.
19. **Ott, I., R. Gust.** Non platinum metal complexes as anti-cancer drugs. - *Arch. Pharm. (Weinheim),* **340**(3), 2007, 117-126.
20. **Popova, T., R. Alexandrova, R. Tudose, E.-M. Mosoarca, O. Costisor.** Antimicrobial activity in vitro of four nickel complexes. - *BJAS,* **18**(3), 2012, 446-450.
21. **Popova, T., R. Alexandrova, R. Tudose, O. Costisor.** Preliminary in vitro investigations on antimicrobial activity of two copper complexes. - *Compt. Rend. Acad. Bulg. Sci.,* 57(6), 2004, 105-110.
22. **Popova, T. P., R. I. Alexandrova, R. Tudose, E.-M. Mosoarca, O. Costisor.** Antibacterial activity in vitro of four cobalt (II) complexes with Mannich type ligands. - *Compt. Rend. Acad. Bulg. Sci.,* **59**(5), 2006, 551-556.
23. **Repetto, G., A. del Peso, J. L. Zurita.** Neutral red uptake assay for the estimation of cell viability/cytotoxicity. - *Nat Protoc.,* **3**(7), 2008, 1125-1131.
24. **Roman, G.** Mannich bases in medicinal chemistry and drug design. - *Eur. J. Med. Chem.,* **89,** 2015, 743-816.
25. **Śliwka, L., K.Wiktorska, P. Suchocki, M. Milczarek, S. Mielczarek, K. Lubelska, T. Cierpiał, P. Łyżwa, P. Kiełbasiński, A. Jaromin, A. Flis, Z. Chilmonczyk.** The Comparison of MTT and CVS Assays for the Assessment of Anticancer Agent Interactions. - *PLoS One.* **11**(5), 2016, e0155772. https://doi.org/10.1371/journal.pone.0155772.
26. **Torbett, N. E., A. Luna, Z. A. Knight, A. Houk, M. Moasser, W. Weiss, K. M. Shokat, D. Stokoe.** A chemical screen in diverse breast cancer cell lines reveals genetic enhancers and suppressors of sensitivity to PI3K isotype-selective inhibition. - *Biochem. J.,* **415**(1), 2008, 97-110.
27. **Yang, T., W. Qin.** Transition metal manganese(II), nickel(II), copper(II) and zinc(II) complexes of a new Schiff base ligand: Synthesis, characterization and antitumor activity studies. - *Polish Journal of Chemistry,* **80**(10), 2006, 1657-1662.
28. **Zdrojewicz, Z., E. Popowicz, J. Winiarski.** Nickel - role in human organism and toxic effects. – *Pol. Merkur. Lekarski,* **41**(242), 2016, 115-118 [in Polish].

Institute of Experimental Morphology, Pathology and Anthropology with Museum
Bulgarian Anatomical Society

Acta morphologica et anthropologica, 25 (1-2)
Sofia ● 2018

Mast Cells in the Rat Carotid Body

Dimitrinka Atanasova[1, 2], Angel Dandov[3], Todor Kirov[3], Nikolai Lazarov[1, 3]*

[1] *Institute of Neurobiology, Bulgarian Academy of Sciences, Sofia, Bulgaria*
[2] *Department of Anatomy, Faculty of Medicine, Trakia University, Stara Zagora, Bulgaria*
[3] *Department of Anatomy and Histology, Medical University of Sofia, Sofia, Bulgaria*

* Corresponding author e-mails: didiatan@bio.bas.bg; didi_atanasova@yahoo.com

The carotid body (CB) is the main peripheral arterial chemoreceptor in mammals that registers the oxygen and carbon dioxide levels in blood, and responds to their changes by adequately adapting the cardiovascular and respiratory homeostasis. The basic morphofunctional unit of the CB called 'glomerulus' consists of two juxtaposed cell types: chemosensory neuron-like type I or glomus cells, and type II or sustentacular cells, the latter being supporting glial-like cells. The purpose of this study was to determine the presence and distribution of mast cells in the rat CB by using staining techniques with Toluidine blue and Bismarck brown. In particular, the mast cells were predominantly located in the interlobular connective tissue of the CB and were closely associated with blood vessels, but they were not found within the cell clusters. A few were observed in a close association with the islands of cells, and they were related to the sustentacular cells. Thus, the mast cells are not directly associated with glomus cells and probably do not functionally determine chemosensory properties. It is likely that mast cells are involved in the regulation of the blood supply within the CB by acting on small blood vessels.

Key words: carotid body, mast cells, blood vessels, toluidine blue, Bismarck brown

Introduction

The carotid body (CB) is the peripheral arterial chemoreceptor that registers the levels of pO2, pCO2 and pH in the blood and responds to their changes by adequately adapting the cardiovascular and respiratory homeostasis. It is strategically located in the bifurcation region of each common carotid artery. The organ consists of "glomeruli" composed of two cell types, glomus and sustentacular cells, interspersed by blood vessels and nerve bundles, and separated by connective tissue.

Mast cells (MCs) have a widespread tissue distribution [4] and are considered to be multifunctional immune cells involved in health and several diseases. Due to their extensive tissue distribution and adaptability they are able to react to environmental changes by comunicating with other cells implicated in physiological and immunological responses.

MCs are plentiful in the CB of humans; their numbers vary in different animal species [10] and are not related to the CB histology. However, there is no difference in the number of MCs in the CBs of young patients with prominent glomus cells and adults with many supporting cells or age-related acellular fibrosis [10].

Chiocchio et al. [3] suggested that dopamine might be stored in the MCs of the cat CB and it might be a precursor of other catecholamines. In addition, there is evidence for serotonin-like immunoreactivity not only in the glomus cells but also in the MCs of the rat CB [7].

Therefore, we set as a goal of this study to provide morphological data on the presence and distribution of MCs in the rat CB using classical histological techniques.

Materials and Methods

The experiments were carried out on eight male Wistar rats, weighing 220 – 250 g. The study was performed in agreement with the European Communities Council Directive 2010/63/EU for the protection of animals used for scientific purposes. The experimental procedures have been approved by the Institutional Ethics Committee at the Institute of Neurobiology of the Bulgarian Academy of Sciences.

The animals were deeply anesthetized and transcardially perfused first with 0.05 M phosphate-buffered saline (PBS), pH 7.4, followed by 4% paraformaldehyde (PFA) in 0.01 M phosphate buffer (PB), pH 7.4. The carotid bifurcations were dissected out and postfixed in the same fixative overnight at 4°C. Thereafter, the tissues were embedded in paraffin and cut into 6 μm thick serial sections. Adjacent serial sections were mounted on glass slides coated with chrome alum-gelatin and processed for Hematoxylin and Eosin (H&E), Toluidine blue (TB) and Bismarck brown (BB) staining, respectively.

For the Toluidine blue staining samples were deparaffinized with xylene and ethanol and rehydrated with distilled water. Staining of the slides was carried out by immersing the sections in a 0.5% aqueous solution of Toluidine blue for a few minutes, under visual control of the staining intesity. Subsequently, sections were rinsed in distilled water, then dehydrated, cleared in xylene, and coverslipped in Entellan.

For the application of Bismarck brown staining we used the modified protocol of Tomov and Dimitrov [13]. According to it, the sections were deparaffinized with xylene and rehydrated to 70% ethanol. Then they were immersed in a solution of 500 mg Bismarck brown in 80 ml 96% ethanol and 10 ml 1N HCl for 2 hours at room temperature. Following a three-time differentiation in 70% ethanol, the sections were counterstained with Mayer's haematoxylin solution. Thereafter they were dehydrated, cleared in xylene, and coverslipped in Entellan.

Serial sections with both staining techniques were analyzed as the positive mast cells have been calculated for a greater precision in an area of 0.25 mm^2. To compare the results from both staining methods we applied the Student's t-test. Statistical analysis was carried out by SigmaStat® 11.0 software and $p<0.05$ value was accepted as a significant difference.

The specimens were observed and photographed with a Nikon research microscope equipped with a DXM 1200c digital camera.

Results

The CB in rats is bilaterally located at the bifurcation of each common carotid artery, between the external and internal carotid arteries **(Fig. 1A)**. The organ is composed of cell clusters, blood vessels, connective tissue and nerve fibres **(Fig. 1B).** The clusters comprised of two cell types, i.e. neuron-like type I or glomus cells and glial-like type II or sustentacular cells. Postganglionic sympathetic neurons innervating the CB via the ganglioglomerular nerves have their cell bodies in the superior cervical ganglion **(Fig. 1A)**.

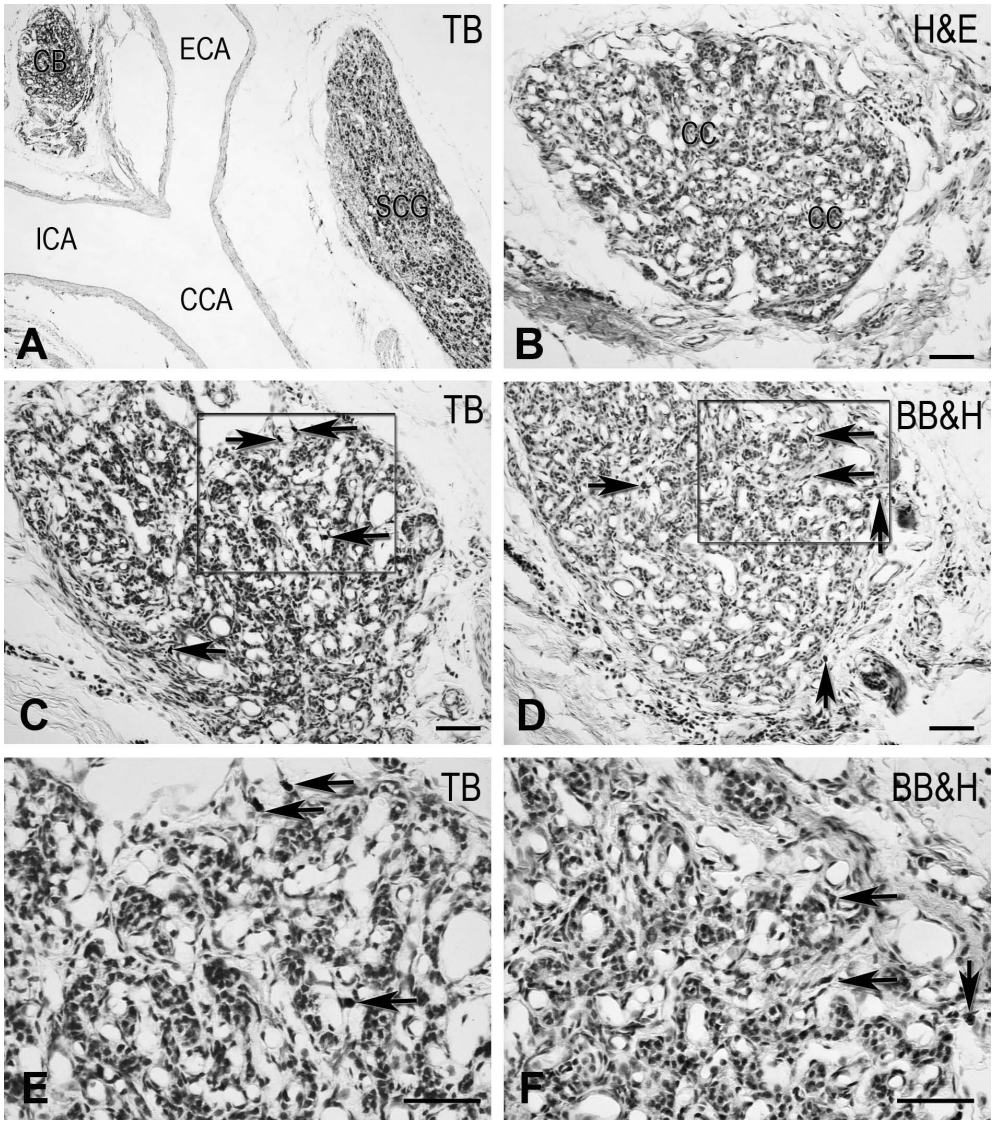

Fig. 1. Localization and distribution of mast cells in the rat carotid body (CB). **(A)** A representative Toluidine blue-stained section of the common carotid artery (CCA) bifurcation area showing the localization of the CB between the external carotid artery (ECA) and the internal carotid artery (ICA) and the superior cervical ganglion (SCG). **(B)** H&E staining illustrates the organization of the rat CB. The glomic tissue is arranged in cell clusters (CC). Low- **(C)** and high- **(E)** power photomicrographs of the Toluidine blue-stained (TB) mast cells (arrows) in the rat CB shown in **A** and **B** displaying the distribution of mast cells. Note that they are predominantly located in the interlobular stroma of the CB and are closely associated with blood vessels. **(F)** Higher magnification of the boxed area in **(D)** demonstrating Bismark brown-stained (BB) mast cells (arrows). Scale bars = 50 μm.

To evaluate the distribution of MCs in the CB of Wistar rats, we applied two classical histological staining techniques for their visualization, i.e. Toluidine blue **(Fig. 1A, C, E)** and Bismarck brown **(Fig. 1D, F).** We observed that the MCs were predominantly located in the interlobular stroma of the CB and were closely associated with blood vessels and no MCs were found within the cell clusters. In particular, a few of the observed MCs were tightly packed to the covering shell of sustentacular cells but were not related to the central core of glomus cells. The average density and distribution of MCs per unit area of 0.25 mm^2 in the rat CB, for both types of staining, was similar: 5.778±0.339 (TB-positive MCs) and 5.929±0.412 (BB-positive MCs) **(Fig. 2).**

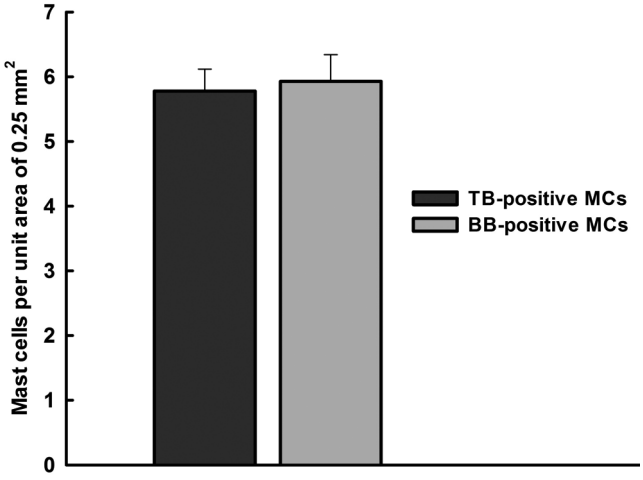

Fig. 2. Vertical bar chart shows the distribution of stained with Toluidine blue and Bismarck Brown mast cells per unit area of 0.25 mm^2. Data are presented as mean±SEM.

Discussion

The results of our study confirm the observations of previous authors [6, 10, 11] that MCs are present in the CB of humans and other mammals. In addition, their number is species-specific and they most frequently occur in bovines [1]. When comparing our data on MC density per unit area in rats (20 – 25 mast cells/mm^2) with the data of other authors [10] on MC density in human CBs (20 – 60 mast cells/mm^2, and mainly in a narrower range of 30 – 60/mm^2) [10], it appears that in the human CB there is a greater MC density and the cells are more abundant than in the rat. Although a difference in their density in the CB of rats and humans exists, it is interesting to point out that distributional patterns remain similar. The MCs are mostly restricted to the interlobular connective tissue where they are often closely related to the small blood vessels. A few MCs are found in a close apposition to the cell islands, but even in that case they are predominantly associated with the sustentacular glial cells. Given that MCs are not directly related to neuron-like glomus cells they are probably not involved in regulating the function of the glomus cells. However, this does not exclude their involvement in the control of small blood vessels and the blood supply within the CB.

The density of MCs remains constant throughout life and is not affected by age and age-related histological appearance of the CB that develops in time. Moreover, certain histopathological conditions involving the CB such as systemic hypertension and chronic obstructive lung disease [8, 12] or coarctation of the aorta [9] do not affect the density and distribution of the MCs.

Conclusion

It can be inferred that the MCs are a constant population in the rat CB and they are most probably related to the functional control of its blood flow via the vasoactive substances they liberate. Further efforts are needed to elucidate their exact chemical nature and physiological mechanism.

Acknowledgements: This work was supported by the Medical Faculty of Trakia University, Stara Zagora, Bulgaria, contract No. 13/2017 and No.10/2018.

References

1. **Arias-Stella, J., F. Bustos.** Chronic hypoxia and chemodectomas in bovines at high altitudes. - *Arch. Pathol. Lab. Med.,* **100,** 1976, 636-639.
2. **Atanasova, D. Y., M. E. Iliev, N. E. Lazarov.** Morphology of the rat carotid body. - *Biomed. Rev.,* **22,** 2011, 41-55.
3. **Chiocchio, S. R., A. M. Biscardi, J. H Tramezzani.** Catecholamines in the carotid body of the cat. - *Nature, Lond.,* **212,** 1966, 834-835.
4. **Dimitrov, N.** Normal morphology of biologically active point BAP/ST36 rat. - *Acta morphol. et anthropol.,* **19**, 2012, 34-37.
5. **Gonzaez, C., L. A1maraz, A. Obeso, R. Rigual.** Carotid body chemoreceptors: from natural stimuli to sensory discharges. - *Physiol. Rev.,* **74**, 1994, 829-898.
6. **Grimley, P. M., G. G.** Glenner. Histology and ultrastructure of carotid body paragangliomas. Comparison with the normal gland. - *Cancer,* **20,** 1967,1473-1488.
7. **Grönblad, M., P. Liesi, L. Rechardt.** Serotonin-like immunoreactivity in the rat carotid body. - *Brain Res.,* **276,** 1983, 348-350.
8. **Heath, D., P. Smith, R. Jago.** Hyperplasia of the carotid body. - *J. Pathol.,* **138,** 1982, 115-127.
9. **Heath, D., P. Smith, G. Hurst.** The carotid bodies in coarctation of the aorta. - *Br. J. Dis. Chest.,* **80,** 1986, 122-130.
10. **Heath, D., P. Lowe, P. Smith.** Mast cells in the human carotid body. - *J. Clin. Pathol.,* **40,** 1987, 9-12.
11. **Pryse-Davies, J. I., I. M. P. Dawson, G. Westbury.** Some morphologic, histochemical and chemical observations on chemodectomas and the normal carotid body, including a study of the chromaffin reaction and possible ganglion cell elements. - *Cancer,* **17,** 1964, 195-202.
12. **Smith, P., R. Jago, D. Heath.** Anatomical variation and quantitative histology of the normal and enlarged carotid body. - *J. Pathol.,* **137,** 1982, 287-304.
13. **Tomov, N., N. Dimitrov.** Modified Bismarck brown staining for demonstration of soft tissue mast cells. - *Trakia J. Sci.,* **3,** 2017, 195-197.

Institute of Experimental Morphology, Pathology and Anthropology with Museum
Bulgarian Anatomical Society

Acta morphologica et anthropologica, 25 (1-2)
Sofia ● 2018

Periungual Pilomatrixoma – a Case with Very Rare Localization

Valentina Broshtilova[1], Ivan Litov[2], Mary Gantcheva[3]*

[1] *Department of Dermatology and Venereology, Faculty of Medicine, Medical University Sofia, Bulgaria*
[2] *Department of Dermatology, Eurohealth, Sofia, Bulgaria*
[3] *Institute of Experimental Morphology, Pathology and Antropology with Museum, Bulgarian Academy of Science, Sofia, Bulgaria*

* Corresponding author e-mails: mary_gant@yahoo.com

A 54-year-old woman with a slowly growing periungual tumor mass, pathologically verified as pilomatrixoma, is described. A multi-aspect overview of the clinical, diagnostic, and therapeutic features of this hair matrix-derived benign neoplasm are presented to accentuate the importance of a proper clinico-pathological approach and raise the suspicion index, even on such an anecdotally rare predilection.

Key-words: pilomatrixoma, periungual localization

Introduction

Pilomatrixomas are subcutaneous benign neoplasms of hair matrix origin, usually localized on face, neck, and upper extremities [15]. The versatile morphology and unusual clinical appearance, as well as the low prevalence, extremely deteriorates the diagnostic verification of the tumor, challenging even the most experienced clinicians.

Herein, a very rare periungual localization of pilomatrixoma is presented.

Case report

A 54-year-old Caucasean woman with a three-year history of slowly enlarging flesh coloured mass on the lateral margin of the left upper thumb is presented. She did not recall traumatic impact or any pre-existing nail abnormality. Keratolytic and anti-mycotic topical agents proved ineffective. Physical examination showed an oval tumor with firm consistency and a diameter of 7mm, with no change of the overlying skin. The presumptive clinical differential diagnosis included a myxoid cyst, ossifying hematoma, fibroxanthoma, glomangioma, and foreign-body granuloma. X-ray analysis showed microcalcifications in the subcutaneous mass. Surgical excision with histological examination was performed. The pathological picture revealed a well-circumscribed

nodulo-cystic tumor with islands of eosinophilic cells derived from basaloid proliferations **(Fig. 1)**, centrally forming anucleated ghost cells **(Fig. 2)** and zones of calcification. The diagnosis of pilomatrixoma was made. The patient was free of recurrences till the 7th month after surgery.

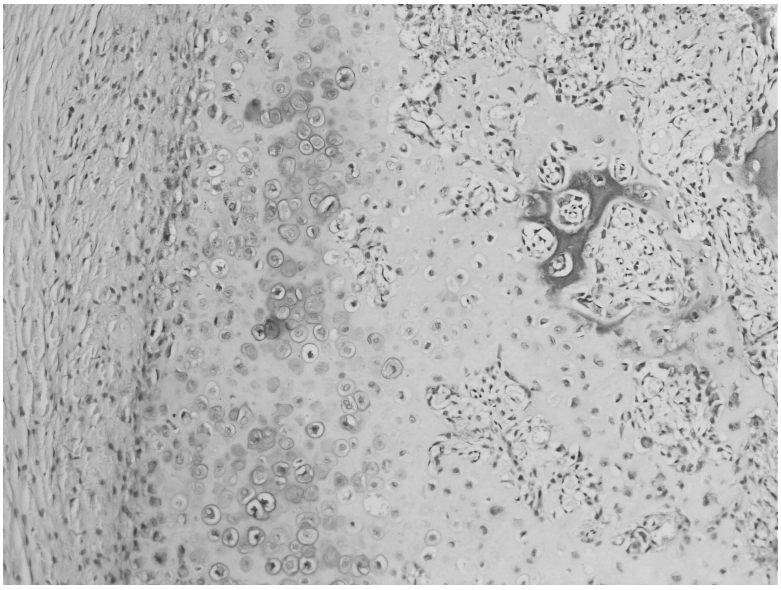

Fig. 1. Basaloid proliferations with central degeneration towards anucleated cells. HE x 100

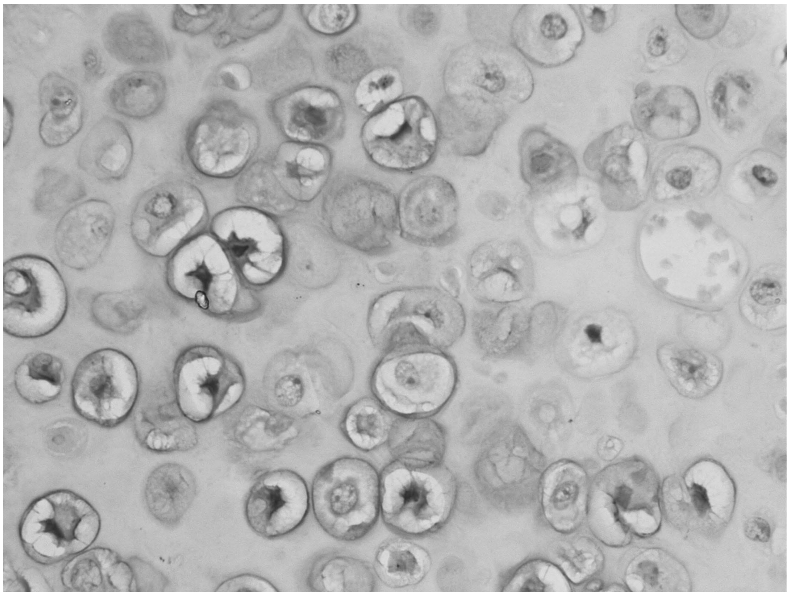

Fig. 2. Ghost cells. HE x 400

Discussion

Pilomatrixomas were first described by Malherbe and Chenantais in 1880 [10]. Although Jones and Campbell coined the term, when discovered a subcutaneous tumor in a pediatric population, it was later fully recognized that the tumor also affects adults [6]. Moreover, despite its low incidence in the elderly population, the only malignant transformations have been described only in this age group [8]. It seems that the pilomatrixoma carcinomas appear on head and neck of middle aged patients. The exact rate of malignant transformation is not clear. No more than 20 cases have been described worldwide, and it is still unknown whether this is a malignant case arising de novo, or represents a degeneration of pre-existing pilomatrixoma [7].

The diagnostic verification of the tumor is extremely challenging [9]. First, there are no specific clinical features. Usually a subcutaneous mass has been growing slowly for some years. The overlying skin can be unchanged, erythematous, slightly livid, or with yellowish discoloration [11]. The tumor is well-circumscribed and very firm on palpation.

The anatomic localization is usually on the head and neck region, less commonly - on the upper extremities [14]. To our knowledge, no periungual localization has been described to date. It seems rather unusual since no hair follicles are presented in close proximity to the nail bed. The differential diagnosis of tumors, arising around the nail apparatus, includes periungual fibroma, pyogenic granuloma, superficial acralfibroxanthoma, periungual melanoma and squamous cell carcinoma [12]. Some inflammatory reaction patterns can also show such localization - periungual warts, foreign body granuloma, residual haemangiomas [13]. The case presented showed an extremely rare variant of periungual tumor, probably arising from an ectopic stem follicle in conjunction with the nail martix. Such a predilection is exceptional, and makes this observation highly anecdotal and extremely difficult for diagnosis.

Imaging diagnosis has proven not to be highly specific. Conventional X-ray, shows milliar micro-calcifications, which can be seen in all cases of dystrophic calcification [5]. Ultrasound is not very discriminating, either. Heterogeneous echotexture, internal echogenic foci in scattered-dot pattern, and posterior shadowing with hypoechoic rim are not considered informative, since they can be seen in any long-standing subcutaneous tumors [1,4]. Sebaceous cysts, foreign body reactions and metastatic bone formations share the same computer-tomographic features as pilomatrixomas – uniform, homogenous on T1 weighted signal with varying results on T1 with contrast and T2 imaging [16].

The golden standard for reliable diagnostic verification remains pathological evaluation 3. It is defined by monomorphous basaloid proliferations with degradation towards amorphic ghost (shadow) cells representing hair cortex differentiation. The foci of calcification originate secondarily due to dystrophic calcium deposition [2].

The proper therapeutic approach acquires surgical excision. A low recurrence rate of 2.6% is expected, and radical excision margins of 2 cm are, therefore, approved. Patients' population that has been follow-up showed free of recurrence interval of 3 to 37 months [17]. Re-appearance of the tumor raises a suspicion of malignancy evoking aggressive surgical excision, which is supposed to be sufficient and curative treatment with excellent prognosis.

Conclusions

The periungual case presented here is a rare example of pilomatrixoma with unusual localization, unpredictable clinical evolution and extremely difficult surgical access. It

demonstrates the importance of complex clinico-pathological correlation and surgical skills, needed to precisely cure, monitor, and prevent such anecdotal hair matrix proliferation.

References

1. **Choo, H. J., S. J. Lee, Y. H. Lee, J. H. Lee, M. Oh, M. H. Kim, E. J. Lee, J. W. Song, S. J. Kim, D. W. Kim.** Pilomatricomas: the diagnostic value of ultrasound. Skeletal Radiology, Blackwell Publishing, 2009.
2. **El Moussaoui, N., B. Hassam.** Pilomatricoma: a tumor to know. - *Pan. Afr. Med. J.,***18,** 2014, 182.
3. **Hernandez-Nunez, A., L. Najera Botello, A. Romero Mate, L. Nájera Botello, Romero Maté, C. Martínez-Sánchez, M. Utrera Busquets, A. CalderónKomáromy, J. Borbujo Martínez.** Retrospective study of pilomatricoma: 261 tumors in 239 patients. - *Actas Dermosifiliogr.,***105,** 2014; 699-705.
4. **Hughes. J., A. Lam, M. Rogers.** Use of ultrasonography in the diagnosis of childhood pilomatrixoma. - *Pediatr. Dermatol.,***16,** 1999, 341-344.
5. **Julian, C., P. Bowers.** A clinical review of 209 pilomatricomas. - *J. Am. Acad. Dermatol.,* **39,** 1998, 191-195.
6. **Jones, P., P. Campbell.** Pilomatrixoma: a not uncommon hamartoma of infancy and childhood. - *Aust. Paediat. J.,* **5,** 1969, 162-166.
7. **Kurokawa, I., K. Yamanaka, Y. Senba, H. Sugisaki, A. Tsubura, T. Kimura, H. Mizutani.** Pilomatricoma can differentiate not only towards hair matrix and hair cortex, but also follicular infundibulum, outer root sheath and hair bulge. - *Exp. Dermatol.,* **18,** 2009, 734-737.
8. **Lan, M. Y., M. C. Lan, C. Y. Ho, W. Y. Li, C. Z. Lin.** Pilomatricoma of the head and neck: a retrospective review of 179 cases. - *Arch. Otolaryngol. Head Neck Surg.,***129,** 2003, 1327-1330.
9. **Lopansri, S., M. Mihm.** Pilomatrix carcinoma or calcifying epitheliocarcinoma of Malherbe: a case report and review of literature. - *Cancer,* **45,** 1980, 2368- 2373.
10. **Malherbe, A., J.** Chenantais. Note on epithelioma calcified sebaceous glands. - *Progres Medical,* **8,** 1880, 826-828.
11. **Moehlenbeck, F.** Pilomatrixoma (calcifying epithelioma): a statistical study. - *Arch. Dermatol.,* **108,** 1973, 532-534.
12 **Morales-Cardona, C., A. Luque-Acevedo, L. Bermudez-Bula.** Onychomatricoma: an often misdiagnosed tumor of the nails. - *Cutis,* **96,** 2015, 121-124.
13. **Perrin, C., L. Langbein, J. Schweizer, G. E. Cannata, T. Balaguer, B. Chignon-Sicart, J. M. Garzon, M. Benchetrit, J. F. Michiels.** Onychomatricoma in the light of the microanatomy of the normal nail unit. - *Am. J. Dermatopathol.,* **33,** 2011, 131-139.
14. **Roche, N., S. Monstrey, G. Matton.** Pilomatricoma in children: common but often misdiagnosed. – *Acta Chir. Beld.,* **110,** 2010, 250-254.
15. **Schwartz, R. A.** Skin Cancer: Recognition and Management. 2nd ed. Malden, MA: Blackwell Publishing 2008.
16. **Som, P., J. Shugar, A. Silvers.** CT of pilomatrixoma in the cheek. - *Am. J. Neuroradiol.,* **19,** 1998, 1219-1220.
17. **Thomas, R., W., J. A. Perkins, J. L. Ruegemer, J. A. Munaretto.** Surgical excision of pilomatrixoma of the head and neck: a retrospective review of 26 cases. - *Ear Nose Thorat. J.,* **514,** 1999, 544-546.

Institute of Experimental Morphology, Pathology and Anthropology with Museum
Bulgarian Anatomical Society

Acta morphologica et anthropologica, 25 (1-2)
Sofia ● 2018

Hormonal Production of the Developing Gastrointestinal Tract of Rat

Nadya Penkova[1], Petar Hrischev[2], Pepa Atanassova[1]*

[1] Department of Anatomy, Histology and Embryology, Medical University - Plovdiv, Bulgaria
[2] Department of Physiology, Medical University-Plovdiv, Bulgaria

* Corresponding author e-mail: nadja_penkova@abv.bg

The aim of our study was to investigate the production of ghrelin and serotonin in the developing gastrointestinal tract of a rat and its paracrine role in the gastrointestinal wall. The earliest occurrence of ghrelin-producing cells we founded in the endoblastic epithelium of rat embryos on 12th day gestation. In the following periods this number increased. GHSR-1 was expressed during the same period in endoblast and myoblast cells of the developing digestive tube of embryos and fetuses as well as in the covering epithelium and glands of the stomach and small intestine of newborn rats. Serotonin-producing cells we found as late as one-day old rats. At that time there was presence of 5-HTR3 in smooth muscle cells. In conclusion, ghrelin-producing cells are among the earliest differentiating cells in the digestive tube and the presence of GHS-R1 reveals the ability of ghrelin to carry out paracrine regulation of organogenesis and histogenesis of the gastrointestinal tract. After birth serotonin-producing cells are already differentiated and the gastrointestinal wall is ready to respond to serotonin and ghrelin signals through the GHSR-1 and 5-HTR3 in the smooth muscle and glandular cells.

Key words: ghrelin, GHS-R1, serotonin, 5-HTR3, gastrointestinal tract, embryo

Introduction

Local regulation of digestion in the gastrointestinal tract is performed by a large number of hormones produced by the enteroendocrine cells in its mucosa. In their totality they form the gastroenteropancreatic endocrine system which is part of the diffuse neuroendocrine system. It includes more than 19 types of cells secreting more than 30 types of hormones. Some of the earliest described cells are the serotonin-producing cells [24,18]. As a gastrointestinal hormone serotonin participates in the regulation of motility, secretion of the glands, sensitivity to pain [21,11,5].

Ghrelin is a recently discovered hormone. It is an oligopeptide of 28 amino acid residues isolated for the first time from rat stomach. It was first identified by Masayasu Kodzima et al. in 1999, they ascertained that serum levels of ghrelin in slim rats are higher than those of fat ones [17]. Ghrelin participates in the formation of severe feeling

of hunger through its connection with specific receptors in the nuclei of the diencephalon. It releases growth hormone secretion through receptors in the adenohypophysis. Maturation of the digestive tube is carried out through complex intercellular signaling between the consecutively differentiating tissues which form it. The differentiating endoderm releases a number of signaling cells which influence the underlying mesenchyme and smooth muscle cells are differentiated in it. The signal pathways of the endodermal - mesenchymal interactions are conservative glycoprotein families with a long evolutionary history. These are growth factors which carry out cascade transductions between embryonic cells. Numerous signal pathways of this interaction are familiar: BMP, Hedgehog (Hh), Sonic hedgehog (Shh), PDGF, TGF-β, Wnt, TCP, Notch etc. Bidirectional intercellular interactions of the endoderm and mesenchyme of the developing digestive tube are carried out through these molecular mechanisms [3,8,22].

Some of the earliest differentiating cells in the wall of the future gastrointestinal tract are endocrine cells. In birds they have been found on 9th day of incubation [15]. In rats they are found on 18th day gestation [12], and in man in 8th day gestation [19].

The occurrence of enteroendocrine cells with signs of hormonal production prior to the definitive differentiation of tissues presupposes participation of the gastrointestinal hormones in the histogenetic processes in the digestive tube.

The aim of our study was to investigate the production of ghrelin and serotonin in the developing gastrointestinal tract of a rat and its paracrine role in the gastrointestinal wall.

Materials and methods

The material of study is white Wistar rats. We studied rat embryos, fetuses and GIT fragments of one-day-old rats. It is obtained from 24 male white rats inseminated through contact with male specimen fixed in time. The material is distributed in four age groups: 1st group of 8th-11th -day-old rat embryos; 2nd- group of 12-15th -day-old rat embyos; 3rd group of 16th-20th gestation day old rat fetuses; 4th group of one-day old newborn rats. We performed an immunohistochemical study of ghrelin, ghrelin receptor GHSR-1; serotonin and serotonin receptor 5-HTR3. Immunohistochemical reactions were performed according to the ABC method through rabbit ABC Staining System (Santa Cruz Biotechnology, USA) with the respective primary antibody&goat polyclonal ghrelin antibody: sc-10368; goat polyclonal antibody GHSR-1: sc-10351; goat polyclonal antibody, SR-3A: sc-19150 - Santa Cruz Biotechnology USA and rabbit polyclonal antibody, MAB352 serotonin - Chemicon USA.We used a semi-quantitative evaluation method for the obtained results. The specificity of immunohistochemical reactions for each studied antigen is confirmed by negative controls. Observation and photo documentation of microscopic preparations are performed with digital photo microscopic camera of a light microscope “Olympus BX51”.

Results

In the developing gastroduodenal tract of rat embryos 12th-15th gestation day we established a positive immunohistochemical occurrence of ghrelin. Individual ghrelin-positive cells were localized among the endoderm of the digestive tube **(Fig. 1A).** Immunohistochemical reaction for ghrelin was positive in the stomach and small intestine of 16th-20th gestation day rat fetuses. Black granules were observed in a small number of stomach wall endoderm cells. **(Fig. 1B).** In one-day-old rats there was presence of positive expression of ghrelin in the stomach and small intestine. In the gastric cardia gherlin was expressed in single cells located in the base of cardiac glands **(Fig. 1C).**The reaction is positive also in the single cells from the small intestine epithelium **(Fig. 1D).**

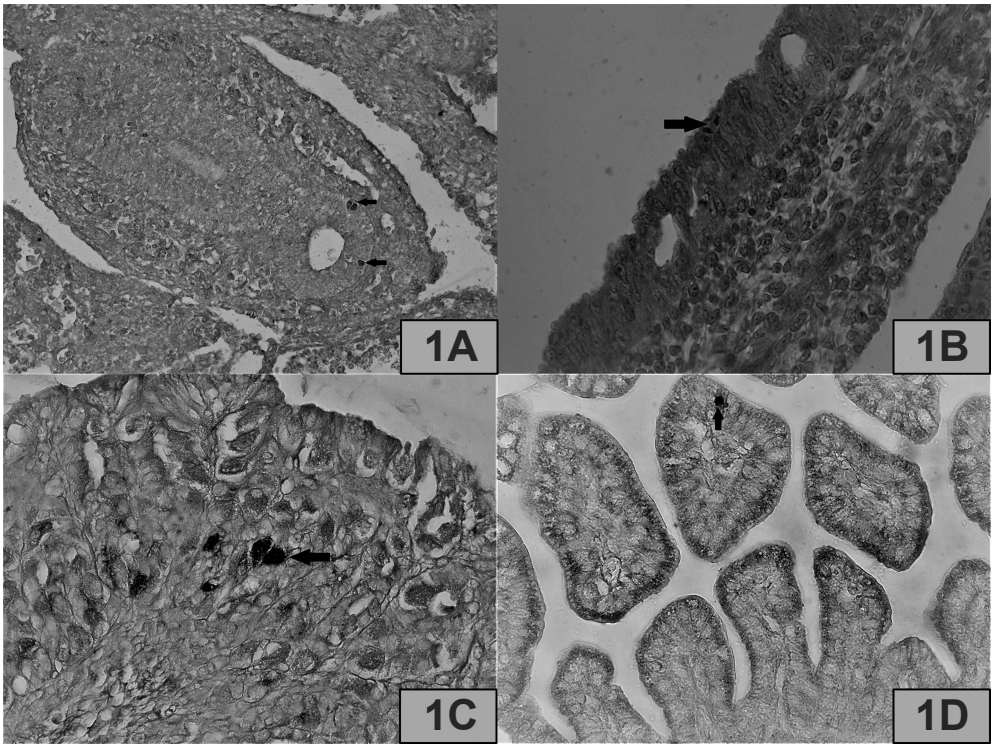

Fig 1. Ghrelin-producing cells in developing gastrointestinal tract of rat. IHC reaction for ghrelin. A. Digestive tube of rat embryos on 12th gestational day. Positive. x 100. B. Rat fetus stomach 16th gestation day. Single ghrelin positive cells in the multilayered endodermal epithelium. x 400. C. Stomach of a one-day-old rat - fundus. Positive ghrelin expression in a small number of cells at the base of the chief glands. x 400. D. Small intestine of a one-day-old rat - cross section. Single ghrelin positive cell in the covering epithelium of the villus. x 400.

For the first time the reaction for ghrelin and its receptor GHS-R1 was positive on 12th gestation day. Expression of GHS-R was found in individual endodermal cells from the covering epithelium as well as in myoblast cells from the surrounding mesenchyme **(Fig. 2A).** Immunohistochemical reaction for GHS-R1 was positive in the wall of the developing stomach of 16th-20th gestation day rat fetuses. There was presence of fine brown granulation in groups of endodermic cells. Expression of GHS-R1 was also found in a thin layer of smooth muscle cells in the periphery of the gastric wall **(Fig. 2B)**. Ghrelin receptor GHS-R1 was expressed in the gastric wall of one-day-old rats. The reaction was positive in individual cells of the covering epithelium and the glands **(Fig. 2C)** and in the the covering epithelium of the intestinal villus **(Fig. 2D).**

Immmunohistochemical reaction for serotonin was positive in the small intestine of one-day-old rats.The reaction is positive for a small number of cells. They were located singly between the resorptive cells in the covering epithelium of the intestinal villus. They were found along the villi and in their peak area. **(Fig. 3)**. Serotonin receptor 5HTR3 was expressed in the gastric wall of one-day-old rats. The reaction was visualized through brown granulation which fills the cytoplasm of a large number of smooth muscle cells from the muscle lining of the stomach **(Fig. 4).**

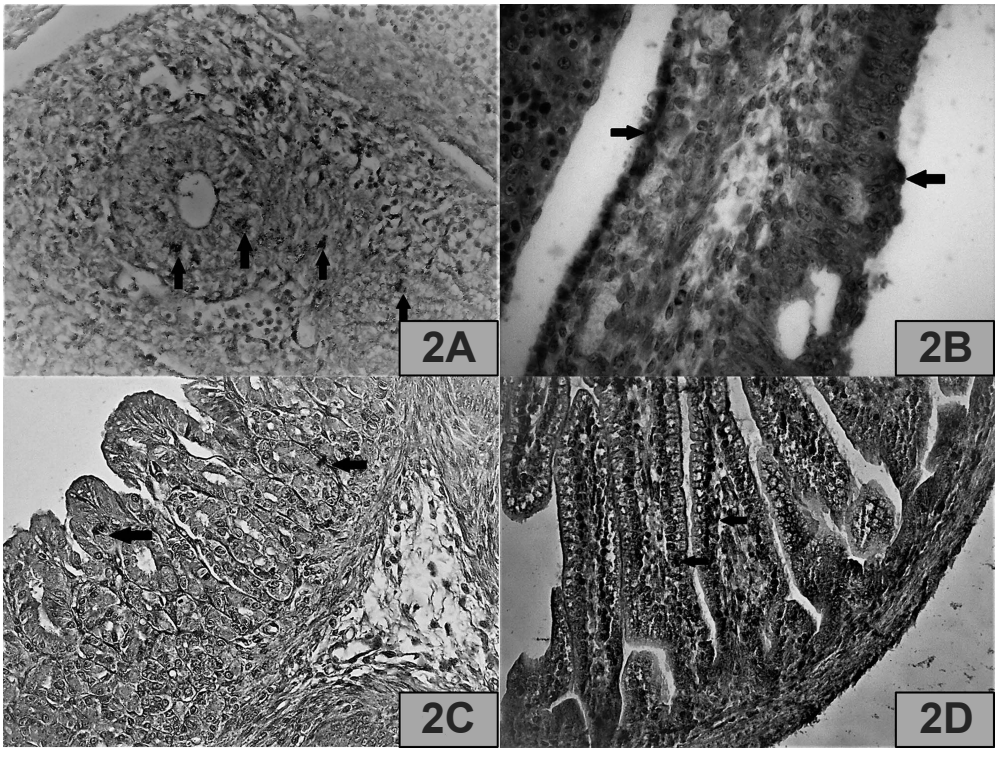

Fig. 2. Ghrelin receptor GHS-R1in developing gastrointestinal tract of rat.IHC reaction for GHS-R1. A. Digestive tube of rat embryos 12th gestation day. Positive GHS-R1 expression in endodermal and myoblast cells. x 200. B. Rat fetus stomach 16th gestation day. Positive GHS-R1 reaction in the multi-layered endodermal epithelium and peripheral smooth muscle layer. x 400. C. Stomach of a one-day-old rat. Positive GHS-R1 expression in single cells from the glands of the gastric mucosa. x 200. D. Small intestine villi of one-day-old rat - longitudinal section. Positive GHS-R1 expression in the epithelial cells. x 200.

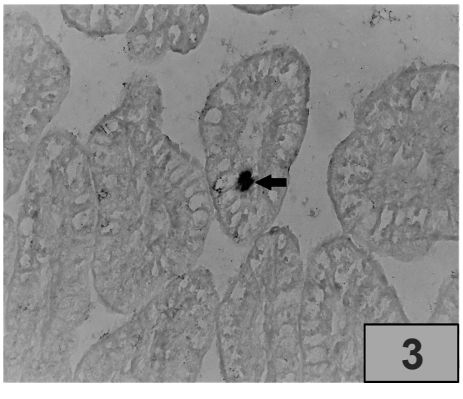

Fig. 3. Small intestine villi of one-day-old rat-cross section. Positive expression of serotonin in the basal part of epithelial cells. IHC. x 200.

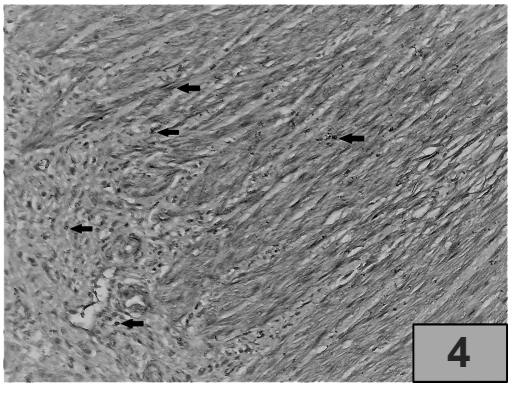

Fig. 4. Stomach of a one-day-old rat. Positive expression for serotonin receptor 5-HTR3 in smooth muscle cells. IHC. x 400.

Discussion

The earliest presence of differentiated ghrelin-producing cells we found in rat embryos on 12th gestation day. They are single cells dispersed among the endodermal epithelial cells of the esophageal tube. Our results show that in 16th gestation day rat fetuses and in one-day-old rats ghrelin-producing cells are already localized in the stomach as well as in the small intestine. The immunohistochemical expression of ghrelin receptor GHS-R1 is parallel with that of the hormone itself.The earliest occurrence of ghrelin-producing cells in rat is reported in fetal stomach on 18th gestation day [6,2]. However, some authors do not ascertain presence of positive ghrelin expression in gastric cells of rat fetuses although they found high plasma levels of ghrelin in the fetus [1,2,10]. Sakata et al., while studying ghrelin production in rat from 1st to 8th week of the postnatal period and in adult rats, ascertain that initially ghrelin-producing cells occur in the base of the chief glands of the stomach. Around the 3rd week their number increases and they spread to the corpus and neck of the glands [16].The presence of ghrelin receptor GHS-R in the prenatal period of rat is found as early as 20th day gestation namely in the pancreas. Wierup et al., study the expression of ghrelin and ghrelin receptor GHS-R in islets of Langerhans of fetal and neonatal pancreas of rat. They prove the presence of ghrelin receptor in the islet cells of 20th gestation day rat fetuses. It is through these receptors that ghrelin exerts a paracrine effect directly on β-cells [23]. Kitazawa et al. report of presence of GHS-R1 in gastrointestinal tract of rat and guinea pig [7]. There is immunohistochemical evidence for an endocrine/paracrine role for ghrelin in the reproductive tissues [9].

In our study we find serotonin expression in one-day-old rats. The small number of serotonin-producing cells is probably due to the unfinished processed of maturation in the small intestine wall. The localization of these cells, found by us, in the peak areas of the small intestine villi and not in their typical location- crypts of Lieberkuhn may be explained with the intensive processes of proliferation of stem cells in the developing crypts and epithelial cell migration along the radiant crypt-villus axis of the small intestine wall. The migration processes are performed also in the mature small intestine. At the bottom of the intestine glands a small group of stem cells, which provide several cellular phenotypes- resorptive, cup-like, endocrine. These cells constantly migrate to the adjacent villi [13, 14].Presence of serotonin receptor 5-HTR3 we found in the gastric wall of one-day-old rats. It is localized in a large number of smooth muscle cells both in the transverse and longitudinal layers of the muscle sheath of the stomach. Glatzle et al. ascertain 5-HTR3- immunoreactivity both in the gastric wall and in the duodenal wall but in adult rats [4]. The effects of serotonin on motility are achieved by 5-HT3R, localized on cholinergic neurons which stimulate smooth muscle cells [20].

Conclusion

Ghrelin-producing cells are among the earliest differentiating cells in the digestive tube and the presence of ghrelin receptor GHS-R1 reveals the ability of ghrelin to perform paracrine regulation in the earliest stages of organogenesis and histogenesis of the gastrointestinal tract. Serotonin regulates the motility, secretion and sensory function of the gastrointestinal tract. Immediately after birth serotonin-producing cells have already been differentiated and the wall of the gastrointestinal wall is ready to respond to serotonin and ghrelin signals through the presence of receptors for serotonin and ghrelin in smooth muscle and glandular cells.

Reference

1. **Bancs, W. A., M. Tschop, S. M. Robinso, M. L. Heiman.** Extent and direction of ghrelin transport across the blood-brain barrier is determined by its unique primary structure. - *J Pharmacol. Exp. Ther.,* **302,** 2002, 822-827.
2. **Chanoine, J-P., K. de Waele, P. Walia.** Ghrelin and the growth hormone secretagogue receptor in growth and development. - *Int. J. Obes. (Lond).,* **33,** 2009, S48-52.
3. **Faure, S., P. de Santa Barbara, D. J. Roberts, M. Whitman.** Endogenous patterns of BMP signaling during early chick development. - *Dev. Biol.,* **24,** 2002, 44–65.
4. **Glatzle, J., C. Sternini, C. Robin, T. Zittel, H. Wong, J. Reeve, H. Raybould.** Expression of 5-HT3 receptors in the rat gastrointestinal tract. - *Gastroenterol.,* **123,** 2002, 217-226.
5. **Hansen, M. B., A. B. Witte.** The role of serotonin in intestinal luminal sensing and secretion. - *Acta Physiol. (Oxf).,* **193,** 2008, 311-323.
6. **Hayashida, T., K. Nakahara, M. Mondal, Y. Date, M. Nakazato, M. Kojima, K. Kangawa, N. Murakami.** Ghrelin in neonatal rats: distribution in stomach and its possible role. - *J. Endocrinol.,* **173,** 2002, 239–245.
7. **Kitazawa, T., T. Nakamura, A. Saeki, H. Teraoka, T. Hiraga, H. Kaiya.** Molecular identification of ghrelin receptor (GHS-R1a) and its functional role in the gastrointestinal tract of the guinea-pig. - *Peptides,* **32,** 2011, 1876-1886.
8. **Lickert, H., A. Kispert, S. Kutsch, R. Kemler.** Expression patterns of Wnt genes in mouse gut development. - *Mech. Dev.,* **105,** 2001, 181–184.
9. **Miller, D. W., J. L. Harrison, Y. A. Brown, U. Doyle, A. Lindsay, C. L. Adam, R. G. Lea.** Immunohistochemical evidence for an endocrine/paracrine role for ghrelin in the reproductive tissues of sheep. - *Reprod. Biol. Endocrinol.,* **31;** 2005, 60.
10. **Nakahara, K., M. Nakagawa, Y. Baba, M. Sato, K. Toshinai, Y. Date, M. Nakazato, M. Kojima, M. Miyazato, H. Kaiya, H. Hosoda, K. Kangawa, N. Murakami.** Maternal ghrelin plays an important role in rat fetal development during pregnancy. - *Endocrinol.,* **147,** 2006, 1333-1342.
11. **Niesler, B., B. Frank, J. Kapeller, G. A. Rappold.** Cloning, physical mapping and expression analysis of the human 5-HT3 serotonin receptor-like genes HTR3C, HTR3D and HTR3E. - *Gene,* **310,** 2003, 101–111.
12. **Ono, E., Y. Doi, H. Furucava, K. Hirata, S. Fujimoto.** The differentiation of entero - endocrine cells of pre- and postnatal rats: light, and electron microscopy and immunocytochemestry. - *Acta Anat. Basel.,* **149,** 1994, 81–88.
13. **Pacha, J.** Development of intestinal transport function in mammals. - *Physiol. Rev.,* **80,** 2000, 1633-1667.
14. **Quinlan, J., W. Yu, M. Hornsey, D. Tosh, J. Slack.** In vitro culture of embryonic mouse intestinal differentiation and introduction of receptor genes. - *BMC Development Biol.,* **6,** 2006, 24.
15. **Rawdon, B. B., A. Andrew.** Gut endocrine cells in birds: an overview, with particular reference to the chemistry of gut peptides and the distribution, ontogeny, embryonic origin and differentiation of the endocrine cells. - *Prog. Histochem. Cytohem.,* **32,** 1999, 3–82.
16. **Sakata, I., T. Tanaka, M. Matsubara, M. Yamazaki, S. Tani, Y. Hayashi, K. Kangawa, T. Sakai.** Postnatal changes in ghrelin mRNA expression and in ghrelin-producing cells in the rat stomach.- *J. Endocrinol.,* **174,** 2002, 463–471.
17. **Salzet, M., R. Day.** Endocrine markers of cellular immunity: defining the endocrine phenotype. - *J. Soc. Biol.,* **197,** 2003, 97–101.
18. **Simonsson, M., S. Eriksson, R. Hakanson, T. Lind, H. Lonroth, L. Lundell, D. O'Connor, F. Sundler.** Endocrine cells in the oxynic mucosa. - *Scdn. J. Gastroenterol.,* **23,** 1988, 1089-1099.
19. **Stein, B. A., A. M. Buchan, J. Morris, J. M. Polak.** The ontogeny of regulatory peptide-containing cells in the human fetal stomach: an immunocytochemical study. - *J. Histochem. Cytochem.,* **31,** 1983, 1117-1125.
20. **Takahara, E., M. Yamamoto, H. Ito, F. Shimamoto, K. Sumii.** The effects of gastrin on the ultrastructure of ratstomach endocrine cells. - *Exp. Molec. Path.,* **35,** 1981; 211-218.
21. **Voutilainen, M., M. Juhova, R. Pijkanen, M. Farkkila, P. Sipponen.** Immunohistochemical study of neuroendocrine cells at the gastric cardia mucosa. - *J. Clin. Pathol.,* **55,** 2002, 767–769.
22. **Wodarz, A., R. Nusse.** Mechanisms of Wnt signaling in development. - *Ann. Rev. Cell Dev. Biol.,* **14,** 1998, 59–88.
23. **Wierup, N., S. Yang, R. J. McEvilly, H. Mulder, F. Sundler.** Ghrelin is expressed in a novel endocrine cell type in developing rat islets and inhibits insulin secretion from INS-1 (832/13) cells. - *J. Histochem. Cytochem.,* **52,** 2004, 301-310.
24. **Zavidcic, M., M. Brozman, J. Jaubovsky.** Influence of fasting and stimulation on the rat gastric endocrine cells. - *Histochemestry,* **49,** 1976, 315-325.

Institute of Experimental Morphology, Pathology and Anthropology with Museum
Bulgarian Anatomical Society

Acta morphologica et anthropologica, 25 (1-2)
Sofia ● 2018

The Aging Kidney - a Quantitative Study on Superficial and Juxtamedullary Nephrons in Wistar Rats

Stancho Stanchev, Alexandar Iliev, Lina Malinova, Boycho Landzhov*

Department of Anatomy, Histology and Embryology, Medical University of Sofia, Bulgaria

* Corresponding author e-mail: stanchev_1989@abv.bg

Renal senescence is characterized by numerous morphological alterations, which are associated with reduction in the renal functional capacity. Glomerulosclerosis is a nonspecific feature observed in the normal process of aging, as well as in pathological conditions such as hypertension and diabetes. In literature, two types of sclerotic glomeruli have been described, based on their light microscopic appearance. However, the qualitative evaluation of the glomerular changes is sometimes not sufficient for distinguishing the etiology of the kidney damage. The present study represents a detailed morphometric study on the postnatal changes in the areas of the renal corpuscles and glomerular capillary tufts of the superficial and juxtamedullary nephrons in Wistar rats.

Key words: glomerulosclerosis, renal corpuscles, morphometry, Wistar rat

Introduction

Aging is a biologically inevitable process, which is characterized by numerous alterations in many organs and systems, including the kidney. The features of renal senescence comprise both macroscopic and histological changes. During the postnatal development, the kidney weight progressively increases and reaches its maximum at four decades of life, followed by gradual reduction [5, 19]. There are convincing data, which represent a positive correlation between aging and the formation of parenchymal calcifications and simple renal cysts [8]. Furthermore, the histological examination of the aging kidney reveals morphological changes in both cortex and medulla leading to declining renal function – an increased number of sclerotic glomeruli, periglomerular and intraglomerular fibrosis, myointimal thickening of the blood vessels and hyaline arteriosclerosis. The tubulointerstitial changes include significant expansion of extracellular collagen fibers, as well as tubular atrophy along the proximal and distal tubular segments – flattening of the covering epithelium, resulting in dilation of the luminal diameter and formation of diverticula [12].

On light microscopy level, two types of glomerulosclerosis can be described - shrinkage of glomerular capillary tuft and increased space between the parietal and visceral layers of the Bowman's capsule or mesangial proliferation accompanied with glomerular enlargement [6]. However, the pathogenesis of age-related renal alterations

is still misunderstood and factors such as gender, race and genetic background have been discussed [1]. Indeed, all described features of the morphological changes in the senescent kidney are not specific and can be observed under pathological conditions such as hypertensive nephrosclerosis and diabetic nephropathy [2, 4].

The aim of the present study was to analyze and compare the areas of the renal corpuscles and glomerular capillary tufts of the superficial and juxtamedullary nephrons traced among three age groups (4-month-old, 6-month-old and 12-month-old) male Wistar rats.

Materials and Methods

In the present study, we used histological material from the kidneys of male Wistar rats. The total number of Wistar rats was 9, distributed in three age groups, each containing three animals: four months old; six months old and twelve months old. All experiments were conducted with the approval of the University Committee on Animal Resources (№ 4866). All animals received humane care in compliance with the "Principles of laboratory animal care" formulated by the National Society for Medical Research and the "Guide for the care and use of laboratory animals" prepared by the National Institute of Health (NIH publication No. 86-23, revised 1996). The rats were anaesthetised intraperitoneally with Thiopental 40 mg/kg body weight. The chest cavity was opened and transcardial perfusion was made with 4% paraformaldehyde in 0.1 M phosphate buffer, pH 7.2. Kidneys were quickly removed and fixed in 10% neutral-buffered formalin. After routine embedding, serial coronal 5 μm thick sections were cut and stained routinely with haematoxylin and eosin. Haematoxylin and eosin staining was conducted in the following way: after removal of the paraffin with xylol, we washed the slides with water and stained them with haematoxylin for 5 minutes. They were then stained with an eosin solution for 10 minutes, washed again with water and embedded in entellan.

The morphometric analysis was performed on five slides from the kidney of each animal. Quantitative data were obtained with a computerised system for image analysis NIS Elements Advanced Research (Ver. 2.30). The areas of interest in each slide were first found on low magnifications (x100, x200), taking into account the respective age group. Results were obtained through assessment of randomly selected zones of the renal cortex with no significant ruptures resulting from the processing technique of the histological material that could compromise the proper data analysis. The standardization of the zone where the areas of renal corpuscles and glomeruli were measured was performed in line with the following criteria in order to certify the authenticity of the results: 1. only renal corpuscles with clearly demarcated vascular and tubular poles were included in this study; 2. the selected renal corpuscles of the superficial nephrons were situated in the periphery of the cortex; 3. the analyzed renal corpuscles of the juxtamedullary nephrons were located adjacent to the medulla. The following morphometric parameters of the superficial and juxtamedullary nephrons during the postnatal development of Wistar rats were analyzed: area of the renal corpuscles of the superficial nephrons (μm^2), glomerular area of the superficial nephrons (μm^2), area of the renal corpuscles of the juxtamedullary nephrons (μm^2), glomerular area of the juxtamedullary nephrons (μm^2). The obtained quantitative data were demonstrated with Bar Chart/Bar Plot diagrams and were statistically evaluated through a Student-T-test. Statistically significant differences were read in the case of $p<0.05$. Microsoft Office Excel 2010 was used to process the data and to demonstrate the obtained results in an adequate way.

Results

The comparative analysis of the parameter area of the renal corpuscles among the young group of 4-month-old Wistar rats showed similar values in the outer and inner cortex with quite higher prevalence in the superficial nephrons. As aging advanced, in 6-month-old rats, we noted a slight increase in the parameter, which was more pronounced in juxtamedullary nephrons. That trend was also observed in the group of senescent 12-month-old Wistar rats, where the areas of the renal corpuscles of the nephrons in the outer and inner cortex reached the highest value. We should note that the analyzed parameter among the juxtamedullary nephrons in 6-month-old rats was comparable with the results obtained from the superficial nephrons in 12-month-old rats **(Fig. 1, Table 1)**.

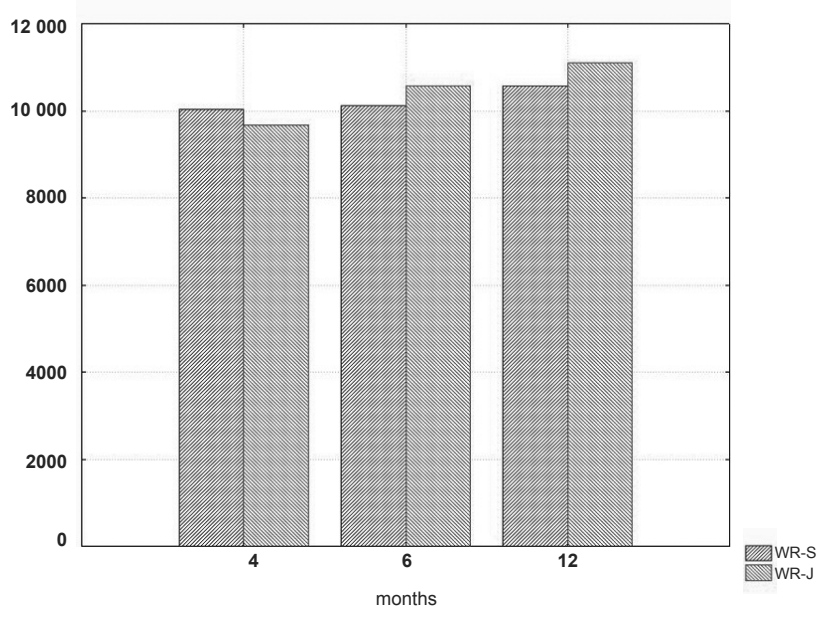

Fig. 1. Graphical representation of the comparative analysis of the morphometric parameter area of renal corpuscles of superficial (WR-S) and juxtamedullary nephrons (WR-J) in Wistar rats. Y-axis: area of renal corpuscles (μm^2)

Table 1. Numerical representation of the comparative analysis of the morphometric parameter area of renal corpuscles in Wistar rats (SD - standard deviation)

WR	Superficial nephrons		Juxtamedullary nephrons		TTEST
	Area of renal corpuscles		Area of renal corpuscles		
Age	Mean value	SD	Mean value	SD	
4 months	10035.7	660.5	9664.4	487.9	p< 0.0001
6 months	10120.3	375.3	10561.1	377.1	p< 0.000001
12 months	10560.8	617.4	11092.8	563.7	p< 0.000001

The representation of the comparative analysis of the area of renal corpuscles of superficial and juxtamedullary nephrons by a Box Plot diagram indicated that in 4-month-old rats the average value of the parameter obtained from the outer cortex was higher compared to the inner cortex. In the groups of 6- and 12-month-old rats, the increase of the area of renal corpuscles was more pronounced in juxtamedullary nephrons **(Fig. 2).**

In the group of 4-month-old Wistar rats, the comparative analysis of the area of the glomerular tufts in the outer and inner cortex showed comparable values, with quite higher prevalence in the juxtamedullary nephrons. The results obtained from 6-month-old rats revealed a progressive increase in the analyzed parameter and the trend for higher value of the area of glomerular tufts was preserved. In the group of 12-month-old animals there was a significant increase in the parameter in juxtamedullary nephrons, where it reached its highest value. In contrast, the increased area of the glomerular tufts of superficial nephrons was less pronounced and was comparable with the results obtained from juxtamedullary nephrons in the 6-month-old group **(Fig. 3, Table 2)**.

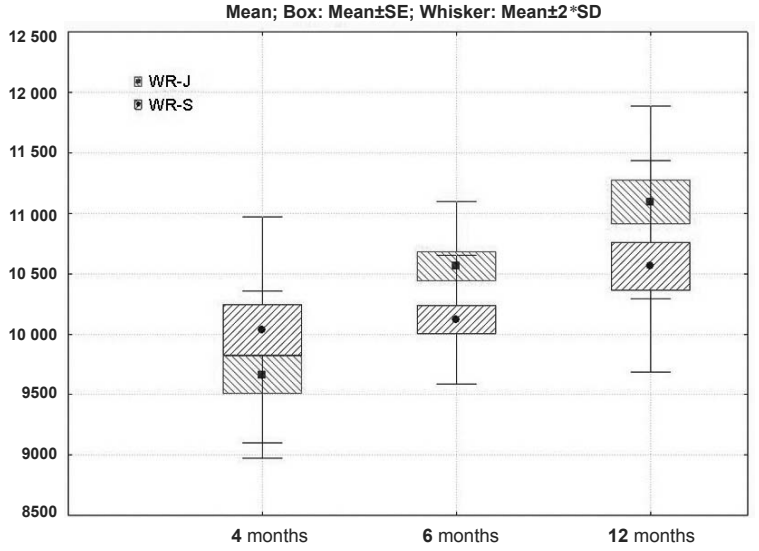

Fig. 2. Box Plot graphical representation of the comparative analysis of the morphometric parameter area of renal corpuscles of superficial (WR-S) and juxtamedullary nephrons (WR-J) in Wistar rats

Table 2. Numerical representation of the comparative analysis of the morphometric parameter glomerular area in Wistar rats (SD - standard deviation)

WR	Superficial nephrons		Juxtamedullary nephrons		TTEST
	Glomerular area		Glomerular area		
Age	Mean value	SD	Mean value	SD	
4 months	6572.4	386.7	6866.1	334.4	p< 0.00001
6 months	7287.1	261.2	7510.8	445.8	p< 0.0001
12 months	7738.1	864.0	9767.5	225.5	p< 0.000001

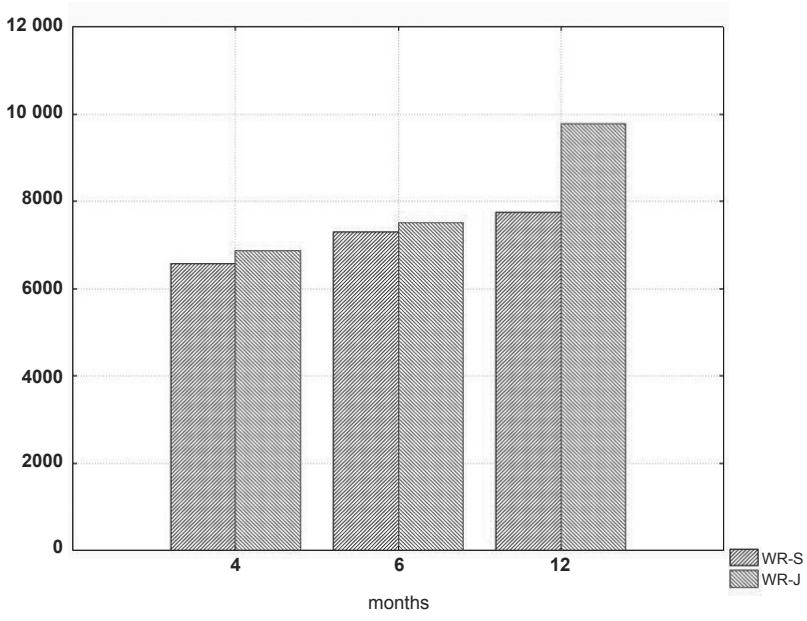

Fig. 3. Graphical representation of the comparative analysis of the morphometric parameter glomerular area of superficial (WR-S) and juxtamedullary nephrons (WR-J) in Wistar rats. Y-axis: glomerular area (μm^2)

Discussion

The current study represents a detailed comparative morphometric analysis of the changes in the areas of the renal corpuscles and glomerular capillary tufts of the superficial and juxtamedullary nephrons during the postnatal development in Wistar rats. The change in the areas of renal corpuscles was not so pronounced, but the trend for higher value of the analysed parameter in juxtamedullary nephrons was preserved in 6- and 12-month-old rats. Comparing 4-month-old with 6-month-old animals, we noted a gradual increase in the glomerular tuft areas of the nephrons in the outer and inner cortex, as well as a well-expressed increase in the parameter in juxtamedullary nephrons of 12-month-old rats, where it reached its highest value.

In the process of aging, the remaining functional capacity of the kidneys depends on the number of intact glomeruli. Numerous studies have shown a positive correlation between age and development of glomerulosclerosis [13]. Furthermore, a formula for estimation of the percentage of the senescent sclerosed glomeruli was suggested by Smith et al. [15]. On the other hand, the evaluation of glomerulosclerosis is based not only on qualitative criteria. In fact, the development of glomerulosclerosis includes initial enlargement of the glomerular capillary tuft described by the term glomerular hypertrophy, which is followed by collapsing of the glomerulus in the late stages [17]. Therefore, the glomerular size changes in the different stages of glomerulosclerosis and the morphometric analysis of the renal corpuscles can contribute to the complex evaluation of renal senescence. In the present study, both superficial and juxtamedullary nephrons were characterized by progressive increase in the areas of glomerular capillary tufts, which was most pronounced in the juxtamedullary nephrons

in the group of 12-month-old rats. Our results indicate that glomerular hypertrophy affected mostly nephrons in the inner rather than the outer cortex in the process of aging. There is evidence that the aged rat kidney is characterized by hypertrophic podocytes, which undergo apoptosis [18]. In contrast, some studies have shown a prevalence of sclerotic glomeruli in the outer cortical zone, as well as inversely proportional correlation between age and glomerular size [10, 11]. Moreover, Kasiske demonstrated a positive correlation between globally sclerotic glomeruli, intrarenal vascular alterations and age [7]. The reason for the opposite results obtained can be explained by the use of different experimental models. Under pathological conditions such as hypertension, glomerulosclerosis is more severe in the inner cortex [3]. This was confirmed by our previous comparative morphometric study on spontaneously hypertensive rats, where juxtamedullary nephrons were characterized by significant decrease in glomerular tuft area – a feature of the late stages of glomerulosclerosis [16]. The role of hemodynamic changes leading to glomerular hyperperfusion has also been discussed in the genesis of age-related glomerulosclerosis [14]. Some authors have commented on the presence of atubular glomeruli, which are non-functional and on the possibility for sclerosed glomeruli to disappear with age [9, 17]. Therefore, these circumstances should be taken into account in the evaluation of the severity of renal morphological alterations.

Conclusion

The current study is a detailed morphometric study on the postnatal changes in the areas of renal corpuscles and glomerular capillary tufts of the superficial and juxtamedullary nephrons in Wistar rats. Such quantitative information can be used in the evaluation of the severity of kidney damage under pathological conditions.

R e f e r e n c e s:

1. **Bolignano, D., F. Mattace-Raso, E. J. Sijbrands, C. Zoccali.** The aging kidney revisited: a systematic review. - *Ageing Res. Rev.,* **14,** 2014, 65-80.
2. **Caetano, E. R., R. Zatz, L. B. Saldanha, J. N. Praxedes.** Hypertensive nephrosclerosis as a relevant cause of chronic renal failure. - *Hypertension,* **38**(2), 2001, 171-176.
3. **Feld, L. G., J. B. Van Liew, R. G. Galaske, J. W. Boylan.** Selectivity of renal injury and proteinuria in the spontaneously hypertensive rat. - *Kidney Int.,* **12**(5), 1977, 332-343.
4. **Fioretto, P., M. Mauer.** Histopathology of diabetic nephropathy. - *Semin. Nephrol.,* **27**(2), 2007, 195-207.
5. **Gourtsoyiannis, N., P. Prassopoulos, D. Cavouras, N. Pantelidis.** The thickness of the renal parenchyma decreases with age: a CT study of 360 patients. - *Am. J. Roentgenol.,* **155**(3), 1990, 541-544.
6. **Hughson, M. D., V. G. Puelles, W.E. Hoy, R. N. Douglas-Denton, S. A. Mott, J. F. Bertram.** Hypertension, glomerular hypertrophy and nephrosclerosis: the effect of race. - *Nephrol. Dial. Transplant.,* **29**(7), 2014, 1399-1409.
7. **Kasiske, B. L.** Relationship between vascular disease and age-associated changes in the human kidney. - *Kidney Int.,* **31**(5), 1987, 1153-1159.
8. **Lorenz, E. C., J. C. Lieske, T. J. Vrtiska, A. E. Krambeck, X. Li, E. J. Bergstralh, L. J. Melton 3rd, A. D. Rule.** Clinical characteristics of potential kidney donors with asymptomatic kidney stones. - *Nephrol. Dial. Transplant.,* **26**(8) 2011, 2695-2700.
9. **Marcussen, N.** Tubulointerstitial damage leads to atubular glomeruli: significance and possible role in progression. - *Nephrol. Dial. Transplant.,* **15**(6), 2000, 74-75.
10. **Newbold, K. M., A. Sandison, A. J. Howie.** Comparison of size of juxtamedullary and outer cortical glomeruli in normal adult kidney. - *Virchows Arch. Pathol. Anat. Histopathol.,* **420**(2), 1992, 127-129.

11. **Nyengaard, J. R., T. F. Bendtsen.** Glomerular number and size in relation to age, kidney weight, and body surface in normal man. - *Anat. Rec.,* **232**(2), 1992, 194-201.
12. **Pannarale, G., R. Carbone, G. Del Mastro, C. Gallo, V. Gattullo, L. Natalicchio, A. Navarra, A. Tedesco.** The aging kidney: structural changes. - *J. Nephrol.,* **23**(15), 2010, 37-40.
13. **Rule, A. D., H. Amer, L. D. Cornell, S. J. Taler, F. G. Cosio, W. K. Kremers, S. C. Textor, M. D. Stegall.** The association between age and nephrosclerosis on renal biopsy among healthy adults. - *Ann. Intern. Med.,* **152**(9), 2010, 561-567.
14. **Silvia, F. G.** The aging kidney: a review - part I. - *Int. Urol. Nephrol.,* **37,** 2005, 419-443.
15. **Smith, S. M., W. E. Hoy, L. Cobb.** Low incidence of glomerulosclerosis in normal kidneys. - *Arch. Pathol. Lab. Med.,* **113**(11), 1989, 1253-1255.
16. **Stanchev, S., A. Iliev, G. Kotov, L. Malinova, B. Landzhov.** A comparative morphometric study of the superficial and juxtamedullary nephrons during the postnatal development in spontaneously hypertensive rats. - *Arch. Anat. Physiol.,* **3**(1), 2018, 001-004.
17. **Stojanović, V. R., I. D. Jovanović, S. Z. Ugrenović, L. P. Vasović, V. S. Živković, M. V. Jocić, B. K. Kundalić, M. N. Pavlović.** Morphometric analysis of nonsclerosed Glomeruli size and connective tissue content during the aging process. - *Sci. World J.,* **2012,** 2012, 845046.
18. **Wharram, B. L., M. Goyal, J. E. Wiggins, S. K. Sanden, S. Hussain, W. E. Filipiak, T. L. Saunders, R. C. Dysko, K. Kohno, L. B. Holzman, R. C. Wiggins.** Podocyte depletion causes glomerulosclerosis: diphtheria toxin-induced podocyte depletion in rats expressing human diphtheria toxin receptor transgene. - *J. Am. Soc. Nephrol.,* **16**(10), 2005, 2941-2952.
19. **Zhou, X. J., D. Rakheja, X. Yu, R. Saxena, N. D. Vaziri, F. G. Silva.** The aging kidney. - *Kidney Int.,* **74,** 2008, 710-720.

Institute of Experimental Morphology, Pathology and Anthropology with Museum
Bulgarian Anatomical Society

Acta morphologica et anthropologica, 25 (1-2)
Sofia ● 2018

Effects of Agomelatine and Lacosamide on Kainate-Induced Status Epilepticus, Epileptogenesis and EEG Seizure Activity in Wistar Rat

Tzveta Stoyanova[1], Natasha Ivanova[1], Jana Tchekalarova[1], Lidia Kortenska[1], Dimitrinka Atanasova[1, 2], Nikolai Lazarov[1, 3]*

[1] *Institute of Neurobiology, Bulgarian Academy of Sciences, Sofia, Bulgaria*
[2] *Department of Anatomy, Faculty of Medicine, Trakia University, Stara Zagora, Bulgaria*
[3] *Department of Anatomy and Histology, Medical University of Sofia, Sofia, Bulgaria*

* Corresponding author e-mail: janetchekalarova@gmail.com

The antidepressant Agomelatine (Ago), unlike to classical antidepressants, possesses an unique receptor profile by activation of MT1 and MT2 receptors and antagonism on 5-HT2C receptor. The aim of the present study was to explore the effect of Ago on kainate (KA)-induced status epilepticus (SE) and chronic epilepsy in Wistar rats. Repeated i.p. injection with Ago (40 mg/kg) at the 1st, 6th, 24th, 32th, 48th h after KA neither alleviated the number of paroxysmal events and their duration (electrographic seizures) during SE nor EEG and behavioral spontaneous seizures during the chronic phase of epilepsy. The positive control with lacozamide (LCM) (50 mg/kg) significantly alleviated the SE-induced epileptiform activity. The present results revealed that Ago is unable to prevent SE and is ineffective against EEG registered spontaneous seizures.

Key words: status epilepticus; EEG; agomelatine; lacosamide; BDNF/TrkB

Introduction

The newly developed antidepressant Agomelatine (Ago) is characterized with a unique receptor profile by activation of MT1 and MT2 receptors and antagonism on 5-HT2C receptor that give it an advantage compared to serotonin reuptake inhibitors (SSRIs) to possess chronobiotic activity both in rodents and human [7]. Several previous studies reported that Ago has anticonvulsant effects after acute injection in seizure tests on non-epileptic naïve rodents [1, 4]. However, this antidepressant was able to suppress seizures after single injection but not after chronic treatment due to receptor internalization [4]. Our research team for the first time reported that chronic treatment with Ago after kainate (KA) induced status epilepticus exerts a strong neuroprotection in limbic structures but was ineffective against epileptogenesis and concomitant spontaneous seizures [10]. Moreover, Ago alleviated the comorbid depression through suppression of inflammatory signaling (IL-1β and gliosis) during the chronic epileptic phase in rats.

Lacosamide (LCM), approved by EMEA and FDA, belongs to a new class of antiepileptic drugs (AED) and is used in patients with partial seizures as an adjuvant [2]. This drug possesses different mechanism of action, with sodium channels' modulation, compared to other anticonvulsants such as Lamotrigine, Carbazepine, Phenytoine. The anticonvulsant effects of LCM are confirmed in experimental models of epilepsy [2, 3, 8]. LCM suppressed sound-induced seizures, generalized tonic-clonic seizures, tonic-extension seizures induced by maximal electroshock seizure (MES) test as well as 6-Hz psychomotor seizures in mice and rats [2]. Moreover, LCM is effective in hippocampal kindling model of epilepsy [3] and against SE [8].

In the present study, we aimed further to explore the effect of Ago against SE and spontaneous epileptiform activity recorded during the acute and chronic epileptic phase in KA model of temporal lobe epilepsy. The same protocol of treatment was applied for LCM considered as a positive control.

Materials and Methods

The procedures used in this study are in agreement with the European Communities Council Directives of 24 November 1986 (86/609/EEC). The experimental design was approved by BFSA (contract # D-65/02.05.2017).

Animals

Male Wistar rats (breeding facility of the Institute of Neurobiology, Bulgarian Academy of Sciences, 200-250 g at the beginning of experimental procedure) were housed in groups (4-5 per cage) for habituation a week prior to experiments. After SE, they were housed individually in transparent labeled cages. Standard conditions (20±3°C, 40-50% humidity; 12/12-h light/dark cycle with lights on at 06:00 a.m.) were freely available.

Electrode implantation

Rats were anesthetized with a mix of ketamine (80 mg/kg) and xylazine (20 mg/kg), i.p. and a local anesthesia with procaine 0.5%. Implantation of electrodes was performed as described previously [9]. Electrodes were placed, according to the atlas of Paxinos and Watson, above the frontal (A = +1, L = ±2) and parietal cortex (A = - 4.2, L = ± 3.0), and the reference and the ground electrodes, above the nasal bone with a stainless steel screw attached at the end. The electrode assembly was connected to a six-plug female connector (Plastic One MS363/E363/0) which was fixed to the skull with dental acrylic. The rats were injected intramuscularly (i.m.) with antibiotic to prevent infection and allowed to recover for at least of 7-10 days.

Induction of status epilepticus (SE) and EEG/video recording and analysis

After at least of 30 min baseline EEG was obtained, SE was induced by i.p. injection of kainic acid (KA) (10 mg/kg, diluted in sterile saline, Abcam, UK). Seizure severity was evaluated by a modified Racine's scale as described previously [9]. Electrographic activity of SE and chronic epileptic phase was recorded for 12 h. Ictal events were calculated manually off-line through inspections of the files using Acknowledge software ACK100W (BIOPAC Inc., USA). Seizure activity during SE was assessed by counting the number, total duration and percent duration of paroxysmal events that lasted at least 5 s, had a frequency (≥8 Hz) and amplitude ≥two time baseline as described previously [5]. This data were analyzed separately i) before treatment (i.e. 0-1 h after beginning of SE) and ii) after the 1st treatment (2-6 h after SE).

For characterization of EEG activity during the chronic phase, the following indices were quantified: the number and total duration of "spike-trains" (<5 s and >20 s) and paroxysmal events (<20 s) as described previously [8].

A video monitoring system (infrared-sensitive colored cameras S-2016, AVTECH, Taiwan, no. AVC307R connected to a computer with software analyzing video-records) was used for continuous recording (24 hr/day for four months) to detect spontaneous behavioral seizures of class IV-V. Partial seizures of class I and II from video-recording were neglected from final analysis.

Experimental design and drug administration

The rats received i.p. injection of vehicle (veh), agomelatine (Ago) (40 mg/kg, dissolved in hydroxyethyl cellulose (HEC)1%, kindly gifted by Servier Company, France) or lacozamide (LCM) (50 mg/kg) at the 1st, 6th, 24th, 32th, 48th h after injection of KA. The drug doses were chosen on the doses used in previous reports in rats [9, 10, 11].

Statistical analysis

All dataare presented as mean±S.E.M. Statistical analyses were performed using Sigma Stat software. Nonparametric statistics were used in all experiments because the distribution of values was not normal due to small number of animals in groups. Data were analyzed using Kruskal-Wallis test followed by Mann-Whitney post hoc test. Statistical analysis was performed with SigmaStat® 11.0. A $p<0.05$ was accepted as statistically significant.

Results

Effect of agomelatine and lacosamide on the severity of status epilepticus

The electrographic data during SE are presented in Table 1. Following systemic administration of KA at a convulsant dose of 10 mg/kg, rats presented continuous scratching, mastication and staring occurring during the first 10 min, which were not associated with obvious changes in the cortical EEG. The electrographic onset of SE that occurred within the following 30-40 min was associated with behavior of class III and IV. There was no difference among the three groups in the number of paroxysmal events and their duration during the 1st h after KA injection. However, unlike the LCM group that had a lower number and shorter duration of paroxysmal events compared to vehicle group, a tendency for increase in paroxysmal events was observed in the Ago group compared to vehicle group after the 1st injection of Ago without reaching significance (**Table 1**). After the second injection, the LCM group was characterized with significantly lower duration of paroxysmal events than vehicle-treated group while the Ago-treated group showed a tendency of higher number in paroxysmal events.

Effect of repeated treatment with agomelatine and lacosamide on spontaneous epileptiform activity (spontaneous electrographic and behavioral seizures) during the chronic phase of epilepsy

All rats treated with either vehicle or agomelatine during SE developed epilepsy with appearance of electrographic and behavioral spontaneous seizures. No difference in the total number of behavioral motor seizures was detected between KA-veh and KA-Ago group four months after SE **(Fig. 1).** Three out of five rats (60%) treated repeatedly with LCM during SE did not exhibited behavioral motor seizures registered during continu-

ous 24-h video-monitoring until the fourth month after SE while two rats in LCM group exhibited lower number of spontaneous behavioral seizures than KA-veh group. However, no difference between the vehicle and Ago group in the number of paroxysmal events and their duration (electrographic seizures) and behavioral seizures was detected **(Fig. 1, Table 2)**. The EEG of LCM group was characterized with occasional paroxysmal events, with significantly decreased number of spike trains and seizures compared to vehicle group four months after SE **(Fig.1, Table 2)**.

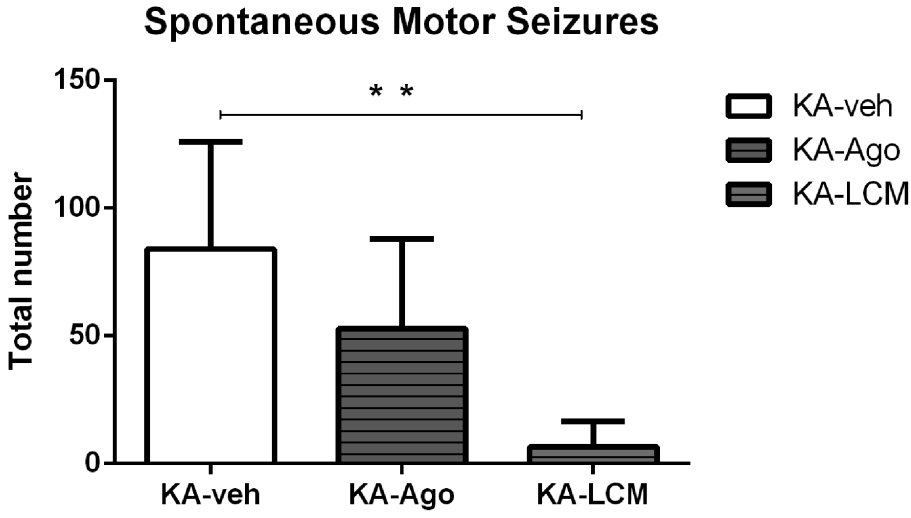

Fig. 1. Vertical bar chart shows the total number of behavioral motor seizures between KA-veh (KA group treated with vehicle), KA-Ago (KA group treated with agomelatine) and KA-LCM (KA group treated with lacosamide) group four months after SE.Data are presented as mean±S.E.M.**p<0.01 compared to the vehicle group(Mann-Whitney test).

Table 1. Characteristics of status epilepticus in different treatment groups. Data are presented as mean±S.E.M. Number of animals is given in parenthesis. *p<0.05 compared to the vehicle group (Normality test).

Group	No. of paroxysmal events		Duration of paroxysmal events (sec)	
	Before treatment (0-1 h)	After the 1st treatment (2-6 h)	Before treatment (0-1 h)	After the 1st treatment (2-6 h)
Vehicle (n=5)	39.3± 7.5	56.8±10.0	3079.3±815.9	6728.5±131.7
Agomelatine (n=5)	36.5±13.5	98.8±15.8	2047.8±306.0	7666.8±275.9
Lacosamide (n=5)	33.0± 8.5	26.5±2.4*	1541.5±388.0	180.0±478.0*

Table 2. Cortical paroxysmal activity in different treatment groups four months after kainate-induced status epilepticus. Data are presented as mean±S.E.M. Number of animals is given in parenthesis. *p<0.05 compared to the vehicle group (Mann-Whitney test).

Group/Rat	Chronic phase			
	No. of paroxysmal events (sec)	No. of spike-trains	No. of seizures	Duration of paroxysmal events (sec)
Vehicle (n=5)	155±27	36.0±10	112±9.7	7503±1154
Agomelatine (n=5)	119±17	88.7±17	110±6.7	6773± 154
Lacosamide (n=5)	81±13*	14.5± 3*	75±17	6344±1583

Discussion

The results of this study are in accordance with our previous work revealing that chronic Ago treatment after KA-induced SE is unable to mitigate the development of epileptogenesis and onset of spontaneous seizures (EEG and video recorded) in the same model of TLE in rats. Moreover, recently we have found that Ago exacerbate the beginning of the chronic phase through decrease of the latent seizure-free period and increase of the frequency of behavioral seizures in the first month after SE. In the present study, we applied another protocol with repeated treatment of this drug in short intervals simultaneously with appearance of SE. The positive control LCZ confirmed results from other experimental studies in rodents [11] confirming that this drug is effective against SE and epileptiform activity during the chronic phase of epilepsy. Numerous preclinical studies, including our results suggest that melatonin is effective against seizure activity in both seizure tests and models of epilepsy [10]. The role of MT1 melatonin receptor in the anticonvulsant effect of melatonin is proposed. Experimental data focused on the role of 5-HT2C receptors in seizure susceptibility are ambiguous [6]. Therefore, it can be speculated that the effects of Ago in the present study might be mediated by antagonism on 5-HT2Creceptors.

Conclusion

To summarize, in the KA-induced SE model Ago is ineffective against development of SE and concomitant spontaneous epileptiform activity compared to the positive control with LCM detected by continuous EEG and video recording. Future studies are required to elucidate the role of MT and 5-HT2Creceptors in its effect.

Acknowledgements: This work was supported by the National Science Fund of Bulgaria (research grant № DN 03/10; DM 11/4), Medical University D-65/02.05.2017.

References

1. **Aguiar, C. C., A. B. Almeida, P. V. Araújo, G. S. Vasconcelos, E. M. Chaves, O. C. do Vale, D. S. Macêdo, F. C. de Sousa, G. S.Viana, S. M. Vasconcelos.** - Anticonvulsant effects of agomelatine in mice. - *Epilepsy Behav.,* **24,** 2012, 324-328.
2. **Beyreuther, B. K., J. Freitag, C. Heers, N. Krebsfänger, U. Scharfenecker, T. Stöhr.** - Lacosamide: a review of preclinical properties. - *CNS Drug Rev.,* **13,** 2007, 21-42.
3. **Brandt, C., A. Heile, H. Potschka, T. Stoehr, W. Löscher.** Effects of the novel antiepileptic drug lacosamide on the development of amygdala kindling in rats. - *Epilepsia,* **47,** 2006, 1803-1809.
4. **Dastgheib, M., L. Moezi.** Acute and chronic effects of agomelatine on intravenous penthylenetetrazol-induced seizure in mice and the probable role of nitric oxide. - *Eur. J. Pharmacol.,* **736,** 2014, 10-15.
5. **Pitkänen, A., I. Kharatishvili, H. Karhunen, K. Lukasiuk, R. Immonen, J. Nairismägi, O. Gröhn, J. Nissinen.** Epileptogenesis in experimental models. - *Epilepsia,* **48,** 2007, 13-20.
6. **Séjourné J, D. Llaneza, O. J. Kuti, D. T. Page.** Social Behavioral Deficits Coincide with the Onset of Seizure Susceptibility in Mice Lacking Serotonin Receptor 2c. - *PLoS One,* **10,** 2015, 0136494.
7. **Stahl, S. M.** Mechanism of action of agomelatine: a novel antidepressant exploiting synergy between monoaminergic and melatonergic properties. - *CNS Spectr.,* **19,** 2014, 207-212.
8. **Stöhr, T., H. J. Kupferberg, J. P. Stables, D. Choi, R. H. Harris, H. Kohn, N. Walton, H. S. White.** Lacosamide, a novel anti-convulsant drug, shows efficacy with a wide safety margin in rodent models for epilepsy. - *Epilepsy Res.,* **74,** 2007, 147-154.
9. **Tchekalarova, J., Z. Nenchovska, D. Atanasova , N. Lazarov, L. Kortenska, M. Stefanova, L. Alova, M. Atanasova.** Long-term consequences of prophylactic treatment with agomelatine on depressive-like behavior and neurobiological abnormalities in pinealectomized rats. - *Behav. Brain Res.,* **302,** 2016, 11-28.
10. **Tchekalarova J., D. Atanasova, Z. Nenchovska, M. Atanasova M, L. Kortenska, R. Gesheva, N Lazarov.** Agomelatine protects against neuronal damage without preventing epileptogenesis in the kainate model of temporal lobe epilepsy. - *Neurobiol. Dis.,* **104,** 2017, 1-14.
11. **Wasterlain, C. G., T. Stöhr, A. Matagne.** The acute and chronic effects of the novel anticonvulsant lacosamide in an experimental model of status epilepticus. - *Epilepsy Res.,* **94,** 2011, 10-17.

Institute of Experimental Morphology, Pathology and Anthropology with Museum
Bulgarian Anatomical Society

Acta morphologica et anthropologica, 25 (1-2)
Sofia ● 2018

Petri Net Representation and Analysis of Mannose Type O-Glycan Biosynthesis

*Jordan Stoyloff**

Institute of Experimental Morphology, Pathology and Anthropology with Museum, Bulgarian Academy of Sciences, Sofia, Bulgaria

* Corresponding author e-mail: jstoyloff@gmail.com

We provide a model and analysis of mannose type O-glycan biosynthesis. Synthesis of Core M1, M2 and M3 glycans is a complex biochemical pathway with numerous interdependent processes. We used Petri nets mathematical formalism to construct the synthesis and extension of Core M1, M2 and M3 glycans. Our analysis show that (Man)1 (Ser/Thr)1 is a critically important substrate for synthesis of all three types of glycans. Gene mutations in POMT1/POMT2 {1'} enzyme lead to muscular dystrophies type A, B and C, congenital muscular dystrophies (CMDs) and limb-girdle muscular dystrophy (LGMD). Core M1 [(Gal)1 (GlcNAc)1 (Man)1 (Ser/Thr)1] and Core M2 [(Gal)2 (GlcNAc)2 (Man)1 (Ser/Thr)1] glycans are also indispensable, as gene mutations in {3'} and {5'}, involved in Core M1 and M2 synthesis, bring forward congenital disorders of glycosylation (CDG) type II.

Key words: O-type glycosilation, Petri nets

Introduction

Biosynthesis of mammalian O-mannosyl glycans is initiated by the transfer of mannose from mannose-P-Dol to serine or threonine residue, followed by extensions with N-acetylglucosamine (GlcNAc) and galactose (Gal) to generate core M1, M2 and M3 glycans. Core M1 and M2 glycans can then be further attached by fucose residues, sialic acid and sulfated glucuroinc acid. Core M3 glycan is involved in the synthesis of alpha-dystroglycan, a heavily glycosylated protein found in muscle and brain tissues. Core M3 glycan contains a tandem repeat of ribitol 5-phosphate (Rbo5P) and -alpha3-GlcA-beta3-Xyl- repeating structures. Defects of genes encoding core glycans and modified core M3 glycans are associated with various congenital diseases, such as muscular dystrophies caused by reduced O-mannosylation of alpha-dystroglycan in skeletal muscles.

Computational systems biology, which is a sub-discipline of systems biology, has developed both as a tool supporting the processing of accumulated biological data and as a modeling discipline, building upon this data in order to predict biological behavior [7], [1]. Qualitative models of biochemical networks are a central component of modern systems biology. Building and managing these complex models is a major challenge that can benefit from the application of formal methods adopted from theoretical

computing science [3]. Petri nets provide graphical representation of the biochemical networks, from which it is possible to perform different kinds of analysis [12]. Petri nets are bipartite graphs with two types of nodes, one corresponding to molecules ('places'), the other corresponding to reactions ('transitions') [4]. The arcs (edges) connecting the nodes encode information about reaction, and involved substrates and products.

Material and Methods

The main source of pathway information was mannose type O-glycan biosynthesis pathway represented in KEGG/ENZYME database. Bipartite Petri graphs G = (V1, V2; E) were constructed from two disjoint sets of nodes, called places (V = P) and transitions (V = T), V1, $\in$ V2 =V, which are connected by edges e $\in$ E $\subseteq$ V. The input range I (x) of an element x $\in$ P $\in$ T of a Petri net is given by I (x) ={y|(y, x) $\in$ E}, the output range as O(x) ={y|(x, y) $\in$ E} [9] and [10].

Results

The mannose type O-glycan biosynthesis pathway starts with addition of dolichyl phosphate D-mannose to [Protein]-L-serine or [Protein]-L-threonine by dolichyl beta - D - mannosyl - phosphate: L - threonyl/L - seryl - [protein] O-D-mannosyltransferase {1'}, see **Fig.1.** Man-β-Dol is available through the N-glycan biosynthesis pathway. Deficiency of Dol-P-Man synthase subunit DPM3 bridges the congenital disorders of glycosylation with the dystroglycanopathies. Investigation of the Dol-P-Man-dependent glycosylation pathway in the ER reveal strongly reduced O-mannosylation of alpha-dystroglycan in a muscle biopsy, thereby explaining the clinical phenotype of muscular dystrophy [14].

Core M3 is synthesized from (Man)1 (Ser/Thr)1 {3} with the help of two enzymes: UDP-N-acetyl-alpha-D-glucosamine:alpha-D-mannosyl-threonyl-[protein] 4 - beta - N - acetyl - D - glucosaminyltransferase [[EC:2.4.1.312] and UDP-N - acetyl - alpha - D - galactosamine: N - acetyl - beta - D - glucosaminyl - (1->4) - alpha - D - mannosyl - threonyl - [protein]3 - beta - N-acetyl - D - galactosaminyltransferase [EC:2.4.1.313], see **Table 1.**

Core M3 is converted by ATP: O3 - [N-acetyl-beta-D-galactosaminyl-(1->3) - N-acetyl - beta - D-glucosaminyl - (1->4) - alpha - D - mannosyl] - L - threonyl/L-seryl-[protein] 6 - phosphotransferase {3.3'} to (GalNAc)1 (GlcNAc)1 (Man)1 (P)1 (Ser/Thr)1 {3.3}. This product and D-ribitol {3.6} are substrates for FKTN {3.5'}. Next, by a series of enzymes, Core M3 is extended to the final product of this branch of mannose type O-glycan biosynthesis, namely α-Dystroglycan.

Next the enzyme, beta-1,2-N-acetylglucosaminyltransferase {2'}, branches the pathway leading to synthesis of Core M1 and M2 glycans, see **Fig. 1.**

Synthesis of Core M1 glycans start from (ClcNAc)1(Man)1(Ser/Thr) [5] through action of B4GALT1 (beta-1,4-galactosyltransferase 1 [EC:2.4.1.22 2.4.1.90 2.4.1.38 2.4.1.-]), see **Table 2.**

Core M2 glycans are not obtained directly from (ClcNAc)1(Man)1(Ser/Thr) [4]. First (ClcNAc)1(Man)1(Ser/Thr) is transformed to (GlcNAc)2 (Man)1 (Ser/Thr)1 [13] by MGAT5B (mannosyl alpha-1,6-glycoprotein beta-1,6-N-acetyl-glucosaminyltransferase, isozyme B [EC:2.4.1.-]) {4'}. Core M2 are synthesized from (GlcNAc)2 (Man)1 (Ser/Thr)1 with the aid of B4GALT1 (beta-1,4-galactosyltransferase 1 [EC:2.4.1.22 2.4.1.90 2.4.1.38 2.4.1.-]), see **Table 3.**

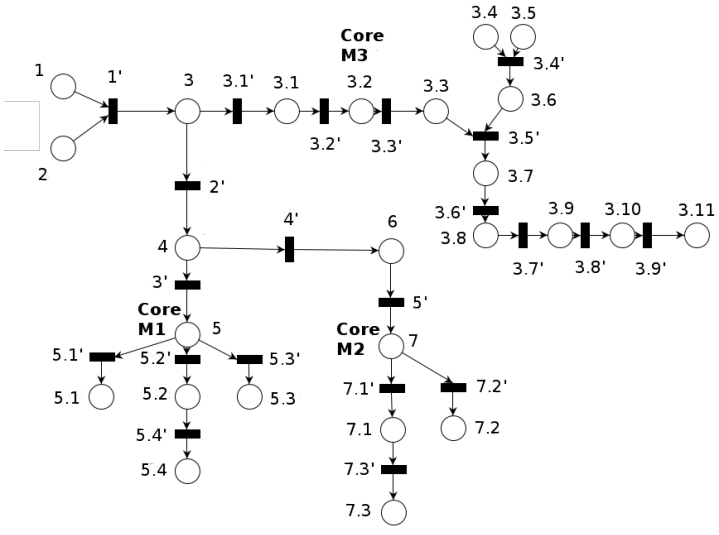

Fig. 1. Petri net representation of mannose type O-glycan biosynthesis pathway

Table 1. Reactions involved in synthesis and extension of Core M3 glycans. Note: Substrates and products are given in curly brackets. Enzymes are given in curly brackets, preceded and followed by '=>'. Numbers in curly brackets correspond to those in Fig. 1.

1'	Dolichyl phosphate D-mannose {1} + [Protein]-L-serine {2} => dolichyl-phosphate-mannose-protein mannosyltransferase [EC:2.4.1.109] {1'} => (Man)1 (Ser/Thr)1 {3} Dolichyl phosphate D-mannose {1} + [Protein]-L-threonine {2} => {1'} => (Man)1 (Ser/Thr)1 {3}
2'	UDP-N-acetyl-alpha-D-glucosamine + (Man)1 (Ser/Thr)1 {3} => protein O-mannose beta-1,4-N-acetylglucosaminyltransferase [EC:2.4.1.312] {3.1'} => UDP + (GlcNAc)1 (Man)1 (Ser/Thr)1 {3.1}
3'	UDP-N-acetyl-alpha-D-galactosamine + [(GlcNAc)1 (Man)1 (Ser/Thr)1] {3.1} => beta-1,3-N-acetylgalactosaminyltransferase 2 [EC:2.4.1.313] {3.2'} => UDP + (GalNAc)1 (GlcNAc)1 (Man)1 (Ser/Thr)1 {3.2} **[Core M3]**
4'	ATP + (GalNAc)1 (GlcNAc)1 (Man)1 (Ser/Thr)1 {3.2}=> glycoprotein-mannosyl O6-kinase [EC:2.7.1.183] {3.3'} => ADP + (GalNAc)1 (GlcNAc)1 (Man)1 (P)1 (Ser/Thr)1 {3.3}
5'	CTP {3.4} + D-ribitol 5-phosphate {3.5} => D-ribitol-5-phosphate cytidylyltransferase [EC:2.7.7.40] {3.4'} => diphosphate + CDP-ribitol {3.6}
6'	(GalNAc)1 (GlcNAc)1 (Man)1 (P)1 (Ser/Thr)1 {3.3} + CDP-ribitol {3.6} => fukutin [EC:2.7.8.-] {3.5'} => (GalNAc)1 (GlcNAc)1 (Man)1 (Rib-ol)1 (P)2 (Ser/Thr)1 {3.7}
7'	(GalNAc)1 (GlcNAc)1 (Man)1 (Rib-ol)1 (P)2 (Ser/Thr)1 {3.7} => fukutin-related protein [EC:2.7.8.-] {3.6'} => (GalNAc)1 (GlcNAc)1 (Man)1 (Rib-ol)2 (P)3 (Ser/Thr)1 {3.8}
8'	(GalNAc)1 (GlcNAc)1 (Man)1 (Rib-ol)2 (P)3 (Ser/Thr)1 {3.8} => ribitol beta-1,4-xylosyltransferase [EC:2.4.2.-] {3.7'} => (GalNAc)1 (GlcNAc)1 (Man)1 (Rib-ol)2 (Xyl)1 (P)3 (Ser/Thr)1 {3.9}
9'	(GalNAc)1 (GlcNAc)1 (Man)1 (Rib-ol)2 (Xyl)1 (P)3 (Ser/Thr)1 {3.9} => beta-1,4-glucuronyltransferase 1 [EC:2.4.1.-] {3.8'} => (GalNAc)1 (GlcA)1 (GlcNAc)1 (Man)1 (Rib-ol)2 (Xyl)1 (P)3 (Ser/Thr)1 {3.10}
10'	(GalNAc)1 (GlcA)1 (GlcNAc)1 (Man)1 (Rib-ol)2 (Xyl)1 (P)3 (Ser/Thr)1 {3.10} => glycosyltransferase-like protein LARGE [EC:2.4.2.- 2.4.1.-] {3.9'} => alpha-Dystroglycan {3.11}

Table 2. Reactions involved in synthesis and extension of Core M1 glycans. Note: Substrates and products are given in curly brackets. Enzymes are given in curly brackets, preceded and followed by '=>'. Numbers in curly brackets correspond to those in Fig. 1.

2'	UDP-GlcNAc + (Man)1(Ser/Thr) {3} => beta-1,2-N-acetylglucosaminyltransferase [EC:2.4.1.-] {2'} => UDP + (ClcNAc)1(Man)1(Ser/Thr) {4}
3'	(ClcNAc)1(Man)1(Ser/Thr) {4} => beta-1,4-galactosyltransferase 1 [EC:2.4.1.22 2.4.1.90 2.4.1.38 2.4.1.-] {3'} => (Gal)1 (GlcNAc)1 (Man)1 (Ser/Thr)1 **[Core M1]** {5}
5.1'	CMP-N-acetyl-beta-neuraminate + (Gal)1 (GlcNAc)1 (Man)1 (Ser/Thr)1 {5} => neolactotetraosylceramide alpha - 2,3 - sialyltransferase (sialyltransferase 6) [EC:2.4.99.6] {5.1'} => CMP + (Sia)1(Gal)1 (GlcNAc)1 (Man)1 (Ser/Thr)1 {5.1}
5.2'	UDP-alpha-D-glucuronate + (Gal)1 (GlcNAc)1 (Man)1 (Ser/Thr)1 {5} => galactosylgalactosylxylosylprotein 3-beta-glucuronosyltransferase 1 [EC:2.4.1.135] {5.2'} => UDP + [protein]-3-O-(beta-D-GlcA-(1->3)-beta-D-Gal-(1->3)-beta-D-Gal-(1->4)-beta-D-Xyl)-L-serine {5.2}
5.3'	GDP-beta-L-fucose + (Gal)1 (GlcNAc)1 (Man)1 (Ser/Thr)1 {5} => 4-galactosyl-N-acetylglucosaminide 3-alpha-L-fucosyltransferase [EC:2.4.1.152] {5.3'} => GDP + (Gal)1 (GlcNAc)1 (LFuc)1 (Man)1 (Ser/Thr)1 {5.3}
5.4'	[protein]-3-O-(beta-D-GlcA-(1->3)-beta-D-Gal-(1->3)-beta-D-Gal-(1->4)-beta-D-Xyl)-L-serine {5.2} => carbohydrate 3-sulfotransferase 10 [EC:2.8.2.-] {5.4'} => (Gal)1 (GlcA)1 (GlcNAc)1 (Man)1 (S)1 (Ser/Thr)1 [5.4]

Table 3. Reactions involved in synthesis and extension of Core M2 glycans. Note: Substrates and products are given in curly brackets. Enzymes are given in curly brackets, preceded and followed by '=>'. Numbers in curly brackets correspond to those in Fig. 1.

4'	(ClcNAc)1(Man)1(Ser/Thr) {4} => mannosyl alpha-1,6-glycoprotein beta-1,6-N-acetylglucosaminyltransferase, isozyme B [EC:2.4.1.-] {4'} => (GlcNAc)2 (Man)1 (Ser/Thr)1 {6}
5'	(GlcNAc)2 (Man)1 (Ser/Thr)1 {6} => beta-1,4-galactosyltransferase 1 [EC:2.4.1.22 2.4.1.90 2.4.1.38 2.4.1.-] {5'} => (Gal)2 (GlcNAc)2 (Man)1 (Ser/Thr)1 {7} **[Core M2]**
7.1'	(Gal)2 (GlcNAc)2 (Man)1 (Ser/Thr)1 {7} **[Core M2]** => galactosylgalactosylxylosylprotein 3-beta-glucuronosyltransferase 1 [EC:2.4.1.135] {7.1'} => (Gal)2 (GlcA)1 (GlcNAc)2 (Man)1 (Ser/Thr)1 {7.1}
7.2'	(Gal)2 (GlcNAc)2 (Man)1 (Ser/Thr)1 {7} **[Core M2]** => neolactotetraosylceramide alpha-2,3-sialyltransferase (sialyltransferase 6) [EC:2.4.99.6] {7.2'} => (Gal)2 (GlcNAc)2 (Man)1 (Neu5Ac)2 (Ser/Thr)1 {7.2}
7.3'	(Gal)2 (GlcA)1 (GlcNAc)2 (Man)1 (Ser/Thr)1 {7.1} => carbohydrate 3-sulfotransferase 10 [EC:2.8.2.-] {7.3'} => (Gal)2 (GlcA)1 (GlcNAc)2 (Man)1 (S)1 (Ser/Thr)1 {7.3}

Discussion

Muscular dystrophies due to reduced glycosylation of alpha-dystroglycan are a common group of conditions, referred to as dystroglycanopathies. The most severe clinical spectrum (type A) are characterized by congenital muscular dystrophy with severe structural brain and eye abnormalities. Muscular dystrophy-dystroglycanopathy type B (MDDGB) is less severe and is characterized by early onset of muscle weakness, mental retardation, and mild brain anomalies. The mildest form (type C) are limb-girdle muscular dystrophy. Gene mutations of O-D-mannosyltransferase {1'} lead to muscular dystrophy-dystroglycanopathy type A [8], B [4] and C [2]. Another class of diseases connected with mannose type O-glycan biosynthesis are congenital muscular dystrophies (CMDs). They are a heterogeneous group of inherited disorders characterized by muscle weakness from birth and variable clinical manifestations of the eye and central nervous system. Defects in genes encoding for POMT1/POMT2 {1'} is a cause for CMDs [6]. Limb-girdle muscular dystrophy (LGMD) is also associated with disruption of the O-glycan biosynthesis pathway. It is a heterogeneous group of inherited disorders characterized by progressive muscle weakness that begins from the proximal limb muscles. Gene mutations of O-D-mannosyltransferase {1'} lead to LGMD [11]. This points out the role of (Man)1 (Ser/Thr)1, which is a product of O-D-mannosyltransferase, and starting point for synthesis of Core M1, M2 and M3 glycans.

Gene mutations in beta-1,4-N-acetylglucosaminyltransferase {3.1'} and beta-1,3-N-acetylgalactosaminyltransferase 2 {3.2'} lead to muscular dystrophy-dystroglycanopathy type A. In the first case beta - 1,4 - N - acetylglucosaminyltransferase obtain (Man)1 (Ser/Thr)1 [3], as we suppose in this case that O-D-mannosyltransferase is functioning normally. Muscular dystrophy-dystroglycanopathy type A is manifested if either the substrate of beta-1,3-N-acetylgalactosaminyltransferase 2 or its product are absent. So [(GlcNAc)1 (Man)1 (Ser/Thr)1] {3.1} or (GalNAc)1 (GlcNAc)1 (Man)1 (Ser/Thr)1 {3.2} [Core M3] are necessary to avoid manifestations of this disease.

Gene mutations in beta-1,2-N-acetylglucosaminyltransferase [EC:2.4.1.-] {2'} lead to same diseases, as mutations in O-D-mannosyltransferase gene, pointing to the role of (ClcNAc)1(Man)1(Ser/Thr) {4}. It appears that ClcNAc attached to (Man)1(Ser/Thr) is necessary to prevent above mentioned diseases. (ClcNAc)1(Man)1(Ser/Thr) is also a branching point for synthesis of Core M1 and Core M2 glycans.

Gene mutations in {3'} and {5'}, involved in Core M1 and M2 synthesis, bring forward a new disorder: congenital disorders of glycosylation (CDG) type II [6]. Multiple subtypes have been identified. In contrast to type I, the type II patients show a more severe psychomotor retardation, no peripheral neuropathy and a cerebellar hypoplasia. Consequently, both Core M1 [((Gal)1 (GlcNAc)1 (Man)1 (Ser/Thr)1)] and Core M2 [((Gal)2 (GlcNAc)2 (Man)1 (Ser/Thr)1)] are essential for prevention of this congenital disorder. Although not mentioned in KEGG database, gene mutations in {1'} and {2'} should also disrupt synthesis of Core M1 an M2 glycans, and consequently have the same pathological manifestation as mutations in {3'} and {5'}. But obviously presence of Man and/or ClcNAc attached to (Ser/Thr)1 are essential for prevention of muscular dystrophy-dystroglycanopathy type A, B and C, congenital muscular dystrophies (CMD/MDC) and limb-girdle muscular dystrophy (LGMD), but not congenital disorders of glycosylation (CDG) type II.

Conclusions:

Petri nets can be used to establish connections between pathology and chemical structure. In this way (Man)1 (Ser/Thr)1 is essential for prevention of muscular dystrophy-dystroglycanopathy types A, B and C. Both Core M1 [((Gal)1 (GlcNAc)1 (Man)1 (Ser/Thr)1)] and Core M2 [((Gal)2 (GlcNAc)2 (Man)1 (Ser/Thr)1)] glycans are essential for prevention of congenital disorders of glycosylation (CDG) type II. In summary, the presence of Man and/or ClcNAc attached to (Ser/Thr)1 are essential for prevention of muscular dystrophy-dystroglycanopathy type A, B and C, congenital muscular dystrophies (CMD/MDC) and limb-girdle muscular dystrophy (LGMD), but not congenital disorders of glycosylation (CDG) type II.

References

1. **Alberghina, L., F. Chiaradonna, M. Vanoni.** Systems biology and the molecular circuits of cancer. - *Chembiochem.,* **5,** 2004, 1322-1333.
2. **Balci B., G. Uyanik, P. Dincer, C. Gross, T. Willer, B. Talim, G. Haliloglu, G. Kale, U. Hehr, J. Winkler, H. Topaloglu.** An autosomal recessive limb girdle muscular dystrophy (LGMD2) with mild mental retardation is allelic to Walker-Warburg syndrome (WWS) caused by a mutation in the POMT1 gene. - *Neuromuscul. Disord.,* **15,** 2005, 271-275.
3. **Rainer B., D. Gilbert, M. Heiner, R. Orton.** A structured approach for the engineering of biochemical network models, illustrated for signalling pathways. - *Briefings in Bioinformatics.,* **9**(5), 2002, 404-421.
4. **Chaouiya C.** Petri net modelling of biological networks. - *Briefings Bioinform.,* **8,** 2007, 210-219.
5. **Godfrey C., E. Clement, R. Mein, M. Brockington, J. Smith.** Refining genotype phenotype correlations in muscular dystrophies with defective glycosylation of dystroglycan. - *Brain,* **130,** 2007, 2725-2735 .
6. **Hansske B., C. Thiel, T. Lubke, M. Hasilik, S. Honing, V. Peters.** Deficiency of UDP - galactose: N - acetylglucosamine beta - 1,4 - galactosyltransferase I causes the congenital disorder of glycosylation type IId. - *J. Clin. Invest.,* **109,** 2002, 725-733 .
7. **Ideker T., T. Galitski, L. Hood.** A new approach to decoding life: Systems Biology. - *Annual Review of Genomics and Human Genetics,* **2,** 2001, 343-372.
8. **Muntoni F., S. Torelli, M. Brockington.** Muscular dystrophies due to glycosylation defects. - *Neurotherapeutics,* **5,** 2008, 627-632 .
9. **Murata, T.** Petri nets: properties, analysis and applications. - *Proc. IEEE,* **77,** 1989, 541-580.
10. **Nagasaki M., A. Doi, H. Matsuno.** A versatile Petri net based architecture for modeling and simulation of complex biological processes. - *Genome Inform.,* **15,** 2004, 180-197.
11. **Nigro V., S. Aurino, G. Piluso.** Limb girdle muscular dystrophies: update on genetic diagnosis and therapeutic approaches. - *Curr. Opin. Neurol.,* **24,** 2011, 429-436 .
12. **Szallasi Z., J. Stelling, V. Periwal.** System Modeling in Cellular Biology. Concepts to Nuts and Bolts. Cambridge, MA: MIT Press, 2006.
13. **Van Reeuwijk J., S. Maugenre, C. van den Elzen, A. Verrips, E. Bertini, F. Muntoni, L. Merlini, H. Scheffer, H. Brunner, P. Guicheney, H. van Bokhoven.** The expanding phenotype of POMT1 mutations: from Walker-Warburg syndrome to congenital muscular dystrophy, microcephaly, and mental retardation. - *Hum. Mutat.,* **27,** 2006, 453-459.
14. **Wevers R., Lefeber, D., J. Schönberger, E. Morava, M. Guillard, K. M. Huyben, K. Verrijp, O. Grafakou, A. Evangeliou.** Deficiency of Dol-P-Man synthase subunit DPM3 bridges the congenital disorders of glycosylation with the dystroglycanopathies. - *AJHG,* **85**(1), 2009, 76-86.

Institute of Experimental Morphology, Pathology and Anthropology with Museum
Bulgarian Anatomical Society

Acta morphologica et anthropologica, 25 (1-2)
Sofia ● 2018

Anthropology and Anatomy

Results from Anthropological Analysis of Bone Remains in Grave No 1 from Archaeological Site at Kremikovtsi Monastery „St. Georgi Pobedonosets“, Sofia

Nadezhda Atanassova[*]*, Vladislav Todorov*

Institute of Experimental Morphology, Pathology and Anthropology with Museum, Bulgarian Academy of Sciences, Sofia, Bulgaria

* Corresponding author e-mail: naditimeva@gmail.com

In 2015 were held excavations of the archeological site in Kremikovtsi Monastery. Well preserved grave (no. 1) with skeleton in anatomical order, orientated West-East, was uncovered in rock base. In the area of the skull, a structure of four reused bricks was established. Radiocarbon dating shows that the grave no. 1 is from the second half of 15th - first quarter of 16th c. The aim of the present study is to provide detailed anthropological information for the skeleton from grave no. 1: age-at-death, sex, stature, body mass, pathological changes and anatomical variations. In view of the high stature, body mass, massive and long bones with a strong relief, it can be concluded that the male buried individual had a very well developed musculoskeletal system and strenuous physical activity in lifetime. A large number of paleopathological changes have been diagnosed on the skull and trunk bones.

Key words: Kremikovtsi Monastery, Ottoman period, human skeleton, anthropological analysis, paleopathology

Introduction

Kremikovtsi Monastery „St. Georgi Pobedonosets“ (St. George the Victorious) is a recognizable monument of the Bulgarian cultural heritage. It is located 3 km above Sofia’s quarter of Kremikovtsi, north-east of the center of Sofia city, in the southern slopes of Stara planina mountain.

Scientific interest about this Monastery was generated at the end of the 19th century [8, 24, 33] and continued throughout the 20th century [5, 15, 17, 21, 22]. Publications described different aspects related to the history, the architecture of the buildings and stylistic features of the frescoes in the old church „St. Georgi Pobedonosets“. In

1987, excavations were carried out in conjunction with restoration work in naos (inner chamber) of the church [19, 20]. Four child skeletons have been discovered by Dr. Slavcho Cholakov [20]. Investigators suggested that two of these children buried in 1493, belonged to the family of Radivoy - ctitor of the church [20]. In 2014, an archaeological observation was made during the construction of a church drainage where archaeological materials were not found [28].

In 2015 under the direction of archaeologist Vladislav Todorov excavations are extended, covering the area north of the old church [26]. During the field work a necropolis is registered. It was compromised by the construction of monastery buildings during the Revival [26] and anthropogenic activities in the 20th century. Scattered human bones from individuals of different ages and sexes are registered. There was also a fully preserved inhumated skeleton in an anatomical order (grave no. 1), orientated West-East. The burial ritual is Christian. In the area of the skull, a structure of four reused bricks is established. Radiocarbon analysis shows that the grave no. 1 dated from the second half of the 15th century – first quarter of the 16th century.

The aim of the present study is to provide detailed anthropological information for the skeleton from grave no. 1, Kremikovtsi Monastery - the condition of the presented bones, age-at-death, sex, stature, body mass, pathological changes and anatomical variations of the buried individual.

Material and Methods

This paper includes results of detailed anthropological investigation of inhumated male skeleton from grave no.1 at archaeological site in Kremikovtsi Monastery, Sofia. The bones are dated from the Scottish Universities Environmental Research Centre via radiocarbon analysis in the second half of the 15th - first quarter of the 16th century. The skeletal remains are in very good condition. Their cortical layers are well preserved which allows establishment of paleopathological changes. The skull is fully represented. The postcranial skeleton is also completed preserved with the exception of some left tarsal bones.

The age-at-death of buried individual is established after symphyseal relief [27] and ossification degree of cranial sutures [1, 6, 13, 30]. Epiphyseal union [25], dental attrition [4, 32] and other general age indicators [3, 6, 7] are also used.

The sex of the buried individual is identified mainly from pelvic girdle bones - the shape of incisura ischiadica major and foramen obturatum, the value of the pubic angle, the breadth and length of the sacrum [3, 12]. The morphology of cranial elements and the measurements of trunk bones are also applied [3, 9, 12].

Assessment of the individual body mass is done after the biomechanical methods [23]. Stature reconstruction is based on the length of the long bones of the limbs by the formulae of Pearson-Lee [18] and Trotter-Gleser [29].

The pathological traces on the bones and normal anatomical variations are assessed after different paleopathological methods [2, 11, 14, 16].

Results and Discusion

Position of the skeleton in situ **(Fig. 1)**

The buried individual was placed in supine position (lying on the back). A structure of four reused bricks covered the skull which lies on the occipital bone. The upper limbs are flexed in the elbow joints. The forearms are parallel and lie on the lower half of the

Fig. 1. Position of the skeleton *in situ* (grave no. 1)

chest. The hands of the buried individual have been laid with their palms up. Lower limbs are stretched out.

Age-at-death estimation

Based on the relief of symphyseal surface of the pubic bone and the degree of ossification (synostosis) of the coronal, sagittal and lambdoid cranial sutures, the age-at-death of individual from grave no. 1 is identified in age group Maturus - between 45 and 49 years.

Sex determination

The sex is defined as male, based on a large number of scopical features of postcranial skeleton and skull: acute subpubic angle (arcus pubicus); the greater sciatic notch (incisura ischiadica major) is narrow; flat auricular surface of ilium (facies auricularis ossis ilii); high and narrow pelvis major; narrow and long sacral bone (os sacrum); the upper orbital margin (margo supraorbitalis) is rounded; the end of zygomatic arch (arcus zygomaticus) continues behind the external auditory opening (porus acusticus externus); mastoid process (processus mastoideus) is large and has a strong relief; the forehead is low; glabella and arcus supercilialis are moderately pronounced; the chin is square; an acute angle of the mandible (angulus mandibulae). The long bones of the limbs are massive with a great length and a strong expressed relief.

Sex is determined also as male by some measurements of postcranial bones **(Table 1).**

Table 1. Measurements of postcranial bones used for sex determination of the individual from grave no. 1, Kremikovtsi Monastery

Bone	(mm)	Sex	Bone	(mm)	Sex
Epycond.D hum. dx	72.0	♂ (Bass 2005)	*D caput radii dx*	25.0	♂ (Kühl 1985)
Epycond.D hum. sin	70.0	♂ (Bass 2005)	*D caput radii sin*	24.5	♂ (Kühl 1985)
Vert D caput humeri dx	47.5	♂ (Bass 2005)	*Trans. D caput hum. dx*	47.0	♂ (Bass 2005)
Vert D caput humeri sin	48.0	♂ (Bass 2005)	*Trans. D caput hum. sin*	47.0	♂ (Bass 2005)
D caput femoris dx	51.0	♂ (Bass 2005)	*D caput femoris sin.*	51.5	♂ (Bass 2005)
Epycond.D fem. dx	87.0	♂ (Bass 2005)	*Epycond.D fem.sin*	87.0	♂ (Bass 2005)
L clavicula dex	149.0	♂ (Bass 2005)	*L clavicula sin*	148.0	♂ (Bass 2005)

Metrical and scopical characteristic of the skull

Investigated skull is characterized by “large” absolute measurements of the cranial part and “medium” length and height of the face. Orbital height is “very small”, while nasal width and height are “very large” and “large”. The length of the palate is also “large”. The lower jaw is with a “large” angular width, a “small” chin height and a “very small” branch width. The indexing characterization showed that the skull is tall and wide, with a slight protuberance of the face.

The scopical skull decription is as follows: vertical norm is ovoid; occiput is flat with a fluent transition in a profile, the occipital bone being slightly protruding and moderate in relief **(Fig. 2)**; mastoid process (processus mastoideus) is large, with a strong relief and a downward direction; frontal eminences (tubera frontalia) are less pronounced; glabella and arcus supercilialis are moderately pronounced; the shape of the face is ellipsoid; orbits are rectangular with a vertical slope; nasal bones are symmetrical, narrow, with medium length and slight shedding; nasal aperture has blunt margins and lower end – anthropina; cheekbones (ossa zygomatica) are slightly protruding and with vertical profiling; fossa canina dextra is medium deep and fossa canina sinistra is shallow, both of them with a slight expressed relief; mandibular bone is small, moderately massive, with a strong relief and a narrow branch (ramus mandibulae). This jaw is deformed by the advanced edentulous ante mortem; the chin is moderately pronounced, triangular, wide-based and without sinking. Occlusion could not be determined due to edentulism of the upper jaw.

Dentition: permanent, incomplete:

right															**left**
0	**0**	**0**	**0**	**0**	**0**	**0**	**0**	**0**	**0**	**0**	**4**	**0**	**0**	**0**	**0**
0	**0**	**0**	**R**	**4**	**3**	**2**	**0**	**0**	**0**	**3**	**4**	**5**	**0**	**0**	**0**

1 - a permanent tooth preserved in the alveolus; 0 - tooth lost before death (*ante mortem*) or tooth agenesis; R - preserved tooth root

Abrasion of the teeth - moderately (3-4 degree).

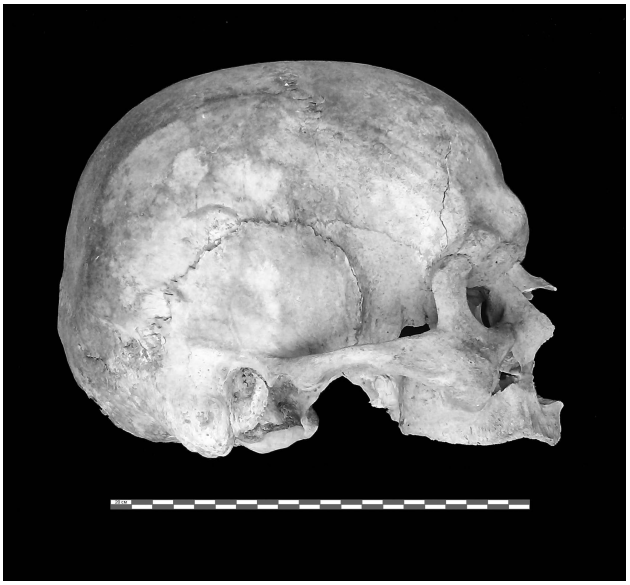

Fig. 2. Skull in *norma lateralis* (grave no.1)

Stature and body mass estimation

The stature of male from grave no. 1 is reconstructed by the lengths of all long bones of the limbs **(Table 2)**. Stature reconstructed by both formulae [18, 29] falls into the category "tall" after Martin-Saller's rubrications [12] for the European population. Heads of both femoral bones are preserved, making it possible to assess the body mass of the individual - 77.01 kg.

Table 2. Lengths of long bone of the limbs used for reconstruction of the stature of the individual from grave no. 1, Kremikovtsi Monastery

Bone	**Length (**cm**)**	**Stature**
Humerus dexter	34,0	169,04 cm (Pearson-Lee 1935) 175,17 cm ±4,05 (Trotter-Gleser 1952)
Humerus sinister	34,0	169,04 cm (Pearson-Lee 1935) 175,17 cm ±4,05 (Trotter-Gleser 1952)
Radius dexter	25,5	175,40 cm ±4,32 (Trotter-Gleser 1952)
Radius sinister	25,5	175,40 cm ±4,32 (Trotter-Gleser 1952)
Femur dexter	48,9	173,24 cm (Pearson-Lee 1935) 177,79 cm ±3,27 (Trotter-Gleser 1952)
Femur sinister	48,8	173,05 cm (Pearson-Lee 1935) 177,55 cm±3,27 (Trotter-Gleser 1952)
Tibia dextra	41,0	181,94 cm±3,37 (Trotter-Gleser 1952)
Tibia sinistra	41,0	181,94 cm±3,37 (Trotter-Gleser 1952)
	Mean value for the stature:	**171,09 cm** (after Pearson-Lee-Lee 1935) **177,55 cm±3,48** (after Trotter-Gleser 1952)

Pathologies, traumas and anatomical variations **(Figs. 3.1. - 3.2.)**

A large number of paleopathological changes have been diagnosed on the skull and trunk bones. A lesion (destruction of the bone) with irregular shape and larger dimensions 2 cm length/1 cm width is observed. It is localized on the right side of the occipital bone. A differential diagnosis could be a malignant bone tumor formation which is the most likely cause for death of the individual **(Fig. 3.1. - 1)**. Four osteomas are identified on the left parietal bone **(Fig. 3.1. - 2)**. Osteoma is a benign tumor and originated by bone-forming connective tissue, which has osteogenic properties. Still etiology is not fully understood. Traces of an infectious process (most likely bacterial) on two parietal and occipital bones, in the area of the intersection of the sagittal and lambdoid cranial sutures are identified **(Fig. 3.1. - 2)**. Ante mortem toothlessness of both jaws is reported **(Fig. 3.1. – 3, 4)**. This type of edentulism could be associated with the advanced age of the individual. Tooth loss has a negative effect on the masticatory function and the occlusion. A jaw cyst is detected in the area of the lower right second premolar, which crown was destroyed by the infectious process **(Fig. 3.1. - 3).** In the skeleton from grave no. 1 it was a deformation (distortion in the form of the letter O) of both tibial bones due to rickets in infancy. There is also asymmetrical deformation of the sacral bone **(Fig. 3.1. - 5)**. Osteoid osteoma is a benign osteoblastic tumor that most commonly affects the femur and tibia at a young age. In the skeleton of grave no. 1, this type of neoplasm is recorded on the lower part of the body of tibia dextra **(Fig. 3.1. - 6)**. Spondylosis traces are observed in the cervical and lumbar areas of the vertebral column with the deformation of the vertebrae and pronounced osteophytes **(Fig. 3.1. - 7)**. Arthritic distortion of right metatarsal bone is also identified. Lateral epicondylitis is a very common condition affecting mainly middle-aged people [31]. Any activity involving excessive and repetitive manual work may cause the tendinosis. In the investigated skeleton from Kremikovtsi Monastery, lateral epicondylitis is found on both shoulder bones, more pronounced on the left, which is an indication that the individual has served primarily with the left upper limb. Myositis ossificans (heterotopic ossification of the muscle) is observed on the medial side of fibula sinistra.

In this skeleton have been diagnosed enthesopathy with formation of hyperostoses on the distal epiphyses of fibula dextra et sinistra **(Fig. 3.2. - 8)** as well as bilateral traumas on the lower half of ulna dextra et sinistra **(Fig. 3.2. - 9).** These fractures and their localization on upper and lower limbs, give us reason to suppose that the male individual buried in Grave no. 1 was tied ante mortem. Traces of trauma are also identified on 4 fragments of ribs **(Fig. 3.2. - 10)** and on left metacarpal bone.

It is established lumbosacral transitional vertebrae (sacralization of fifth lumbar vertebra) **(Fig. 3.1. - 5)**. Metopism **(Fig. 4)** as well as intra sutural bones on lambdoid cranial suture have been detected.

Conclusions

In view of the high stature, body mass, massive and long bones with a strong relief, it can be concluded that the male from grave no. 1 of archaeological site in Kremikovtsi Monastery, had a very well developed musculoskeletal system and strenuous physical activity in lifetime. The mentioned above large number of pathological traces on the bones and anatomical variations are indicative for a generalized ossification and mineralization problem that started in childhood and affected the whole locomotor system of the buried individual.

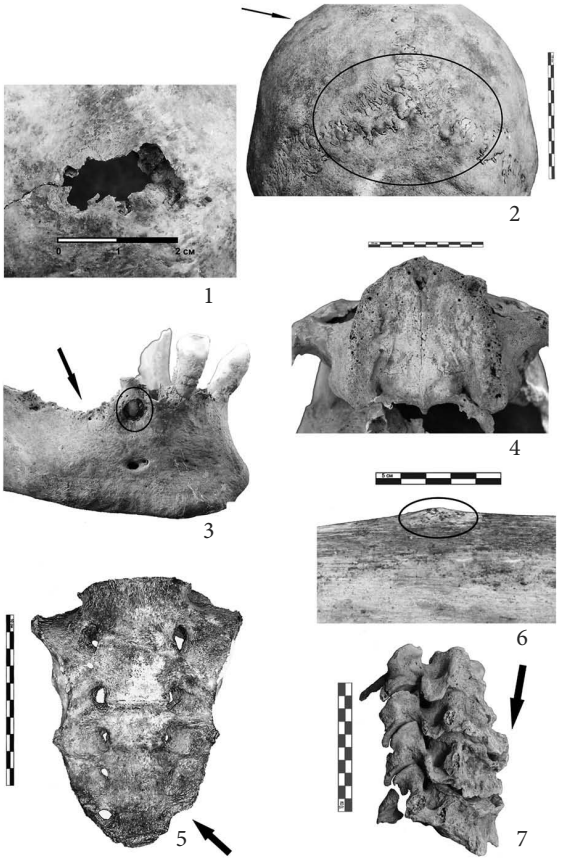

Fig. 3.1. Bone diseases on the skeleton from grave No 1
1 – Lesion on *squama occipitalis*; 2 - Osteoma and traces from an infectious process on the skull; 3 - Toothlessness (edentulism) ante mortem and cyst on the mandibular bone; 4 - Toothlessness (edentulism) ante mortem of maxillary bone; 5 - Asymmetrical deformation of sacral bone and lumbosacral transitional vertebrae; 6 - Osteoid osteoma on the lower part of the body of right tibia; 7 - Spondylosis in the cervical area of *columna vertebralis*;

Figure 3.2. Bone diseases and traumas on the skeleton from grave no 1
8 - Enthesopathy on the distal epiphyses of *fibula dextra et sinistra*; 9 – Traces of fracture on *ulna dextra et sinistra*; 10 - Traces of *fracture on ribs*

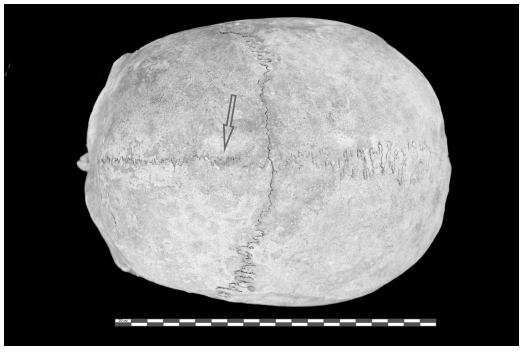

Fig. 4. Metopism (unfused *sutura metopica*) on frontal bone of investigated skeleton

References

1. **Alekseev, V., G. Debets.** Craniometry, methods of anthropological study. Moscow, Nauka, 1964, 228 p. [in Russian].
2. **Aufderheide, C., C. Rodriguez-Martin.** The Cambridge Encyclopedia of Human Paleopathology. Cambridge University Press, 1998, 478 p.
3. **Bass, W.** Human osteology: a laboratory and field manual of the human skeleton. University of Missoury, Special publication no. 2 of the Missouri Archaeological Society, 2005, 365 p.
4. **Brothwell, D. R.** The relationship of tooth wear to aging. - *In: Age markers in the human skeleton* (Ed. M. İşcan), Illinois, Springfield, 1989, 303-316.
5. **Dimitrova, Z., Z. Ganeva, G. Stoyanova.** Sofia Monasteries**.** Origin, development, structure and character. Sofia, Publishing Center at the Ministry of Culture, 1992, 130 p. [in Bulgarian].
6. **Ferembach, D., I . Schwidetzky, M. Stloukal.** Recommendations for age and sex diagnosis of skeletons. - *J. Hum. Evol.,* **9,** 1980, 517-549.
7. **Gerasimov, M.** Reconstruction of the face by the skull. Moscow, Nauka, 1955, 586 p. [in Russian].
8. **Irechek, K.** Principality of Bulgaria, II. Traveling in Bulgaria. Plovdiv, Hristo Danov Publishing House, 1899, 943 p. [in Bulgarian].
9. **Kühl, R.** Skeletal remains from praehistorical cremations and their possibilities for interpretation with with attention to the special problems in Schleswig-Holstein. - *Communications of the Anthropological Society in Wien* (MAGW), **115,** 1985, 113-137 [in German].
10. **Lovejoy, C., R. Meindl, T. Pryzbeck, R. Mensforth.** Chronological metamorphosis of the auricular surface of the ilium: A new method for the determination of adult skeletal Age-at-death. - *Am. J. Phys. Anthropol.,* **68,** 1985, 15-28.
11. **Mann, R., D. Hunt.** Photographic regional atlas of bone disease. A guide to pathologicand normal variation in the human skeleton. Illinois, Charles Thomas Publisher Ltd., 2005, 416 p.
12. **Martin, R., K. Saller.** Lehrbuch der Anthropologie in sistematischer Darstellung, Band I. Stuttgart, G. Fischer Verlag, 1957, 429 –595.
13. **Meindl, R., C. Lovejoy**. Ectocranial suture closure: a revised method for the termination of skeletal age-at-death based on lateral-anterior sutures. - *American Journal of Physical Anthropology,* **68,** 1985, 57-66.
14. **Merbs, C., F. Trauma.** Reconstruction of Life (Eds. M.Y. Iscan, K. Kennedy), New York, Alan R. Liss, 1989, 161-189.
15. **Mihailov, S.** Ctitor portrait in Kremikovtsi church in light of the Bulgarian-Romanian cultural relations in the fifteenth century. – *Archaeology,* **2,** 1960, 23-29 [in Bulgarian].
16. **Ortner, D. J., J. Putschar.** Identification of pathological conditions in human skeletal remains. Washington, Smithsonian Institution Press, 1981, 499 p.
17. **Paskaleva-Kabadieva, K.** The church "St. George" in Kremikovtsi Monastery. Sofia, Publishing house Bulgarian artist, 1980, 164 p. [in Bulgarian].
18. **Pearson, K.** Mathematical Contributions to the Theory of Evolution. V. On the Reconstruction of the Stature of Prehistoric Races. - *Philosophical Transactions of the Royal Society of London. Series A, Containing Papers of a Math. or Phys. Character (1896-1934),* **192,** 1899, 169-244.
19. **Pobornikova, R.** New archeological studies of three medieval monasteries from Sofia. – *Serdica – Sredetc - Sofia,* **2,** 1994, 117-144 [in Bulgarian].
20. **Pobornikova, R.** Archaeological excavations in naos of the medieval church „St. George" in Kremikovtsi Monastery. - *Contributions to Bulgarian Archeology,* **III-IV,** 2006, 173-179 [in Bulgarian].
21. **Protich, A**. A portrait model for Bulgarian masters in 18th-19th century. - *Yearbook of the National Museum,* **4,** 1922, 21-25 [in Bulgarian].
22. **Protich, A.** Denationalization and revival of our art from 1393 to 1879. - *Bulgaria 1000 years, 1930,* 434-435 [in Bulgarian].
23. **Ruff, C. B., W. W. Scott, A. Y. Liu.** Articular and diaphyseal remodeling of the proximal femur with changes in body mass in adults. - *Am. J. Phys. Anthropol.,* **86**(3), 1991, 397–413.
24. **Shindarov, I.** Some notes about Kremikovtsi Monastery near Sofia. - *Collection of folk perceptions,* **XV,** 1898, 304-309 [in Bulgarian].
25. **Stull, K., D. James.** Determination of age-at-death using the acetabulum of the os coxa. - *In: Age Estimation of the Human skeleton* (Eds. K. Latham, M. Finnegan), Springfield, 2010, 134-146.

26. **Todorov, V., N. Atanassova.** Archaeological excavations at Kremikovtzi Monastery "Saint George The Victorious", Sofia municipality, "Kremikovtzi" district. - *A*rchaeological Discoveries and Excavations in 2015. 2016, 748-750 [in Bulgarian, with English summary].
27. **Tood, T. W.** Age changes in the pubic bone I: the male white pubic. - *American Journal of Physical Anthropology,* **3,** 1920, 285-334.
28. **Tranteev, B.** The church "St. George" in PI with identifier 68134.8229.9 at Manastirsky livadi locality, Kremıvotzi district, Sofia city. - *Archaeological Discoveries and Excavations in* 2014. **2015,** 765-766 [in Bulgarian].
29. **Trotter, M., G. Gleser.** Estimation of Stature from Long Bones of American Whites and Negroes. - *American Journal of Physical Anthropology,* **10,** 1952, 463-514.
30. **Valois, H. V.** L'omoplate humaine: Étude anatomique et anthropologique. - *Buletins et Mémoires de la Société d'Anthropologie de Paris,* **3,** 1932, 3-153.
31. **Vaquero-Picado, A., R. Barco, S. A. Antuña.** Lateral epicondylitis of the elbow. - *EFORT Open Rev,* **1,** 2016, 391-397.
32. **Zubov, A.** Odontology. Methods of anthropological investigations. Moscow, Nauka, 1968, 200 p. [in Russian].
33. **Unknown author.** Description of Kremikovtsi Monastery "St. George". - *Religious stories,* **9-10,** 1896, 376-384 [in Bulgarian].

Institute of Experimental Morphology, Pathology and Anthropology with Museum
Bulgarian Anatomical Society

Acta morphologica et anthropologica, 25 (1-2)
Sofia ● 2018

An Anthropological Characteristic of the Distribution of Adipose Connective Tissue in Elderly Bulgarian Females with Type 2 Diabetes Mellitus

*Atanas Baltadjiev**

Department of Anatomy, Histology and Embryology, Faculty of Medicine, Medical University, Plovdiv, Bulgaria

* Corresponding author e-mail: dr_atanas@abv.bg

The purpose of this study was to investigate the distribution of adipose connective tissue in Bulgarian females with T2DM. Subjects: 120 women suffering from T2DM, with age range 61-80 years. Control group: 40 Bulgarian women at the same age range. Measured parameters: height, weight, 9 skinfolds (sf) - sfTriceps, sfBiceps brachii, sfForearm, sfSubscapular, sfXrib, sfAbdomen, sfSuprailiaca, sfThigh, and sfCalf; Bioelectrical Impedance analysis - % body fat tissue and visceral fat tissue. Calculated indexes: BMI, ratio sfTrunk/sfLimbs, ratio skin folds upper half of body/skin folds lower half of body, fat mass and subcutaneous fat mass. Statistically significant differences were found between the means of weight, sfTriceps, sfSuprailiaca, sfAbdomen, sfThigh, sfCalf and subcutaneous fat mass between the diabetic and healthy women. In diabetic females aged 61-80 years the model of subcutaneous adipose tissue distribution was mostly in the upper torso region and less in the limbs. In controls the accumulation of adipose tissue was mostly in the limbs and in the lower part of the body.

Key words: T2DM, females, adipose tissue, distribution

Introduction

In the recent years, Type 2 diabetes mellitus (T2DM) is gaining more signs of social problem due to the rapidly growing number of people affected by the disease worldwide [13]. The number of diabetes mellitus patients in Europe is expected to increase from 52 millions in 2014 to 68.9 millions by 2035, mostly due to increases in overweight and obesity, unhealthy diet and physical inactivity, according to the International Diabetes Federation. Across Europe, around 1 in 11 adults is affected and this number is set to rise as the population ages. It's about 10.3% of men and 9.6% of women aged 25 years and over. In Bulgaria around 8-9% of the population suffers from the disease.

The most researchers are interested in etiology, pathogenesis, clinical course and treatment of the disease. The anthropological status of diabetic patients enjoys little attention. The fat accumulation in the body of diabetic patients occurs primarily in two locations: in the abdomen (central, abdominal, visceral) and subcutaneously (peripheral).

Fat accumulation in the abdominal area is commonly associated with increased risk for T2DM [2, 6, 12, 19]. Not much research has been performed on the subcutaneous distribution of adipose tissue. World literature offers little data on the complex deposition of adipose tissue in patients with T2DM. The purpose of this study was to investigate the distribution of adipose tissue in 61-80 years old Bulgarian females with T2DM.

Matherials and Methods

Subjects of the study were 120 women suffering from T2DM. They were diagnosed by a diabetes specialist and recruited from the Clinic of endocrinology of St. George University Hospital at the Medical University of Plovdiv, Bulgaria. The inclusion criteria were: Bulgarian ethnicity, duration of the disease of not less five years, compensated diabetes at the time of the study, age range 61-80 years (mean 68.95 ±0.57 SEM). The control group included 40 women at the same age range (mean 69.85 ±0.95 SEM). An ethical approval was taken for this study. Informed consents were taken from all patients involved in the study.

The exclusion criteria were: previous or existing metabolic, oncological and other disorder that could compromise the anthropological study. The anthropological methods included:

Directly measured parameters: The body height and body weight, skinfold (sf) thicknesses were measured at 9 locations – sfTriceps, sfBiceps (brachii), sfForearm, sfSubscapular, sfXrib, sfAbdomen, sfSuprailiaca, sfThigh, and sfCalf, using Harpenden Skinfold Calipers (British Indicators Ltd) at standard sites on the right side of the body.

Bioelectrical Impedance analysis (BIA): body fat tissue and visceral fat tissue percent (%) - was measured with a Body Composition Monitor Tanita. BC-532.

Calculated indexes: Body mass index (BMI); sfTrunk/sfLimbs ratio; skinfolds upper half of body/skinfolds lower half of body ratio; fat mass and subcutaneous fat mass.

Statistical analysis. Data were analyzed using statistical software SPSS version 15 (SPSS Inc., Chicago, IL). Parametric statistical methods were relevant. Independent Samples t-Test was used to compare the means of two independent anthropologic parameters in order to determine whether there was statistical evidence that the means were significantly different. The one-way analysis of variance (ANOVA) was used to determine whether there were any significant differences between the means of three or more independent parameters. $P<0.05$ (two tailed) was considered statistically significant. We used Pearson's correlation to assess associations between variables, and Pearson's correlations coefficient (PC) was calculated. The value of the coefficient was used to rate the correlation's strength: low correlation – 0.01-0.30; moderate – 0.30-0.50; strong 0.50-0.70; high – 0.70-0.90; very high >0.90. $P<0.05$ (two tailed) was considered statistically significant.

Results

In the present study significant differences were found between the means of **weight**- the mean value of the diabetic females was higher than the controls ($p<0.05$) and between the means of **height** – the mean value of the diabetic women was higher than the controls ($p<0.001$) **(Table 1)**.

The thickness of **sfTriceps** (brachii) of the diabetic females was significantly lower than the controls ($p<0.05$). The former, however was significantly thicker in comparison to sfBiceps, sfForearm and sfSuprailiaca of diabetic females, but significantly thinner than sfSubscapular, sfXrib and sfAbdomen (ANOVA, $p<0.05$). The correlation

Table 1. Anthropological parameters of elderly Bulgarian females aged 61-80 years with Type 2 diabetes mellitus compared to healthy controls at the same age

	Type 2 diabetes mellitus				Controls				
Parameters	N	Mean	SEM	SD	N	Mean	SEM	SD	P
Age (years)	120	68.95	0.57	5.80	40	69.85	0.95	5.88	>0.05
Height (cm)	120	156.94	0.45	4.66	40	153.93	0.89	5.51	**<0.001***
Weight (kg)	120	75.79	1.13	11.54	40	71.11	2.05	12.64	**<0.05***
sf Triceps (mm)	120	21.88	0.98	8.94	40	25.89	1.46	9.22	**<0.05***
sf Subscapular (mm)	120	24.82	1.20	10.18	40	27.22	1.85	11.38	>0.05
sf X rib (mm)	120	25.36	0.94	7.95	40	23.12	1.51	9.33	>0.05
sfSuprailiaca (mm)	120	18.59	0.78	6.60	40	22.01	1.51	9.28	<**0.05***
sfAbdomen (mm)	120	28.89	1.03	8.80	40	37.22	1.80	11.08	**<0.001***
sfBiceps (mm)	120	12.12	0.59	4.98	40	13.15	0.86	5.29	>0.05
sfForearm (mm)	120	10.71	0.42	3.60	40	10.38	0.66	4.07	>0.05
sfThigh (mm)	120	21.73	1.45	12.29	40	38.15	1.82	11.19	**<0.001***
sfCalf (mm)	120	19.66	1.08	9.18	40	26.79	1.24	7.65	**<0.001***

sf = skinfold

analysis revealed positive correlations ($p<0.05$) between the thicknesses of sfTriceps and other skinfolds, as follows: the correlations were high to sfForearm, sfSubscapular and sfXrib (r = 0.70-0.90); strong - to sfBiceps and sfAbdomen (r = 0.50-0.70) and moderate to sfSuprailiaca (r = 0.48).

The thickness of sfSubscapular in the diabetic females was not significantly different in comparison to the controls ($p>0.05$). The sfSubscapular of diabetic women was significantly thicker in comparison to sfTriceps, sfBiceps, sfForearm, sfSuprailiaca and sfCalf of the same women (ANOVA, $p<0.05$). The sfSubscapulare was significantly thinner than sfAbdomen.The correlation analysis revealed positive significant correlations ($p<0.05$) between the thicknesses of sfSubscapular and other skinfolds, as follows: high correlations to sfForearm, sfTriceps, sfXrib, sfSuprailiaca (r = 0.70-0.90); strong correlations to sfBiceps, sfAbdomen, and sfThigh (r = 0.50-0.70).

The thickness of sfXrib in the diabetic females was not significantly higher than the healthy controls ($p>0.05$). The sfXrib of diabetic women was significantly thicker compared to sfTriceps, sfBiceps, sfForearm, sfSuprailiaca, sfThigh and sfCalf of the same women, but it was thinner than sfAbdomen (ANOVA, $p<0.05$). The correlation analysis revealed significant positive correlations ($p<0.05$) between the thicknesses of sfXrib and other skinfolds, as follows: high correlations to sfTriceps, sfForearm and sfSubscapular (r = 0.70-0.90); strong correlations to sfBiceps, sfAbdomen, sfSuprailiaca and sfThigh (r = 0.50-0.70); moderate to sfCalf (r = 0.41).

A statistically significant difference was found in the thicknesses of **sfSuprailiaca** between the diabetic females and healthy controls ($p<0.05$). It was thicker in the healthy controls than in the diabetic females. The sfSuprailiaca of diabetic women was thicker in comparison to sfBiceps and sfForearm of the same women, but it was thinner than sfTriceps, sfSubscapular, sfXrib and sfAbdomen (ANOVA, $p<0.001$). The correlation analysis revealed positive correlations between the thicknesses of sfSuprailiaca and other skinfolds, as follows: high correlations to sfSubscapular and sfAbdomen in the same topographical area (r = 0.74-0.79); strong correlations to sfXrib, sfForearm and sfBiceps (r = 0.50-0.70); moderate - to sfThigh and sfTriceps.

A statistically significant difference was found in the thicknesses of **sfAbdomen** between the diabetic females and healthy controls ($p<0.001$). It was thicker in the healthy controls than in the diabetic females. The sfAbdomen was significantly the thickest skinfold among all studied skinfolds in the diabetic women. (ANOVA, $p<0.05$). The correlation analysis revealed positive correlations between the thicknesses of sfAbdomen and other skinfolds ($p<0.05$), as follows: high correlation to sfSuprailiaca and sfBiceps ($r = 0.70-0.90$); strong - to sfTriceps, sfForearm, sfXrib, sfSubscapular and sfThigh ($r = 0.50-0.70$); moderate - to sfCalf.

The thickness of sfBiceps in the diabetic females was lower than the controls, but the difference did not statistical significance ($p>0.05$). The sfBiceps was thicker than the sfForearm of diabetic women, however it was thinner than the other skinfolds of the same women (ANOVA, $p<0.05$). The correlation analysis revealed positive significant correlations to the thicknesses of the studied skinfolds ($P<0.05$). The correlations were high to sfForearm, sfAbdomen and sfThigh ($r = 0.70-0.90$); strong - to sfXrib, sfTriceps, sfSubscapular, sfSuprailiaca and sfCalf ($r = 0.50-0.70$).

The thickness of **sfThigh** in the diabetic females was significantly lower than the controls ($p<0.001$). It was thicker in comparison to the sfForearm and sfBiceps, but thinner than sfAbdomen and sfXrib (ANOVA, $p<0.05$). The correlation analysis revealed positive correlations between the thickness of **sfThigh** to the other studied skinfolds ($P<0.05$). The correlations were high to sfBiceps ($r = 0.73$) and sfCalf ($r = 0.84$); strong - to sfTriceps, sfForearm, sfXrib, sfSubscapular, sfAbdomen ($r = 0.50-0.70$); moderate – to sfSuprailiaca.

There was not found a significant difference in the thicknesses of sfForearm between diabetic females and healthy controls ($p>0.05$). The sfForearm was the thinnest among the other studied skinfolds (ANOVA, $p<0.05$). The correlation analysis revealed several positive significant correlations of the sfForearm thickness to the other skinfolds ($p<0.001$), except sfCalf. The correlations were high to sfBiceps, sfTriceps, sfSuprailiaca and sfXrib ($r = 0.70-0.90$); strong to sfAbdomen, sfSubscapular and sfThigh ($r = 0.50-0.70$).

The thickness of **sfCalf** in the diabetic females was significantly lower than in the healthy controls ($p<0.001$). It was thicker than sfForearm and sfBiceps, but it was thinner than sfSubscapular, sfXrib and sfAbdomen (ANOVA, $p<0.05$). The correlation analysis revealed positive correlations of the sfCalf thickness to the other skinfolds ($p<0.05$). The correlation was strong to sfBiceps ($r = 0.55$); moderate to sfXrib and sfAbdomen ($r = 0.30-0.50$).

The accumulation of subcutaneous adipose tissue in patients with Type 2 diabetes mellitus was higher in the torso, than in the limbs. In contrast, the controls exhibited the opposite distribution. In women with Type 2 diabetes mellitus the accumulation of subcutaneous adipose tissue was larger in the upper half of the body, than in the lower half. The controls exhibited the opposite distribution **(Table 2).**

Body composition parameters' results, investigated by Bioelectrical Impedance analysis revealed that the values of the **subcutaneous fat tissue** in the controls were significantly higher compared to those of diabetic women ($p<0.001$).

We didn't detect any significant differences in other body composition parameters: % body fat tissue, visceral fat tissue and fat mass ($p>0.05$) between the diabetic females and healthy controls. It wasn't detected any significant difference in the BMI-indexes between both groups too ($p>0.05$). **(Table 3)**

The data concerning the fat tissue components determinates the body composition of diabetic patients as an important parameter regarding the prognosis of the T2DM.

Table 2. Anthropological indices of elderly Bulgarian females aged 61-80 years with Type 2 diabetes mellitus compared to healthy controls at the same age

	Type 2 diabetes mellitus	Controls
sf trunk/sf limbs	1,22	0,96
sf upper half of the body/ sf lower half of the body	1,11	0,79

sf = skinfold;

Table 3. Body composition of elderly females aged 61-80 years with Type 2 diabetes mellitus compared to healthy controls at the same age

	Type 2 diabetes mellitus				Controls				
Parameters	N	Mean	SEM	SD	N	Mean	SEM	SD	P
BMI	120	30.77	0.44	4.55	40	30	0.80	4.91	>0.05
% body fat tissue	120	41.34	0.86	5.4	40	40.02	1.18	7.26	>0.05
Visceral fat tissue (kg)	120	11.74	0.38	2.35	40	11.4	0.49	3.01	>0.05
Fat mass (kg)	120	31.87	1.36	9.87	40	29.87	1.66	10.48	>0.05
Subcutaneous fat mass (kg)	92	14.44	0.26	2.85	40	17.56	0.45	2.85	**<0.001***

BMI = Body mass index

Discussion

It has been found that abdominal obesity, also known as central or visceral obesity, was more closely related to T2DM than the general obesity. The visceral fat was more metabolically active and produced more insulin resistance (3, 4, 16, 18). Similar data we observed in Bulgarian women aged 40-60, with a diagnosis T2DM. The means of the % body fat tissue, visceral fat tissue and fat tissue were statistically higher in these women with T2DM than in the healthy controls.

It was not found any significant differences in the mentioned parameters between the age group 61-80 years with T2DM and the healthy controls, except the accumulation of subcutaneous fat tissue. It was detected a tendency only, that the values of the mentioned parameters were higher in the diabetic group than the healthy controls ($p>0.05$). It can be explained with the aging of the body in this age group.

Attention should be paid to the distribution of subcutaneous adipose tissue in female patients with T2DM. It was found that in patients with T2DM the accumulation of subcutaneous adipose tissue was mostly in torso and less so in the limbs. Moreover,

the accumulation of adipose tissue consisted predominantly in the upper part of the body compared to the lower, the so-called "apple shaped". These patients have a worse anthropological status, which would lead to a more severe clinical course of the disease [5, 20, 11, 14]. It was considered that this type of obesity increased the risk of pathological changes in other systems, along with the progress of T2DM [10, 9, 8].

In controls the deposition of adipose tissue was predominantly in the limbs and mainly in the lower part of the body, the so-called "pear shaped". An interest induced that skinfolds from topographically neighboring areas were in a stronger correlation with each other than skin folds from distant topographical areas. Some authors have reported the importance of adipose tissue accumulation in the anterior abdominal wall [15]. In this investigation the sfAbdomen was the thickest, compared to the other studied skinfolds in patients with T2DM and the thickness was significant greater in the controls than in the diabetic group. Moreover, significantly greater thickness was measured in some skinfolds in the control group than in the corresponding skinfolds in patients with T2DM: sfTriceps, sfSuprailiaca, sfAbdomen, sfThigh and sfCalf. These facts confirmed the greater importance of the accumulation of visceral than of subcutaneous fat for the course of the disease [7].

The levels of total body weight were higher in diabetic women. They showed that women with T2DM were overweight and fattened compared to healthy controls, but these values had less importance to the course of the disease compared with the above-described parameters [17]. More original data about the anthropological status of Bulgarian patients with T2DM were published in other our publications [1].

This study is part of a larger survey including female patients 40-60 and 61-80 years as well as male patients from both age groups in Bulgaria. The anthropological parameters provided a large data base, specific for Bulgarian population. Using the anthropological parameters it will be possible to calculate the components of the somatotype by Heath and Carter method of somatotyping, as well as other indexes. They will reveal the anthropological status of Bulgarian patients suffering from T2DM.

Conclusion

The body composition of diabetic females aged 61-80 years contained a larger common adipose component than the controls. The study revealed that the accumulation of subcutaneous fat tissue was significant more in the body of healthy controls than the patients ($p<0.001$). The subcutaneous adipose tissue was accumulated mostly on the upper part of the torso than the lower and predominant in torso than in the limbs.

In the group of healthy women (controls) the subcutaneous adipose tissue was accumulated mostly in the peripheral part of the body (arms, thighs and lower legs) and mostly in the lower half of the body than in the upper half of the body.

The bioelectrical impedance analysis of the body composition in this age group didn't demonstrate any significant differences between the female patients suffering from T2DM and healthy women.

The complex study including anthropometry of adipose tissue in women suffering from T2DM would support the evaluation of the clinical course, treatment and prognosis of the disease.

This article is containing original research and has not been submitted/published earlier in any journal and is not being considered for publication elsewhere.

This research did not receive any specific grant from any funding agency in the public, commercial or not-for-profit sector.

References

1. **Baltadjiev, A.** Morpho-anthropological characteristics of patients with type 2 Diabetes mellitus. Monograph, Plovdiv, MU-Plovdiv; 2015.
2. **Folsom, A. R., L. H. Kushi, K. E. Anderson, P. J. Mink, J. E. Olson, C. P. Hong, T. A. Sellers, D. Lazovich, R. J. Prineas.** Associations of general and abdominal obesity with multiple health outcomes in older women: the Iowa Women's Health Study. - *Arch. Intern. Med.,* **160,** 2000, 2117-2128.
3. **Goodpaster, B. H., F. L. Thaete, D. E. Kelley.** Thigh adipose tissue distribution is associated with insulin resistance in obesity and in type 2 diabetes mellitus. - *Am. J. Clin. Nutr.,* **71**(4), 2000, 885 - 892.
4. **Hauner, H.** Managing type 2 diabetes mellitus in patients with obesity. - *Treat Endocrinol.,* **3**(4), 2004, 223-232.
5. **Heshka, S., A. Ruggiero, G. A.Bray, J. Foreyt, S. E. Kahn, C. E. Lewis, M. Saad, A. V. Schwartz.** Altered body composition in type 2 diabetes mellitus. - *Int. J. Obes.,* **32**(5), 2008, 780-787.
6. **Janssen, I, P. T. Katzmarzyk, R. Ross.** Waist circumference and not body mass index explains obesity-related health risk. - *Am. J. Clin. Nutr.,* **79**(3), 2004, 379-384.
7. **Jørgensen, M. E., K. Borch-Johnsen, R. Stolk, P. Bjerregaard.** Fat distribution and glucose intolerance among Greenland Inuit. - *Diabetes Care,* **36**(10), 2013, 2988-2994.
8. **Jung, C. H., B. Y. Kim , K. J. Kim, S. H. Jung, C. H. Kim, S. K. Kang, J. O. Mok.** Contribution of subcutaneous abdominal fat on ultrasonography to carotid atherosclerosis in patients with type 2 diabetes mellitus. - *Cardiovasc. Diabetol.,* **13,** 2014, 67.
9. **Kim, S .R., J. H.Yoo , H. C. Song, S. S Lee, S. J. Yoo, Y. D. Kim, Y. S. Lim, H. W. Kim, C. W. Yang, Y. S. Kim, E. J. Choi, Y. K. Kim.** Relationship of visceral and subcutaneous adiposity with renal function in people with type 2 diabetes mellitus. - *Nephrol. Dial Transplant.,* **26**(11), 2011, 3550-3555.
10. **Kim, T. H., S. S. Lee, J. H. Yoo, S. R. Kim, S. J.Yoo, H. C. Song, Y. S. Kim, E. J. Choi, Y. K. Kim.** The relationship between the regional abdominal adipose tissue distribution and the serum uric acid levels in people with type 2 diabetes mellitus. - *Diabetol. Metab. Syndr.,* **4**(1), 2012, 3.
11. **Livingston, E.H.** Lower body subcutaneous fat accumulation and diabetes mellitus risk. - *Surg. Obes. Relat. Dis.,* **2**(3), 2006, 362-368.
12. **Meisinger, C., A. Döring, B. Thorand, M. Heier, H. Löwel.** Body fat distribution and risk of type 2 diabetes in the general population: are there differences between men and women? The MONICA/KORA Augsburg cohort study. - *Am. J. Clin. Nutr.,* **84**(3), 2006, 483-489.
13. **Melmed, S, S. Kenneth, P. Polonsky, P. R. Larsen, H. M. Kronenberg.** Principles of Endocrinology. *In: Williams textbook of endocrinology,* Philadelphia: Elsevier/Saunders, **12**(1), 2011, 1371–1435.
14. **Patel, P., N. Abate.** Body fat distribution and insulin resistance. – *Nutrients,* **5**(6), 2013, 2019-2027.
15. **Ristic, P., D. Bokonjic, V. Zivkovic, V. Jakovljevic, M. Zdravkovic, J. Pejovic, D. Ristic, J. Mladenovic.** Subcutaneous adipose tissue measurements and better metabolic prediction. – *Centr. Eur. J. Med.,* **8**(2), 2013, 237-243.
16. **Sam, S., S. Haffner, M. H. Davidson, R. B. D'Agostino, S. Feinstein, G. Kondos, A. Perez, T. Mazzone**. Relationship of abdominal visceral and subcutaneous adipose tissue with lipoprotein particle number and size in type 2 diabetes. - *Diabetes,* **57**(8), 2008, 2022-2027.
17. **Shirafkan, A., A. Marjani.** Prevalence of obesity among type 2 diabetes mellitus in Gorgan (South East of Caspian Sea), Iran. - *World Applied Sciences Journal,* **14**(9), 2011, 1389-1396.
18. **Shrestha, O. K, G .L. Shrestha.** Visceral fat versus subcutaneous fat: comparison of their association with type 2 diabetes mellitus. - *Journal of Chitwan Medical College,* **4**(2), 2014, 9-12.
19. **Snijder, M. B., R. M. van Dam, M. Visser, J. C. Seidell.** What aspects of body fat are particularly hazardous and how do we measure them? - *Int. J. Epidemiol.,* **35**(1), 2006, 83-92.
20. **Tafeit, E., R. Möller, T. R. Pieber, K. Sudi, G. Reibnegger.** Differences of subcutaneous adipose tissue topography in type-2 diabetic (NIDDM) women and healthy controls. - *Am. J. Phys. Anthropol.,* **113**(3), 2000, 381-388.

Institute of Experimental Morphology, Pathology and Anthropology with Museum
Bulgarian Anatomical Society

Acta morphologica et anthropologica, 25 (1-2)
Sofia ● 2018

Aortic Arch Aneurysm Represented by a 3D Printing and Simulation of Fluid Movement through It

Ivan Maslarski[1], Yordan Hodzhev[2], Galin Gyulchev[3]*

[1] Anatomy, Histology, Pathology and Forensic Medicine, Faculty of Medicine, SU "St. Kliment Ohridski", Sofia, Bulgaria
[2] Microbiology Laboratory, Institute of Soil Science, Agrotehnologies and Plant Protection "Nikola Pushkarov", Sofia, Bulgaria
[3] Physics, Biophysics and Rentgenology, Faculty of Medicine, SU "St. Kliment Ohridski", Sofia, Bulgaria

* Corresponding author e-mail: maslarsky@gmail.com

Degeneration of the human aorta can occur in the thoracic, abdominal and arch region. Rarely this kind of disease happen in the arch region of aorta closer to the semilunar valve. By definition, an aneurysm is a localized dilation of an artery with a diameter at least 50% greater than normal size. The main objective of the study is to recreate the 3D model of the heart with real aortic arch aneurysm and successive simulation of fluid movement in it and demonstrate a difficulty in the conductivity of the vessel.
Successful testing of a 3D model based on real data of aneurism and achieved with great precision through 3D printing. A satisfactory result has been obtained demonstrating the degree of functional predicament of the aorta in this rare type of aneurysm.

Key words: aortic arch aneurysm, 3D print models, heart anatomy, vascular disorders

Introduction

By definition, an aneurysm is a localized dilation of an artery with a diameter at least fifty percent greater than normal size. This often occurs at human aorta in thoracic, abdominal and arch regions. Relatively more rare the aneurysm affects arch region closer to the semilunar valve. However, it is important condition because ascending aortic aneurysm may be fatal due to its liability to dissect or rupture due to intense blood pressure [5].

3D anatomical models are used like educational method and clinical training of medical students while they study anatomy, physiology and surgery. Simulation based training with 3D models are useful and help recognize the morphology and symptoms of the specific disease such as aneurysm [3]. 3D anatomical models can be computer-generated images from medical data by Computed Tomography (CT), or Magnetic Resonance Imaging (MRI). Another source of 3D anatomical models are 3D surface scanners, printers, skeletal collections, etc.

The main goal of this investigation is: to model the fluid dynamics during aortic arch aneurysm and compare it to normal condition by building realistic 3D model of heart with and without ascending aortic aneurysm and compare model results from simulation of fluid dynamics [1]. We hypothesize that fluid flow measured entering left atrium will differ dramatically by means of speed and pressure between aneurysmal and normal heart models.

Materials and Methods

Tubing model.Two flexible plastic hearts in norm and pathology were digitally rendered and 3D printed. Those were attached to blood flow simulator made by flexible silicone tubes. Fluid flow parameters at specific locations before and after aneurim were measured by flow sensors and were recorded by Arduino Uno-based computer [3]. The three-dimensional heart models are 3D printed with a precision monochrome 3D printer of the Kossel Delta Mini type, using Flexible PLA representing viscoelastic biodegradable plastic material. A melting temperature of the filament is 205 °C, as a print speed of 20 mm/s is used. The experimental set is composed of the 3D printed plastic models of the hearth with normal aortic arch and of the hearth with aortic arch aneurysm, water pump, water flow sensor, water preassure sensor, flexible silicon tubes and plastic tube connectors.

Numerical model. Fluid pressure and particle velocity were measured accordingly. The numerical simulation of fluid gives information about the severity of the impairment of circulatory flow in the arch caused by vortices [5]. This was performed by fluid flow simulation in the software Abaqus 6.1 using surface mesh models of the 3D hearts and computational fluid dynamics module.

Results

Precisely 3D printed models, based on real arch aneurism data,which were the subject of the test, showed increased turbulence in the pathology as compared to normal conditions. It can be seen from the diagram shown on **Fig. 1**. Additionally, a concept of proof for numerical modeling was established.Tubing model represents innterplay bettween physics, anatomy and physiology, focused in particular in fluid- and hemodynamics resistance in large circle of blood circulation in norm and pathology. In this investigation we use a realistic 3D model based on printed medical data from MRI, as it can be seen on **Fig. 2** and **Fig. 3.** The model was useful for medical students, helping them imagine the pathology of the area of aorta arch.

Discussion

We experienced a number of difficulties during the experiment. In the construction of the heart shows that the internal heart morphology does not correspond to the true structure, but the external is realistic and credible. The model has been enforced with a pump in order to stimulate fluid movements without the presence of heart valves.The model of the aortic artery aneurysm is from anactualpatient and allows to create realistic 3D model. The scan we used had the data of the external morphology of the heart and the characteristic pathology of the aorta arch. There is no complete data collected from the main vessels. That was the reason we decided to use the aortic arch as well as a few centimeters of the data available on the cava veins, lung veins and pulmonary trunk.

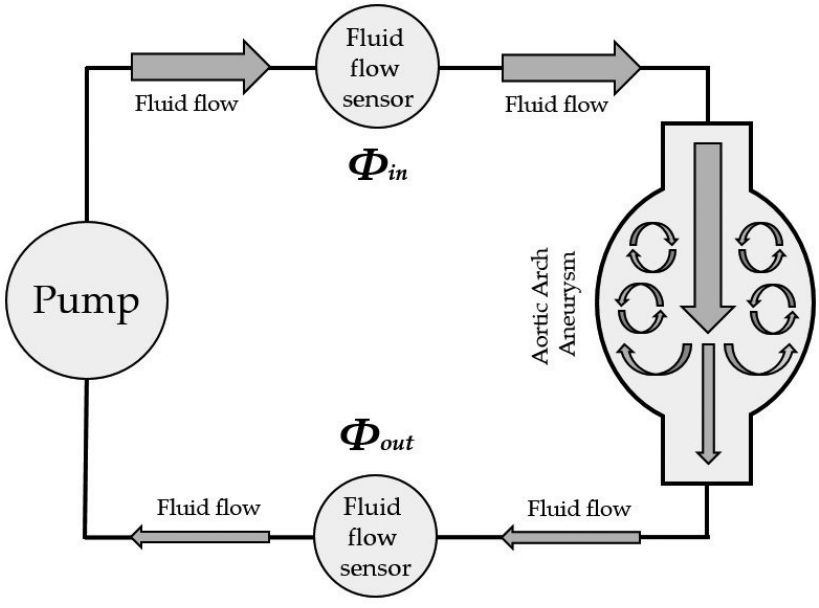

Fig. 1. Diagram of the principle circuit for fluid flow rate measuring in aortic arch

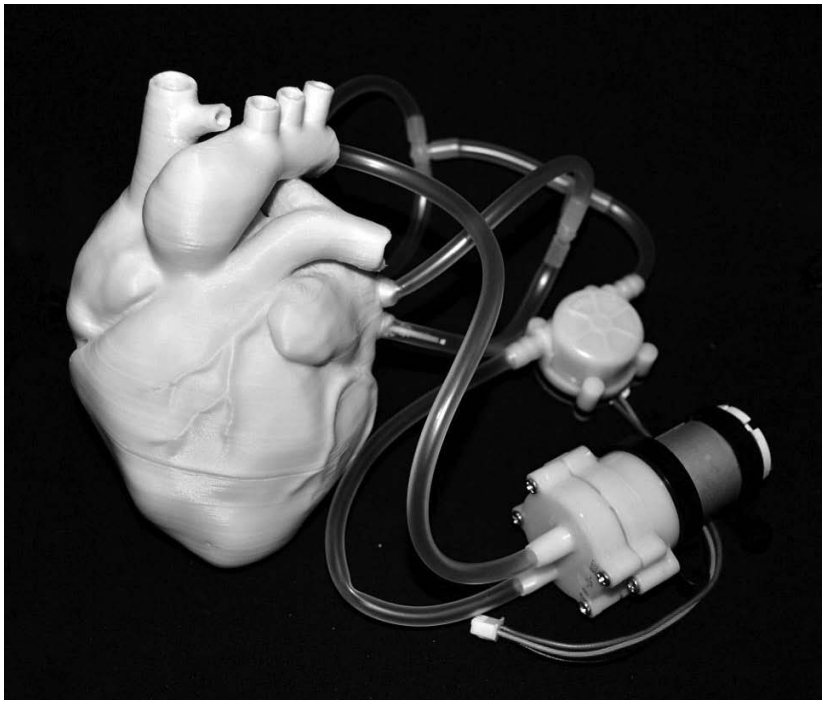

Fig. 2. 3D model of a circuit for fluid flow rate measuring in aortic arch aneurysm

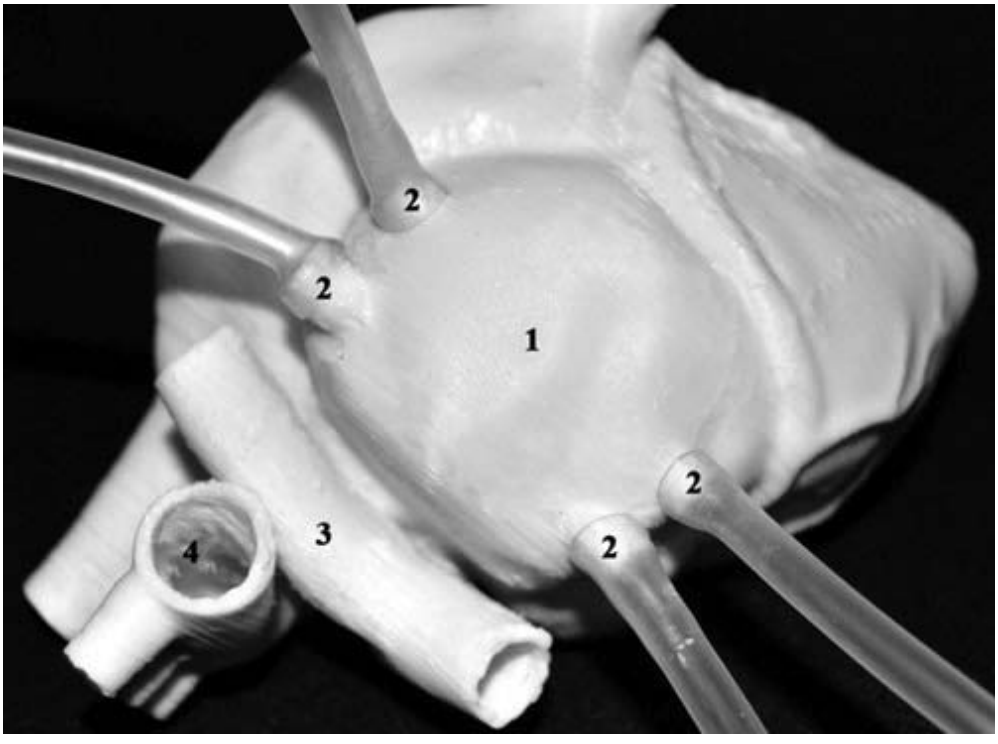

Fig. 3. Connection of the silicon tubes with 3D printed human heart. 1- left atrium, 2 - pulmonary veins, 3 - pulmonary trunk, 4 - aorta.

Another problem occurred while choosing the printing material for the heart and, respectively, the blood vessels. We used not transparent and less elastic material. The model was equipped with an electrical motor, silicone tubes and flow sensor. For fluid we used saline. We used computer program to change the problematic part of the aorta creating second model in order to study the differences in the fluid dynamics of the saline. The fluid model shows reduced blood flow passing through the aorta. The main reason for that is the creation of the vortex fluid movements, which are fed primarily by the kinetic energy of the main fluid flow. A major consequence of this, is a reduction of the velocity and blood flow rate through the aorta. To compensate this shortage the cardiac muscle contractions becomes more powerful and needs more energy consumption. The long term effect of this disease leads to overloading of the heart muscle and causes disruption of the normal function.

The results apparently showed "vortexing" and slowing down the fluid's rate in the area of aortic aneurysm. The deviation of the norm in the movements of the fluid and the reasons for its delay can be observed macroscopic. In our opinion, these models, although without the characteristic of internal heart morphology, can improve motivation and knowledge of medical students related to vascular diseases. Each fluid dynamic model has better training potential than schemes and images and allows to open a new chapter in the scientific research. The 3D modeling of blood vessels could be used in different anatomical areas. This will help to study and actually visualize the presence of thrombosis of varicose disease. The model described in this manuscript could be used together with color duplex of the blood and Doppler check of the blood velocity.

References

1. **Bongert, M., M. Geller, W. Pennekamp, V. Nicolas.** Simulation of personalisedhaemodynamics by various mounting positions of a prosthetic valve using computational fluid dynamics. - *Biomed. Tech.* (Berlin), 2018 bmt-2017-0092.
2. **Dahlberg, T., T. Stangner, H. Zhang, K. Wiklund, P. Lundberg, L. Edman, M. Andersson.** 3D printed water-soluble scaffolds for rapid production of PDMS micro-fluidic flow chambers. - *Scientific Reports*, 2018, doi: 10.1038/s41598-018-21638-w.
3. **Sharzehee, M., S. S. Khalafvand, H. C. Han.** Fluid-structure interaction modeling of aneurysmal arteries under steady-state and pulsatile blood flow: a stability analysis. - *Computer Methods in Biomechanics and Biomedical Engineering*, 2018, doi: 10.1080/10255842.2018.1439478.
4. **Tam, M. D., S. D. Laycock, J. R. Brown, M. Jakeways.** 3D printing of an aortic aneurysm to facilitate decision making and device selection for endovascular aneurysm repair in complex neck anatomy. – *J. Endovasc. Ther.,* 2013, doi: 10.1583/13-4450MR.1.
5. **Tenorio, E. J. R., A. F. F. Braga, D. P. D. C. Tirapelli, M. S. Ribeiro, C. E. Piccinato, E. E. Joviliano.** Expression in whole blood samples of miRNA-191 and miRNA-455-3P in patients with abdominal aortic aneurysm and their relationship to clinical outcomes after endovascular repair. - *Ann. Vasc. Surg.*, 2018, doi: 10.1016/j.avsg.2018.01.086.

Institute of Experimental Morphology, Pathology and Anthropology with Museum
Bulgarian Anatomical Society

Acta morphologica et anthropologica, 25 (1-2)
Sofia ● 2018

Unusual Findings during Upper Limb Dissection

Stoyan Novakov[1], Nina Yotova[1], Ivan Hristov[1], Stefan Prisadov[2]*

[1] Department of Anatomy, Histology and Embryology,
[2] Student, Medical Faculty, Medical University, Plovdiv, Bulgaria

* Corresponding author: e-mail: stoyan67@gmail.com

Human anatomy is a fundamental subject of medical curriculum. Teaching normality is not always easy and persuasive, especially when variations appear in gross anatomy lab. The knowledge of the 'full' anatomy though neglected and is important for the future practice of the undergraduates from first and second year. In an unforced study we describe a number of varieties on upper limbs found during limb dissection in the first semester at anatomy department. Two out of ten limbs showed unusual pattern of an artery, a nerve and a muscle. The first case was an upper limb with a superficial ulnar artery in the forearm. In the second case a third head of biceps brachii muscle coexists associated to communication of musculocutaneous with median nerve. The morphological features and the prevalence of these cases are presented, besides the discussion of its clinical significance.

Key words: human anatomy variation, musculocutaneous nerve, third head of biceps brachii, superficial ulnar artery

Introduction

It is known that anatomy is an ancient science. It is not only part of the base and the beginning of the medicine but it comes before it in searching the knowledge of human morphology [11]. The Latin word normalis means conforming to the rule or pattern. Norma is the Latin name for a carpenter's square; it is used in descriptive anatomy to indicate the standard or normal appearance of a structure [9]. In anatomy, normal are the structures which are most common but not infrequently there are others called variations which are less common but not considered abnormal. Variations ranging from subtle to remarkable change the anatomy of the known human body. They may have important influences on predisposition to illness, symptomatology, clinical examination and investigation, and patient management including operative surgery. Though most of university students should have been familiar with the variabilities met in human morphology from the early stage of their study many of them approach their anatomy studies in expectation that all human beings should be identical [21].

The studies in the field of human anatomy variations reveal that there is difference in their frequency by system. Most usual are the vascular variations followed by muscular and least are those of viscera and nervous system [2, 11]. Usually the ulnar artery is

the principal source of blood supply to the forearm while radial is for the hand [18]. The variation of superficial course of the ulnar artery has its prevalence of 0.7-9.4% of the population [19]. The standard two headed biceps brachii muscle may have supernumerary heads [17]. A coexistence of third head of the muscle and variation of musculocutaneous nerve communicating with median is reported [4].

Materials and Methods

Five upper and five lower limbs were dissected for the need of teaching process in the department of anatomy. The separated limbs from previously embalmed cadavers were used. Standard anatomy dissection technique was made. During the procedure the limbs were examined for the course, availability and branching of the vessels as well as for the position and morphology of the muscles, nerves and the rest of the structures.

Results

Two of the upper limbs were identified as variable.
Case no.1. - A spatial variation of ulnar artery was found on a separate right upper limb. The brachial artery was 5mm in diameter and in the cubital fossa bifurcated into radial and ulnar branch. The former was 4.5 mm wide and after 12 mm of length released common interosseous artery – diameter was 3.5 mm. Anterior interosseous artery was 3mm wide and bigger than usual, while posterior interosseous was normal. The ulnar artery (3 mm wide) originated as a terminal branch of the brachial artery in the cubital fossa. This beginning was standard but the course of the vessel was different from the one described in the anatomy books. On the forearm it passed superficial to all flexor muscles, which originate from the front of the medial epicondyle of the humerus **(Fig. 1).**

As it descended into the lower third of the forearm, it followed the lateral border of the flexor carpi ulnaris muscle and then proceeded into the Guyon's canal and on the hand formed the superficial palmar arch together with the superficial branch of radial artery **(Fig. 2)**.

Case no. 2. - During the dissection of a left upper limb we found two significant variations in the axillary fossa and brachial region. The musculocutaneous nerve originated from the lateral cord and after 60mm it pierced the coracobrachialis muscle. The length of this part of the nerve was in the reported norm, which according to Flatow et al. is from 3 to 12.5 cm [7, 13]. Distally to coracobrachialis its position between biceps brachii and brachialis was typical and several muscular branches were released for the

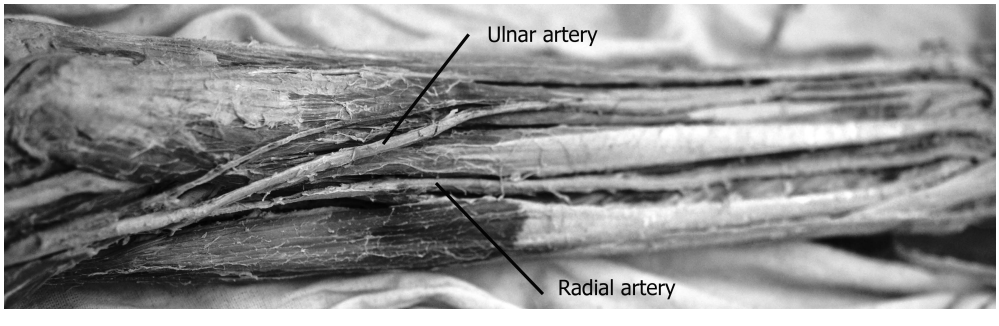

Fig. 1. Right upper limb. Cubital fossa and forearm. Superficial ulnar artery

Fig. 2. Right upper limb. Carpal region and Guyon's canal with the superficial ulnar artery.

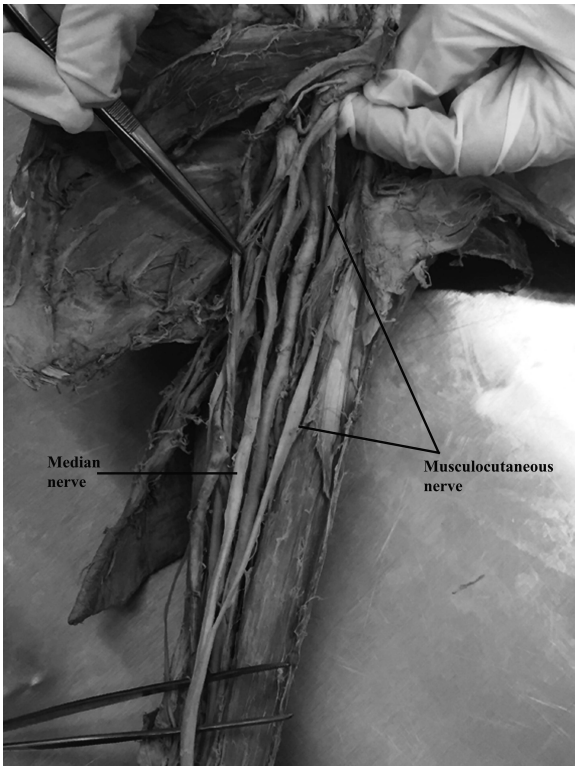

Fig. 3. Left upper limb. Unusual anastomosis between musculocutaneous and median nerves

two muscles after that it joined the median nerve. This part of the nerve is 130 mm or the communicating branch originated 19 cm from the coracoid process. The lateral cutaneous nerve of the forearm was a branch of the musculocutaneous and passed between the body and the third head of the biceps brachii as it appeared on the lateral border of the muscle and descended on the forearm **(Fig. 3).**

The supernumerary third head of biceps brachii muscle was observed during the dissection. The origin of the variable head was at the humeral medial face, at the level of the middle third of the arm, between coracobrachialis insertion and brachialis muscle origin. It was 13.8 cm in length and joined the biceps brachii at the lower third of the arm **(Fig. 4).**

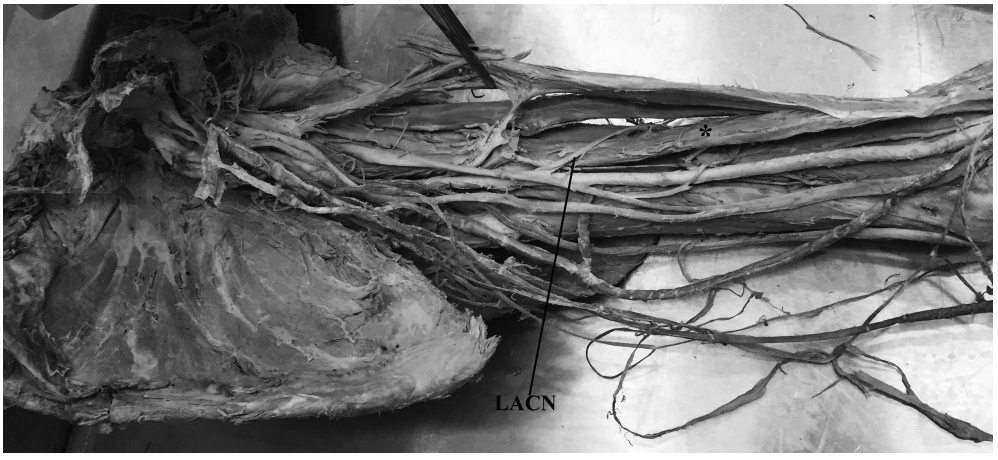

Fig. 4. Left upper limb. Third head of biceps brachii
* - third head, LACN - lateral antebrachial cutaneous nerve

Discussion

The presence of human anatomy variations in the gross anatomy teaching lab is undisputable. They are found in each stage of the teaching process and it is hard to neglect their existence and to escape discussion of their impact on the future clinical work [11].

The anatomical variations of the upper extremity are significant, especially with increasing use of imaging techniques like computed tomography and magnetic resonance imaging [3]. Variations of the arterial pattern of the upper limb are reported in the available literature including axillary artery, brachial artery and ulnar and radial arteries [12]. Superficial ulnar artery is a very common variety with a prevalence of 0.7-9.4% in some studies [19] and 4.2% in others [6]. A high proximal origin of the ulnar artery from axillary, brachial or superficial brachial is termed as "superficial ulnar artery" [14]. The appearance of this variation, when coming from brachial artery, is most often from the lower third, often from the upper and infrequently from the middle one. In these cases the arteries of the forearm are usually more superficial and are lying under the antebrachial fascia or very rarely subcutaneously [2]. Ulnar artery could pass superficial to the superficial muscles of the anterior group of the forearm [16]. In the presented case No1 ulnar artery arises on its usual place from the brachial artery and passes superficial to the flexors of the forearm. Here no prominent branches are given off the main artery. This pattern doesn't correspond to any of the 5 types presented by Latarjet [8].

In case no. 2 the concomitant multiple variations of musculocutaneous and biceps brachii are reported in the literature. The existence of the extra heads of the biceps bra-

chii has been associated with variabilities of musculocutaneous nerve and even more it has been associated with presence of communicating branches between the latter and the median nerve [17]. The embryological development of the upper limbs may help in explaining the upper mentioned variations. During the 5th week of the development, mesoderm invades the upper limb bud to further condense into ventral and dorsal muscle masses [10]. The mesenchyme of these muscles is penetrated by the ventral primary branches of the appropriate spinal nerves. Contact between nerves and a muscle is necessary to provide mesenchymal condensation to form muscles [4]. So the development of the biceps brachii third head and the course and branching of musculocutaneous nerve could be influenced by each other, which may explain the coexistence of the reported neuromuscular variation [1]. From the supernumerary heads of biceps brachii the one with three heads is most common and frequently reported [1, 27] but variable muscle with four or even seven heads was also presented [3]. The multiple varieties of this muscle have resulted on a large number of reports with different classifications [17]. According to Rodríguez-Niedenführ et al. there are three types of variants of the third head of biceps brachii considering its attachment to the humerus: superior humeral head; inferomedial and inferorlateral heads [4]. In our case no. 2 we have the inferomedial positon of the third head, which originates from the anteromedial surface of the humerus between insertion of the coracobrachialis proximally and the origin of brachialis muscle distally. The coexisting variation of musculocutaneous nerve in our case cannot be categorized in the 5 types presented by Le Minor which classification is the most detailed one from several others based on the anastomoses of the nerve and its relation to coracobrachialis. It is similar to type 2 where fibers from medial root of median nerve join musculocutaneous nerve and return back to the former in the midarm. In our case fibers are from the lateral cord and they all join the median nerve in the distal third of the arm.

The clinical significance of the reported variations is specific for each one of them. The superficial position of the ulnar artery in our case could be a reason for unintentionally penetrating the artery during attempts of venipuncture of median cubital vein [5]. This arterial variation is increasing the chance of iatrogenic injury occurring during surgery [14]. The third head of biceps might be misinterpreted with soft tissue tumor [20]. A nerve or artery compression (median nerve or brachial artery) is possible produced by the extra head [15]. Another impact of this variety is the role of biceps brachii in flap surgery and probable unusual bone displacement subsequent to fracture. Clinically, the musculocutaneous nerve variations may be related to entrapment syndrome. If the entrapment of the musculocutaneous nerve coexists with a communicating branch between the musculocutaneous and median nerve may lead symptoms of median nerve neuropathy [4]. The knowledge of the last condition could help differential diagnosis and avoid unnecessary operative treatment of carpal tunnel syndrome [22].

Conclusion

The variations are part of the normal anatomy of human body. Surgeons, radiologists and anatomist are the specialists that can refute the assertion that normality is the only state of human body. The aberrations in position, number and presence of the structures in anatomy are something that they find very often. A new concept of teaching and interpreting anatomy is necessary to have more impact of modern normal morphology on the clinical process of diagnosis and treatment of the diseases especially with surgical procedures.

References

1. **Abu-Hijleh, M. F.** Three-headed biceps brachii muscle associated with duplicated musculocutaneous nerve. - *Clin. Anat.,* **18,** 2005, 376-379.
2. **Bergman, R. A., S. A. Thompson, A. K. Afifi, F. A. Saadeh.** Compendium of human anatomic variation, Baltimore-Munich, Urban & Schwarzenberg, 1988, 72-75.
3. **Catli, M. M., U. Ozsoy, Y. Kaya, A. Hizay, F. B.Yildirim, L. Sarikcioglu.** Four-headed biceps brachii, three-headed coracobrachialis muscles associated with arterial and nervous anomalies in the upper limb. - *Anat. Cell. Biol.,* **45,** 2012, 136-139.
4. **Cerda, A.** Third head of biceps brachii muscle, associated with musculocutaneous and median nerve bilateral communication and with a communicating branch between median nerve roots. - *Int. J. Morphol.,* **32,** 2014, 510-514.
5. **Chin, K. J., K. Singh.** The superficial ulnar artery-a potential hazard in patients with difficult venous access. - *Br. J.Anaesth.,* **94,** 2005, 692–693.
6. **Dartnell, J., P. Sekaran, H. Ellis.** The superficial ulnar artery: incidence and calibre in 95 cadaveric specimens. - *Clin. Anat.,* **20,** 2007, 929-932.
7. **Flatow, E. L., L. U. Bigliani, E. W. April**. An anatomic study of the musculocutaneous nerve and its relationship to the coracoid process. - *Clin. Orthop.Relat. Res.*, **244,** 1989, 166-171.
8. **Latarjet, A.** Testut'sTraited'AnatomieHumaine, Paris, G. Doin & Cie., 1948.
9. **Moore, K. L**. Meaning of "normal". - *Clin. Anat.,* **2,** 1989, 235-239.
10. **Nayak, S., A. Krishnamurthy, M. Kumar, L. Prabhu, V. Saralaya, M. Thomas.** Four-headed biceps and triceps brachii muscles, with neurovascular variation. - *Anat. Sci. Int.,* **83,** 2008, 107-111.
11. **Novakov, S.** Human anatomy variations - part of anatomy and importance for medicine. *PhD thesis,* Medical University Plovdiv, 2017, 167 p. [in Bulgarian]
12. **Olinger, A. Upper limb arteries.** - *In: Bergman's Comprehensive Encyclopedia of Human Anatomic Variation* (Eds. R. Shane Tubbs, Mohammadali M. Shoja, MariosLoukas), Wiley-Blackwell, 2016, 583-618.
13. **Pianezza, A., A. Salces y Nedeo, P. Chaynes, P. E. Bickler, V. Minville**. The emergence level of the musculocutaneous nerve from the brachial plexus: implications for infraclavicular nerve blocks. - *Anesth. Analg.,* **114,** 2012, 1131-1133.
14. **Quadros, L. S., N. Bhat, A. S. D'Souza.** Superficial Ulnar Artery: A Case Report of its Unusual Course. - *Malays. J. Med. Sci.*, **22,** 2015, 65-67.
15. **Rai, R., A. V. Ranade, L. V. Prabhu, M. M. Pai.** Third head of biceps brachii in an Indian population. - *Singapore Med. J.,* **48,** 2007, 929-931.
16. **Rodriguez-Baeza, A., J. Nebot, B. Ferreira, F. Reina, J. Perez, J. R. Sanudo, M. Roig**. An anatomical study and ontogenic explanation of 23 cases with variations in the main pattern of the human brachio-antebrachial arteries. - *J. Anat.,* **187,** 1995, 473-479.
17. **Rodríguez-Niedenführ, M., T. Vázquez, D. Choi, I. Parkin, J. R. Sañudo.** Supernumerary humeral heads of the biceps brachii muscle revisited. - *Clin. Anat.,* **16,** 2003, 197-203.
18. **Romanes, G. J.** Cunningham's manual of practical anatomy, New York, Oxford University Press, 1986, 82-83.
19. **Sieg, P., H. C. Jacobsen, S. G. Hakim, D. Hermes.** Superficial ulnar artery: curse or blessing in harvesting fasciocutaneous forearm flaps. - *Head Neck,* **28,** 2006, 447-452.
20. **Wahengbam, S., R. Karam, K. Thounaojam, E. Remei.** Incidence of third head of biceps brachii in indian population. – *Int. J. Anat. Res.,* **3,** 2015, 1466-1470.
21. **Willan, P. L., J. R. Humpherson**. Concepts of variation and normality in morphology: Important issues at risk of neglect in modern undergraduate medical courses. - *Clin. Anat.,* **12,** 1999, 186-190.
22. **Venieratos, D., S. Anagnostopoulou.** Classification of communications between the musculocutaneous and median nerves. - *Clin. Anat.,* **11,** 1998, 327-331

Institute of Experimental Morphology, Pathology and Anthropology with Museum
Bulgarian Anatomical Society

Acta morphologica et anthropologica, 25 (1-2)
Sofia ● 2018

Study of Fingerprint Patterns in Left-Handed and Right-Handed Bulgarian Individuals

Nadezhda Petrova[2], Emilia Andreenko[2], Cristobal Iglesias[3], Stefan Sivkov[1]*

[1] *Medical University, Plovdiv, Bulgaria*
[2] *University of Plovdiv Paisii Hilendarski, Plovdiv, Bulgaria*
[3] *Medical Faculty of Oviedo's University, Asturias, Spain*

* Corresponding author e-mail: nad87@abv.bg

The aim of the present study is to assess the variability of fingerprint patterns in the individuals of Bulgarian ancestry and establish their relationship with hand dominance. The study includes 390 subjects (277 females and 113 males) aged 19-30 years. Of these, 285 are right-handed, 94 left-handed, and 11 are ambidextrous. The subjects are clinically healthy, of Bulgarian ethnicity.
Rolled fingerprints were obtained by the ink method. Papillary patterns were classified into four main types. The data were analyzed with statistical software SPSS 19.0. A pattern model (U>W>A>Y) of the distribution of papillary fingerprints was found for both hands in left-handers and right-handers. Significant differences were found in the fingerprints of the first ($p = 0.009$), second ($p = 0.008$) and fifth fingers ($p = 0.053$) on the left hand between left-handed and right-handed females. In males the differences did not reach statistical significance ($p>0.05$).

Key words: fingerprint patterns, handedness, Bulgarian individuals

Introduction

Dermatoglyphic ridges are resistant, permanent throughout life and diagnostically sensitive traits, varying in most cases independently from each other. A large number of modern studies address the relationship between fingerprints and genetically determined tendency for hand dominance [3]. S. Coren [4] suggests a genetic mechanism in the development of hand dominance, which allows differentiation between pathological and natural left-handedness.

In a number of studies, attention is paid to sexual dimorphism in papillary fingerprints of right-handed and left-handed people [16]. According to W. Buchwald [2], in most cases a higher degree of variety of images is found in males, and in terms of fourth finger, diversity is equally valid for both sexes.

A major aim in the studies of many authors is the higher bilateral asymmetry of dermatoglyphic traits in the left-handed subjects. In his paper G. Karev, [7] has found

more expressed fluctuating asymmetry in ulnar loops on the first and fourth fingers of right-handed subjects significantly compared with left-handed and ambidextrous subjects. E. Kobyliansky and S. Micle [11] have investigated dermatoglyphic signs of right-handed and left-handed males. In their opinion, fluctuating asymmetry is lower in right-handed persons and the directional asymmetry higher in left-handed persons.

In Bulgaria, dermatoglyphic studies performed have been concerned with ethnicity [8], sexual dimorphism and fluctuating asymmetry [1], clinical application of dermatoglyphics [13, 14, 15]. Less number of studies have examined the differences in the fingerprints between right-handed and left-handed subjects of both sexes [7, 8]. This determined our interest in the present study.

The aim of the present study was to examine the variability of fingerprint patterns in the Bulgarian population and establish their relationship with hand dominance.

Materials and Methods

The study included 390 individuals (277 females and 113 males) aged between 19 and 30 years. Of these subjects 285 were right-handed (73.1%), 94 left-handed (24.1%) and 11 ambidextrous (2.8%). The group of right-handed subjects included 66 males (58.4%) and 219 females (79.1%). The group of left-handed subjects comprised 41 males (36.3%) and 53 females (19.1%). The ambidextrous group included 6 males (5.3%) and 5 females (1.8%).

Potential respondents were excluded from the study in the case of non-Bulgarian ethnicity of one of the parents and grandparents, history of severe neurological disease, history of psychotic disorder, first degree relatives with a history of psychotic disorder, pathological conditions characterized with abnormal dermatoglyphic status: psoriasis, congenital heart disease, diabetes, etc.

The subjects gave their informed consent to participate in the study after the aim, objectives, and procedure of the study had been explained.

Rolled fingerprints were obtained using the ink method and examined with slight magnification (6D). Fingerprint patterns were read as described by Cummins and Midlo [5] and identified as arches (A), ulnar loops (U), radial loops (Y), whorls (W). The whorls group included all varieties of circular images (twin loop, central pocket loop, lateral pocket loop, and accidental).

Hand preference was assessed using the Edinburgh Handedness Inventory [12]. Hand dominance was evaluated on the basis of the laterality index.

The data were analyzed statistically with SPSS 19.0 software. Descriptive statistics was used to summarize the data. Student's t-test was used to test the differences in fingerprints between the groups. The level of significance was set at $p<0.05$.

Results

Fig. 1 shows the percentage distribution of finger papillary patterns for both hands in females. Ulnar loops are most common patterns both in left-handed (60.8%) and in right-handed (53.9%) subjects. The second most common patterns are the whorls, followed by arches. Radial loops are the least common (4.2% for left-handed, 3.2% for right-handed). The fingerprint pattern frequency formula in females is U>W>A>R for both hands.

The fingerprint frequency on each finger in left-handed and right-handed females is shown in **Table 1.** Ulnar loops are the most common fingerprint pattern on both hands in the left-handed subjects, excluding the second finger of the right hand on which the

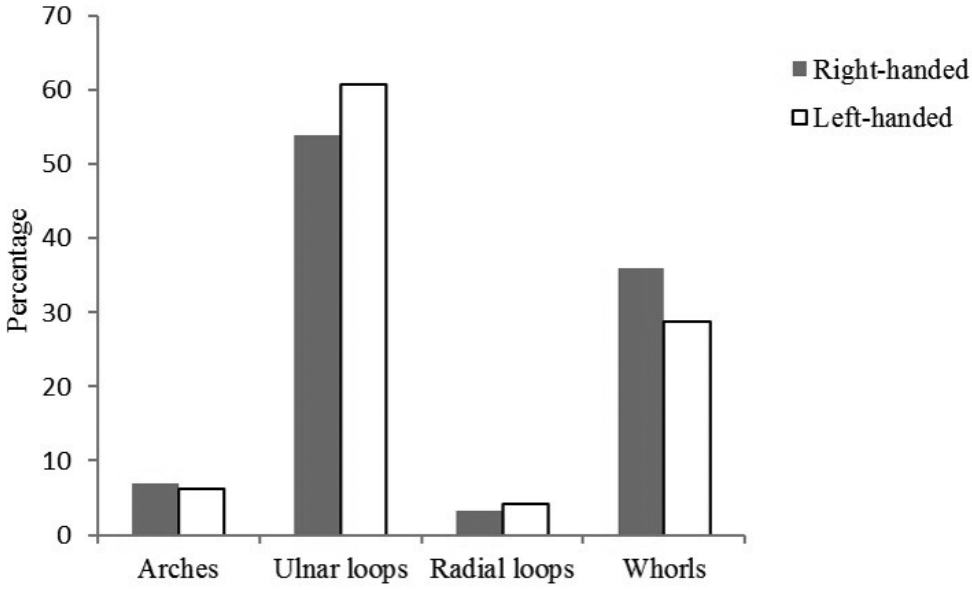

Fig. 1. Finger papillary patterns distribution in both hands of females

Table 1. Percentage of the main papillary pattern types on fingers in right- and left-handed females

Finger	Left-handed females n = 53		Right-handed females n = 219		p value*
	number	%	number	%	
Right hand					
R1					
A	2	3,8	8	3,7	
U	29	54,7	109	49,8	0.652
R	0	0	1	0,5	
W	22	41,5	101	46	
R2					
A	8	15,1	29	13,2	
U	17	32,1	72	32,9	0.078
R	9	17	20	9,1	
W	19	35,8	98	44,8	
R3					
A	1	1,9	18	8,2	
U	45	84,9	151	68,9	0.103
R	0	0	3	1,4	
W	7	13,2	47	21,5	

Continuation of **Table 1.**

Finger	Left-handed females n=53		Right-handed females n=219		p value*
	number	%	number	%	
R4					
A	0	0	2	0,9	
U	27	50,9	107	48,9	0.249
R	0	0	1	0,5	
W	26	49,1	109	49,7	
R5					
A	2	3,8	5	2,3	
U	43	81,1	171	78,1	0.298
R	1	1,9	1	0,5	
W	7	13,2	42	19,1	
Left hand					
L1					
A	3	5,7	12	5,5	
U	35	66	105	47,9	**0.009***
R	0	0	4	1,8	
W	15	28,3	98	44,8	
L2					
A	8	15,1	37	16,9	
U	21	39,6	67	30,6	**0.008***
R	10	18,9	28	12,8	
W	14	26,4	87	39,7	
L3					
A	6	11,3	26	11,9	
U	31	58,5	128	58,4	0.548
R	1	1,9	5	2,3	
W	15	28,3	60	27,4	
L4					
A	1	1,9	9	4,1	
U	30	56,6	95	43,4	0.127
R	0	0	3	1,4	
W	22	41,5	112	51,1	
L5					
A	2	3,8	5	2,3	
U	44	83	175	79,9	**0.053***
R	1	1,9	4	1,8	
W	6	11,3	35	16	

whorls are most common. Ulnar loops are most frequent patterns on the first, third and fifth finger in the right-handed subjects. Whorls are most common on the second and fourth finger. The frequency of arches and radial loops is low on both hands in left-handed and right-handed subjects. Radial loops show the lowest frequency in right-handed subjects. Similar tendency is observed in left-handed females, with the exception of the second finger of both hands, where the arch rate is the lowest.

Table 2 shows the topographic distribution of fingerprint patterns in women with different hand dominance. Arches and radial loops are most commonly found on the second finger of both hands in left-handed and right-handed subjects. Whorls are most common on the fourth fingers of both hands. Ulnar loops show a slightly different trend in their distribution. On the left hands in both groups, they are most commonly found on the fifth finger, while in the left-handed subjects they are most common on the third finger of right hand.

Differences in fingerprint patterns reach statistical significance for the first ($p = 0.009$), second ($p = 0.008$) and fifth ($p = 0.053$) fingers of the left hand between left-handed and right-handed females. On the right hand, the differences do not reach statistical significance ($p>0.05$).

Fig. 2 shows the percentage distribution of the fingerprint patterns for both hands in males. Left-handed and right-handed males have the same model of fingerprint pattern as females. The most common patterns are the ulnar loops (48.3% for left-handed, 53.6% for right-handed subjects), followed by whorls (44.4% for left-handed, 34.8% for right-handed males). Arches and radial loops are observed significantly less frequently in both groups. The formula of fingerprint patterns is U>W>A>R on both hands.

Table 3 shows the frequency of fingerprint patterns on each finger in left-handed and right-handed males. Ulnar loops are the most common pattern on the third and fifth fingers of both hands in left-handed and right-handed subjects. Whorls are most common on the first, second and fourth fingers of the right hand in both groups, and on the left hand only in left-handed subjects. Arches show lower frequency on both hands. Radial loops are the least common pattern on all fingers, except the index one, in the right-handed subjects, and on the index finger of the right hand in the left-handed subjects.

Table 2. Papillary pattern distribution on fingers in left- and right-handed females

Pattern	Left-handed females n = 53	Right-handed females n = 219
	Formulae	Formulae
Right hand		
A	II>I=V>III>IV	II>III>I>V>IV
U	III>V>I>IV>II	V>III>I>IV>II
R	II>V>I=III=IV	II>III>I=IV=V
W	IV>I>II>III=V	IV>I>II>III>V
Left hand		
A	II>III>I>V>IV	II>III>I>IV>V
U	V>I>IV>III>II	V>III>I>IV>II
R	II>III=V>I=IV	II>III>I=V>IV
W	IV>I=III>II>V	IV>I>II>III>V

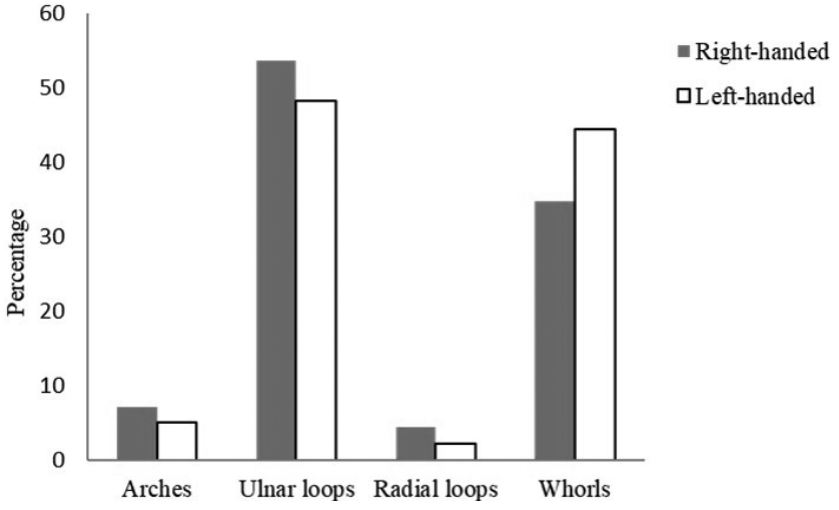

Fig. 2. Finger papillary patterns distribution in both hands of males

Table 3. Percentage of the main papillary pattern types on fingers in right- and left-handed males

Finger	Left-handed males n = 41		Right-handed males n = 66		p value*
	number	%	number	%	
Right hand					
R1					
A	4	9,8	1	1,5	
U	9	22	29	43,9	0.411
R	0	0	0	0	
W	28	68,2	36	54,6	
R2					
A	4	9,8	7	10,6	
U	9	22	22	33,3	0.139
R	7	17,1	11	16,7	
W	21	51,1	26	39,4	
R3					
A	2	4,9	8	12,1	
U	29	70,7	44	66,7	0.968
R	0	0	0	0	
W	10	24,4	14	21,2	
R4					
A	0	0	2	3	
U	12	29,3	21	31,8	0.238
R	0	0	1	1,5	
W	29	70,7	42	63,7	
R5					
A	0	0	3	4,5	
U	28	68,3	47	71,2	0.118
R	0	0	0	0	
W	13	31,7	16	24,3	

Continuation of **Table 3.**

Finger	Left-handed males n = 41		Right-handed males n = 66		p value*
	number	%	number	%	
Left hand					
L1					
A	2	4,9	3	4,5	
U	19	46,3	39	59,1	0.102
R	0	0	0	0	
W	20	48,8	24	36,4	
L2					
A	6	14,6	7	10,6	
U	15	36,6	26	39,4	0.134
R	2	4,9	15	22,7	
W	18	43,9	18	27,3	
L3					
A	1	2,4	10	15,2	
U	30	73,2	43	65,2	0.117
R	0	0	0	0	
W	10	24,4	13	19,6	
L4					
A	0	0	3	4,5	
U	16	39	32	48,5	0.565
R	0	0	2	3	
W	25	61	29	44	
L5					
A	2	4,9	3	4,5	
U	31	75,6	51	77,3	0.796
R	0	0	0	0	
W	8	19,5	12	18,2	

In **Table 4** is shown the fingerprint pattern formulas in males with different hand dominance. Two images - radial loops and whorls - have the same topographic distribution on both hands for left-handed and right-handed subjects. Radial loops are the most common on the second finger, and whorls on the fourth finger. As for the other two images - ulnar loops and arches, there are differences between left and right hand in both groups. Ulnar loops are most often found on the fifth finger of the left hand in both groups, and on the right hand only in right-handed subjects. Arches are most often found on the first and second finger of left-handed subjects and on the third finger of right-handed subjects.

In our study, the differences in the distribution of fingerprint patterns on both hands in males do not reach statistical significance.

Table 4. Papillary pattern distribution on fingers in left- and right-handed males

Pattern	Left-handed males n = 41	Right-handed males n = 66
	Formulae	Formulae
Right hand		
A	I=II>III>IV=V	III>II>V>IV>I
U	III>V>IV>I=II	V>III>I>II>IV
R	II>I=III=IV=V	II>IV>I=III=V
W	IV>I>II>V>III	IV>I>II>V>III
Left hand		
A	II>I=V>III>IV	III>II>I=IV=V
U	V>III>I>IV>II	V>III>I>IV>II
R	II>I=III=IV=V	II>IV>I=III=V
W	IV>I>II>III>V	IV>I>II>III>V

Discussion

The results of our study show well-established differences in fingerprint patterns between left-handed and right-handed females on the first, second and fifth fingers of the left hand. These differences could be due to a greater genetic pressure during the prenatal period. Similar pattern has been observed by B. Wijerathne and G. Rathnayake [16], who found statistically significant differences in fingerprints on the first and second fingers of the left hand between left-handed and right-handed females. The authors have also reported significant differences between left-handed and right-handed males which are not present in our study.

S. Coren, [4] has found significant dermatoglyphic differences in four of the five fingers of the left hand in males and females. In our sample, statistically significant differences are found in three of the five fingers of the left hand only in females.

G. Karev, [7] has examined the frequency of typographic images in men and women with different dominant hand. The author finds that whorls are less and ulnar loops are more common in right-handed than in left-handed subjects from both sexes. Our results support these data, but only for males. In our study in females, the pattern is reversed.

Of all types of patterns in our study, the least represented on both hands are the arches and radial loops. In comparison between left-handed and right-handed, we find a lower incidence of arches in left-handed subjects. The results obtained by K. Cho and S. Kim [3] are slightly different; they notice a lower frequency in right-handed subjects. This may be due to racial peculiarities in fingerprint pattern.

Conclusions

1. There is a similar model of distribution of the fingerprints patterns on both hands (U>W>A>R) in left-handed and right-handed subjects. Differences are expressed by their percentage representation on each finger individually.
2. The distribution of the least represented images (arches and radial loops) on the fin-

gers of the two groups is normal, whereas the higher-frequency images (ulnar loops) show a higher topographic diversity.
3. Statistically significant differences in fingerprint patterns on the first, second and fifth fingers of the left hand are found between females with different hand dominance but not between males.

References

1. **Andreenko, E., S. Baltova.** Sexual dimorphism in dermatoglyphic traits and fluctuating asymmetry in Bulgarians from northeast Bulgaria. - *Homo,* **68**(4), 2017, 316-327.
2. **Buchwald, W.** The morphological diversity of dermatoglyphic patterns on fingers - a simple and objective method for measurement. - *Homo,* **66,** 2015, 60-78.
3. **Cho, K. J., S. I. Kim.** Characteristics of fingerprints according to type of handedness. - *Korean J. Phys. Anthropol.,* **23**(1), 2010, 21-31.
4. **Coren, S.** Are fingerprints a genetic marker for handedness? - *Behav. Genet.,* **24**(2), 1994, 141-8.
5. **Cummins, H., C. Midlo.** Finger prints, palms and soles. An introduction to dermatoglyphics. – Philadelphia, Blakinstone. Reprinted: New York, Dover, 319, 1961.
6. **Hit, G. L., N. A. Dolinova.** Racial differentiation of human. Moscow, Science, 1990, 3-200. [In Russion]
7. **Karev, G.** Finger dermatoglyphics and their asymmetry in Bulgarian right-, mixed- and left-handers. - *Anthropol. Anz.,* **66**(3), 2008, 281-93.
8. **Karev, G.** Three palmar dermatoglyphic traits and their asymmetry in Bulgarian right-, mixed- and left-handers. - *Antropol. Anz.,* **68**(3), 2011, 291-307.
9. **Kavgazova, L., R. Stoev, Z. Mitova.** Dermatoglyphic characteristicsof a population from the Central Rhodopes (South Bulgaria). Anthrop. anz., 57, no. 4, 349-360.
10. **Kavgasova, L.** Dermatoglyphic characteristics of the ethnographic group "Balkandzii". - *Acta morph. et anthropol.,* **9,** 2004, 165-169.
11. **Kobyliansky, E., S. Micle.** Handedness and dermatogliphic directional and fluctuating asymmetry. - *Z. Morph. Anthrop.,* **76**(3), 1986, 313-329.
12. **Oldfield, R. C.** The assessment and analysis of handedness: the Edinburgh inventory. – *Neuropsychologia,* **9**(1), 1971, 97-113.
13. **Sivkov, S., V. Akabaliev, K. V. Akabalieva.** Fluctuating asymmetry in dermatoglyphic traits in schizophrenic patients. - *Folia Med,* **49**(1-2), 2007, 5-10.
14. **Tornjova, S., D. Borissova, D. Topalova.** Fluctuating Asymmetry of dermatoglyphic features in patients with Turner syndrome. - *Acta morph. et anthropol.,* **9,** 2004, 148-159.
15. **Tornjova-Randelova, S., D. Paskova-Topalova, Y. Yordanov.** Dermatoglyphic in anthropology and medicine. - Own studies with individuals with different disorders. Sofia, Academic publishing house "Marin Drinov", 2011, 94-158. [in Bulgarian]
16. **Wijerathne, B. T., G. K. Rathnayake.** Association between digital dermatoglyphics and handedness among Sinhalese in Sri Lanka. - *F1000Res.,* **2,** 2013, 111.

Institute of Experimental Morphology, Pathology and Anthropology with Museum
Bulgarian Anatomical Society

Acta morphologica et anthropologica, 25 (1-2)
Sofia ● 2018

Anatomical Peculiarities and Morphometric Characteristics of the Intramural Part of Porcine Ureter

Nikolay Tsandev[1], Ivailo Stefanov[2], Genadi Kostadinov[1], Angel Vodenicharov[1]*

[1] *Deparment of Veterinary Anatomy, Histology and Embryology, Faculty of Veterinary Medicine, Trakia University, Stara Zagora, Bulgaria*
[2] *Department of Anatomy, Faculty of Medicine, Trakia University, Stara Zagora, Bulgaria*

* Corresponding author e-mail: drcandev@abv.bg

The intravesical part of porcine ureter from 100 (50 male and 50 female) six months, 95-105 b.w. Bulgarian White x Landrace pigs, slaughtered for a meat consumption in accordance with Bulgarian legislation, were studied after silicone filling, radiography and corrosion casts measuring. It was established that the intramural part showed a well expressed curved course (almost 90°) with laterally oriented arch and distension just before transmission into ureteric columns. The statistical data (presented as mean ± SD) of studied morphometric parameters on silicone replicas - diameter and length of both sides of that ureter's part and distance between two ureteral orifices (ostia ureterica), as well, showed little more values in females vs. males ones, with no statistical significance ($P>0.05$, one-way ANOVA). Similarly, the diameter and length of right ureters were with little more values that these of left ones. Also, an asymmetry in ureteric ostia location was observed - 15.4% in males and 38.5% in females, with different position each toward other. Ureteric ectopy was not observed in all studied animals. The original data obtained add a species specific feature and could be useful also for medico-biological studies concerned to man and probably for a xenotransplantation.

Key words: ureter, intravesical part, anatomy, morphometry, pig

Introduction

The intramural part of the ureter, located in the bladder's wall, showed specific peculiarities and for this reason it has a special morphological, functional and clinical interest. Although the ureters penetrating the bladder's wall lose their smooth muscle cells, the remaining ureteric part retains as independent organ, situated dorsally into the bladder's wall. The remaining part of longitudinal smooth musculature does not fuse with those of the bladder, but it is attached to its wall [1, 2, 3, 6, 8, 16]. The intravesical part in domestic animal has different length,varying from several millimeters to 2-3 centimeters and depends mostly on the animal species. It is importantly that as in human, this part has an anatomical narrowing in which a urinary stones could be retained - sometimes provoking inflammation, leading to ureteric musculature spasm. As a result of a particular or full ureter obstruction a hydronephrosis or hydroureteronephrosis is developed

[2, 3, 4]. It is commonly accepted that the oblique situation of ureters into the bladder's musculature, narrowing lumen, muscle cells contraction and pressure of the urine on bladder's wall are factors which prevent urine reflux into the ureter from filled bladder and contraction of its wall [3, 5, 6, 8, 16]

The intravesical part of the ureter and respective area of the bladder form the ureterovesical junction which allows unhindered passage of urine from the ureter to the bladder while preventing the reflux [15, 17]. Comparative study of Shehata [16] on eleven mammalian species showed some differences in the intramural portion of the ureter concerning to submucous ureter, three types of that ureteral part and gender peculiarities in the muscular pattern of both ureter and urinary bladder.

With respect to anti-reflux mechanism of ureterovesical junction the juxta- and intravesical ureter and its relationship to the surrounding musculature have been studied by enzyme histochemistry in pig [15] and in human [10]. The data obtained showed that the ureter orifices are macroscopically located approximately the bladder neck in pig, the porcine trigone is less developed compared to that in human and is located very close to the dorsal aspect of the bladder neck. Also, an enzyme histochemical study revealed a lack of periureteric muscle sheet in pig [10].

Obtaining a complete draft of the pig genome sequence has been central to the development and broad acceptance of the pig as a biomedical model [9, 11, 12, 14].

The absence of data about the direction and running as well as measurements of intravesical part of porcine male and female ureters and increasing importance of pig as model in biomedical research motivated us to perform this study.

Materials and Methods

Animals: The intravesical ureteric part with adjacent area of the bladder from 100 (50 male and 50 female), 6 months old, 95-105 b.w., cross-breeding Bulgarian White and Landrace pigs were collected for this study. The animals were slaughtered for meat consumption in licensed abattoir in accordance with the Bulgarian legislation.

Experimental design: The pelvic parts of the ureters together with whole urinary bladder were carefully removed from the corps immediately after animal slaughtering. After 24 h staying at 40°C in refrigerator they were filled with silicone elastomer (Elite Double 22, Zhermack, BadiaPolesine, Italy), acryl acrylate resin (Duracryl, Spofa Dental, Praha, Czech Republic) and saturated solution of lead tetroxide in 10% water solution of gelatin. In order to fill the specimens with polymerized matter, following respective procedures were used: dissection (silicone elastomer), corrosion in 10% KOH (acrylate resin) and Rö graphy (saturated liquid of lead tetroxide ($\mathbf{PbO_4}$) in 10% water gelatin). Only silicone replicas with visible longitudinal grooves and gyri (reflecting the relief of ureteral mucosa) were used for metric evaluations.

The measures were carried out only on silicone replicas with visible longitudinal grooves and gyri using digital caliper and obtained data were processed using GraphPad Prism 6 for Windows (GraphPad Software, Inc., USA) via one-way analisys of variance (one-way ANOVA). P-values <0.05 were considered statistically significant. The data are presented as mean ± SD.

Results and Discussion

The observations after dissection, as well as on silicone replicas, corrosion casts and Rö grams showed that intravesical part of the ureter has a well expressed course (almost 90°) into the urinary bladder wall with laterally oriented arch. A distension just before

transmission of ureter (juxtavesical ureteral part) into urinary bladder's wall followed by distention within the wall, were also found **(Fig. 1a, b)**.

The morphometric measurements of both right and left ureter replicas diameter, length and distance between two ostia (right and left ostium ureteris) of each studied animal, and asymmetry between the ostia are given on **Table 1.** The data presented showed that as a whole the values of diameter and the length of intramural part silicone replicas in female individuals were higher than in male animals. This fact is difficult to explain, but it could be presume that at that age female pigs are a little more mature than males. The asymmetry between ostia was also found more often in females than in males - 38.5% vs. 15.4%, respectively. Our results about the ostia location asymmetry confirm in part the data of [7] on human ureters where almost all cases with asymmetry were observed in females, and only one in male individuals.

No statistical significance differences were established between studied parameters.

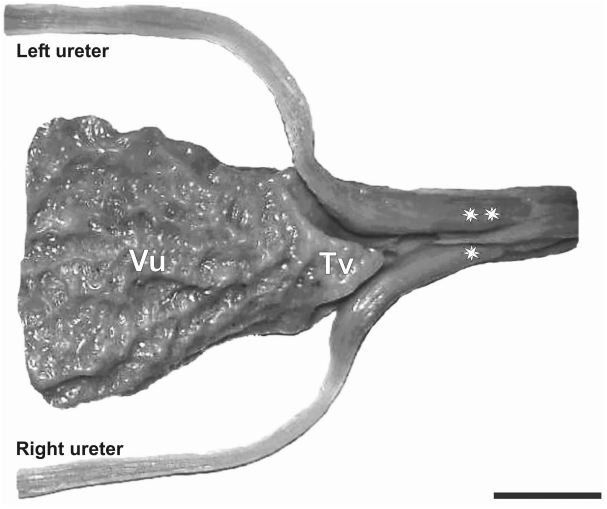

Fig. 1a. Silicone replica of bladder and asymmetry (*, **) of ureters in female pigs. **Tv**-trigonum vesicae; **Vu**-vesicaurinaria; Bar = 1 cm

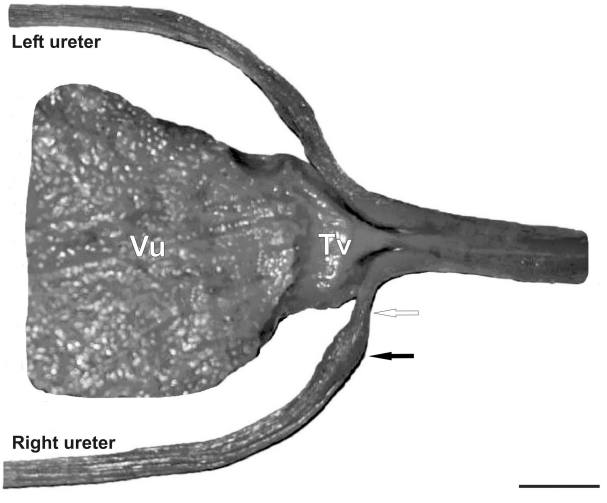

Fig. 1b. Silicone replica of bladder and ureters in female pigs. Silicone replica of bladder and ureters in male pigs. **Tv**-trigonim vesicae; **Vu**-vesical urinaria; enlargement (black arrow) and distension (white arrow) in terminal part of ureter. Bar = 1 cm.

Table 1. Measurements of intramural part of ureters and percentage of ostia location asymmetry between male and female pigs

PARAMETERS	MALES	FEMALES
SILICONE CASTS OF THE URETER INTRAMURAL PART **Diameter** Right Left	 **2.68±1.55** **2.19±0.73**	 **3.02±0.91** **2.79±1.10**
SILICONE CASTS OF THE URETER INTRAMURAL PART **Length** Right Left	 **10.60±2.41** **9.85±1.84**	 **12.86±3.93** **11.75±3.79**
OSTIUM URETERIS **Distance between the two ostia**	 **2.53±1.07**	 **3.65±0.95**
OSTIUM URETERIS **Percentage of asymmetry**	**15.4%** (**7.7%** - right ostium localized behind the left one; **7.7%** - left ostium localized behind the the right one)	**38.5 %** (**23.1%** - right ostium localized behind the left one; **15.4%** - left ostium localized behind the the right one)

Conclusion

The original data obtained about the course, diameter, length of intramural part silicone replicas, distance between the ureteric ostia and percentage of asymmetry in both male and female individuals add the knowledge for ureter anatomy peculiarities in this animal species. Our results could be useful in biomedical researches in relation of man, veterinary clinical practice as well as in further studies concerning xenotransplantation where domestic pig are involved as suitable animal model.

References

1. **Arrabal-Martin, M., A. Zuluaga-Gomez, S. Merino-Salas, M. Nogueras-Ocafia, M. A. Arrabal-Polo.** Endoscopic treatment of ureterovesical junction obstructive pathology: A description of the oblique meatotomy technique and results. - *Can. Urol. Assoc. J.,* **7**(11-12), 2013, 728-731.
2. **Barone, R.** Comparative anatomy of domestic mammals. Vol. **4,** Vigot, Paris, 2001, 46-61. [in French]
3. **Chouchkov, H., W. Ovtscharoff, N. Stoinov.** *Clinical Anatomy,* 1995, 335-358.
4. **Dyce, K. M., W. O. Sack, C. J. G. Wensing.** Textbook of veterinary anatomy. St. Louis, Missouri, Saunders Elsevier, 4th ed., 2010, 181-184.

5. **Goessl, C., Z. Grozdanovic, H. H. Knispel, H. E. H. Wegner, K. Miller.** Nitroxergic innervation of the human ureterovesical junction. - *Urol. Res.,* **23,** 1995, 189-192.
6. **Ham, A. W., D. H. Cotrmack.** Histology. (Russ. ed.) Moscow, Mir, 1983, Vol. 5, 41-45.
7. **Kabakian, H. A., H. K. Armenian, Z. L. Deeb, G. K. Rizk.** Asymmetry of the pelvic ureters in normal females. - *Am. J. Roentgenol.,* **127,** 1976, 723-727.
8. **Köning, H. E., J. Maierl, H.-G. Liebich.** Urinary system (Organa urinaria). - *In: Veterinary anatomy of domestic animals* (Eds. H. E. Köning and H.-G. Liebich), Stuttgart, Schauttauer, 2004, 375-378.
9. **Kuzmuk, K. N., L. B. Schook.** Pigs as model in biomedical science. - *In: The Genetic of the pig* (Eds. M. F. Rothschild, A. Ruvinsky), CAB International, 2011; 426-444.
10. **Roshani, H., N. F. Dabhoiwala, F. J. Verbeek, W. H. Lamers.** Functional anatomy of the human ureterovesical junction. - *Anat. Rec.,* **245,** 1996, 645-651.
11. **Schook, L. B., J. E. Beever, J. Roger, S. Humphray, A. Archibald, P. Chardon, D. Milan, G. Rohrer, K. Eversole.** Swine genome sequencing consortium (SGSC): a strategic roadmap for sequencing the pig genome. - *Comp. Funct. Genom.,* **6,** 2005a, 251-255.
12. **Schook, L. B., C. Beattie, J. E. Beever, S. Donovan, R. Jamison, F. Zuckermann, S. Niemi, M. Rothschild, M. Rutherford, D. Smith.** Swine in biomedical research: creating the building blocks of animal models. - *Anim. Biotech.,* **16,** 2005b, 183-190.
13. **Shehata, R.** A comparative study of the urinary bladder and the intramural portion of the ureter. - *Acta Anat.* **98,** 1977, 380-395.
14. **Swindle, M. M., A. Makin, A. J. Herron, F. J. Clubb, K. S. Frazier.** Swine as models in biomedical-research and toxicology testing. - *Vet. Pathol.,* **49,** 2012, 344-356. DOI: 10.1177/0300985811402846
15. **Thomson, A. S., N. F. Dabhoiwala, F. J. Verbeek, W. H. Lamers.** The functional anatomy of the ureterovesical junction. - *Brit. J. Urol.,* **73,** 1994, 284-291.
16. **Vankov, V., W. Ovtscharoff.** Anatomy of the Man. Sofia, Arso, 10th ed., 337-343.
17. **Vernet, S. G.** Anatomical aspects of vesicoureteral reflux. - *In: Urodynamics upper and lower urinary tract* (Eds. W. Lutzeyer, H. Meldeior,), Springer-Verlag Berlin Heidelberg, 1973, 171-178.

Institute of Experimental Morphology, Pathology and Anthropology with Museum
Bulgarian Anatomical Society

Acta morphologica et anthropologica, 25 (1-2)
Sofia ● 2018

Comparative Dermatoglyphic Study of the Palmar Ridge Count in Breast Carcinoma Patients from Northeast Bulgaria

Galina Yaneva[1], Tsonka Dimitrova[1], Djeni Cherneva[1], Nikoleta Ivanova[1], Ivan Maslarski[2], Stefan Sivkov[3], Dobri Ivanov[1]*

[1] *Department of Biology, Faculty of Pharmacy, Medical University, Varna, Bulgaria*
[2] *Department of Human Anatomy, Histology and Pathology, Faculty of Medicine, US, "St. Kliment Ohridski", Bulgaria*
[3] *Department of Anatomy, Histology and Embryology, Faculty of Medicine, Medical University, Plovdiv, Bulgaria*

* Corresponding author e-mail: galina_yanevaa@abv.bg

The present study was aimed to assess the relationship of quantitative dermatoglyphic analysis of the palmar ridge count and the predisposition for developing of breast cancer.
The study was conducted among 82 women with breast carcinoma diagnosed by histological and mammographic investigations and 60 healthy women for the control group from Northeast Bulgaria. Palmprints were obtained by the ink method. The palmar ridge count was read by the method of Cummins and Midlo. Statistically significant differences were estimated in the total palmar ridge count in b-c and a-d interdigital fields on both hands in cases with breast cancer compared to healthy controls. In a-b and c-d interdigital fields, no statistically significant differences were determined. Statistical significance was examined by SPSS 18.0 software.
The palmar dermatoglyphics is simple, inexpensive, anatomical and non-invasive method and may be used as a reliable tool for screening predisposition of breast cancer.

Key words: dermatoglyphics, breast cancer, total palmar right count, Northeast Bulgaria

Introduction

Dermatoglyphics is a field of science that studies dermal patterns of human hands and feet [15]. Ridges are formed in the early periods of intrauterine development and they remain unchanged throughout the whole period of life. Environmental factors can have an influence only in the period of the ridge formation. The dermatoglyphic pattern reflects congenital and hereditary conditions such as breast carcinoma. Several dermatoglyphic investigations by Bulgarian researchers also represent an undoubted interest, indeed [7-10]. The development of genetic research helps to establish the relationship of certain dermatoglyphic traits with a number of chromosomal aberrations such as Langdon Down syndrome, the Klinefelter syndrome, Turner syndrome, trisomy 17

and 18 [20]. There is evidence for abnormalities in the dermatoglyphic patterns in schizophrenia, congenital heart disease, lupus erythematodes, mental disorders and etc [21]. Carcinoma of the breast is one of the most common and dreadful diseases in Bulgaria as well as worldwide. In 5-10% of the cases breast carcinoma may be hereditary and sporadic, which is due to a mutation during the BRCA1 and BRCA2 genes [16, 19]. The development of the mammary glands starts in the sixth week of embryonic development [13] when the dermal ridges are formed [2]. This suggests that the abnormalities in the mammary glands during this period may be reflected in the dermatoglyphic parameters [3, 22, 12]. One of the most important quantitative dermatological features is the palmar ridge count a-b, b-c, c-d. The palmar ridges (papillary prints) are counted for the first time by Galton in 1895 [5] and the rules for counting the ridges are given by Henry in 1900 [4]. Palmar ridge count consists of the number of ridges that cross or touch the line, drawn from the triradius to the center of the pattern. The triradius is a papillary pattern where three flows of ridges meet.

The aim of the current study is to determine differences in the total palmar ridge count in breast carcinoma female patients compared to healthy controls which may have a prognostic and screening value.

Materials and Methods

The fingerprints were taken by spreading typographic ink over a glass or rubber pad by a roller. Palmprints were recorded in a passive manner on a high-quality paper [14]. For the best print of the central part of the hand the paper was placed on a convex surface. The study was conducted among 82 women with breast carcinoma, diagnosed by histological and mammographic investigations in the Department of Thoracic surgery at St. Marina Hospital in Varna and 60 healthy women as a control group from Northeast Bulgaria.

For reading the palmar prints, we used the basic methodology of Cumis and Midlo [4]. The ridge count between different fingerprint triradii is a quantitative parameter which does not depend on size and age. The ridge count in the interdigital spaces a-b, b-c, c-d is calculated for each hand separately **(Fig. 1)**. The total ridge count is estimated on the left and right hand as well as on both hands. The results were examined with the computer program SPSS 18.0.

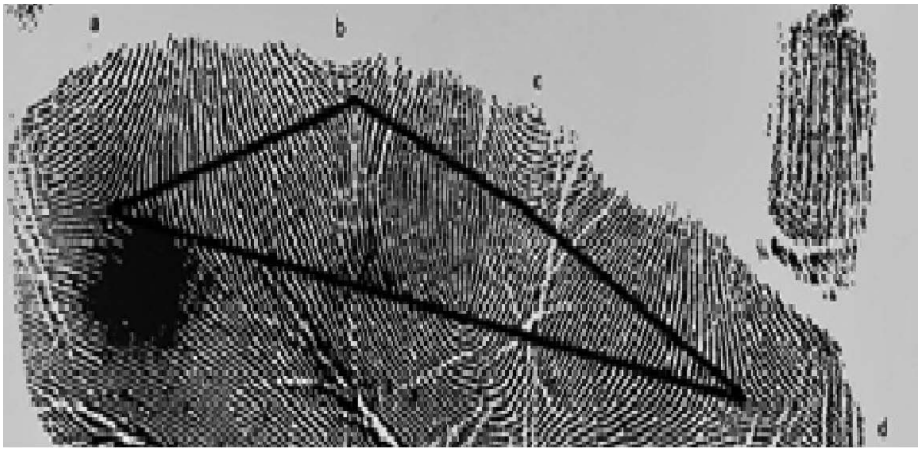

Fig. 1 Palmar ridge count and its calculation in basic a-b, b-c, c-d triradii

Results and Discussion

As it is seen on **Fig. 2**, similar values of the palmar ridge count in the a-b interdigital palmar field on the left hand in women with breast cancer and in control group were observed **(Fig. 2)**. In breast carcinoma patients the palmar ridge count in the c-d interdigital field showed slightly reduced values compared to the control group. Elevated values in the b-c ridge count in breast carcinoma women were established in relation to the control group with statistically significant difference ($p<0.001$). The total ridge count in a-d on the left hand in breast carcinoma patients showed statistically significant differences compared to the control group ($p<0.05$).

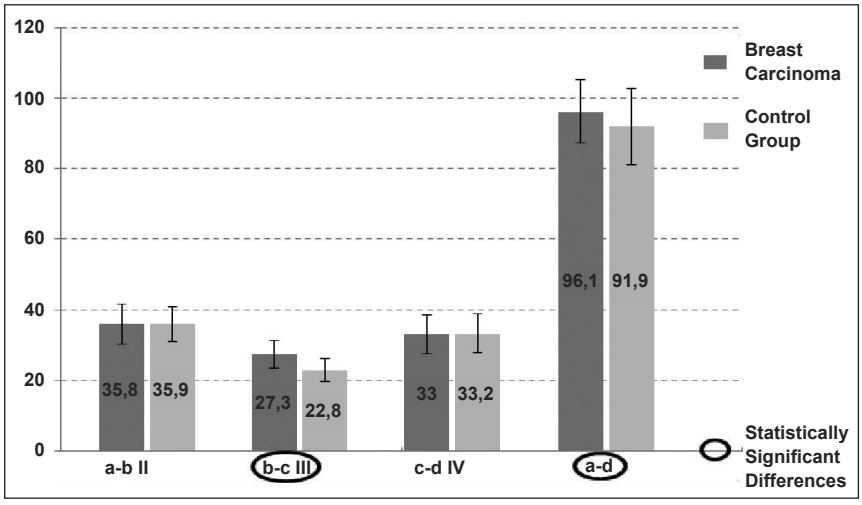

Fig. 2. Average values and standard deviations for palmar ridge count in breast carcinoma patients and control group on the left hand

Slightly elevated values of palmar ridge count in the a-b interdigital field on the right hand were estimated in breast carcinoma patients and the control group, which did not reach statistical significance **(Fig. 3)**.

In women with breast cancer the palmar ridge count in the b-c interdigital field showed increased values in comparison to the control group and the differences were statistically significant ($p<0.001$). No statistically significant differences were found but rather a trend in higher values of the ridge count in c-d interdigital field in women with breast carcinoma compared to healthy controls. In the women patients the values of total ridge count in the a-d field on the right hand demonstrated statistically significant difference in comparison with the healthy controls ($p<0.001$)

Marked interdigital fields on **Fig. 4** indicated higher bilateral differences in the ridge count for women with breast carcinoma compared to the control group (Fig. 4).

Higher values were observed in a-b ridge count on the left and right hand in women with breast carcinoma compared to controls. The b-c ridge count was characterized by relatively high bilateral differences **(Fig. 4)** and reached statistical significance compared to those of the control group ($p<0.001$). The c-d palmar ridge count, on the contrary, showed higher values on the right hands in the patients group compared to the left hands, but did not reach statistical significance in comparison with those of the control group.

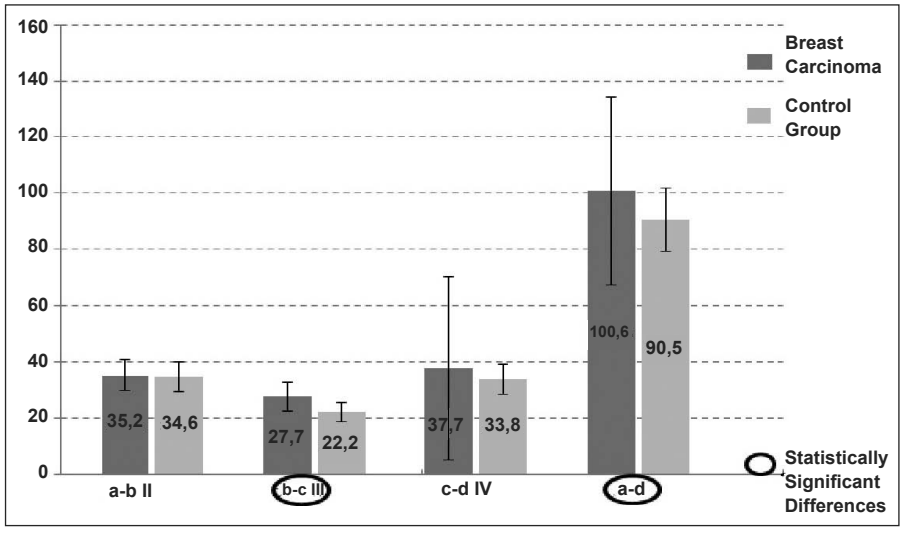

Fig. 3. Average values and standard deviations for palmar ridge count in breast carcinoma patients and control group on the right hand

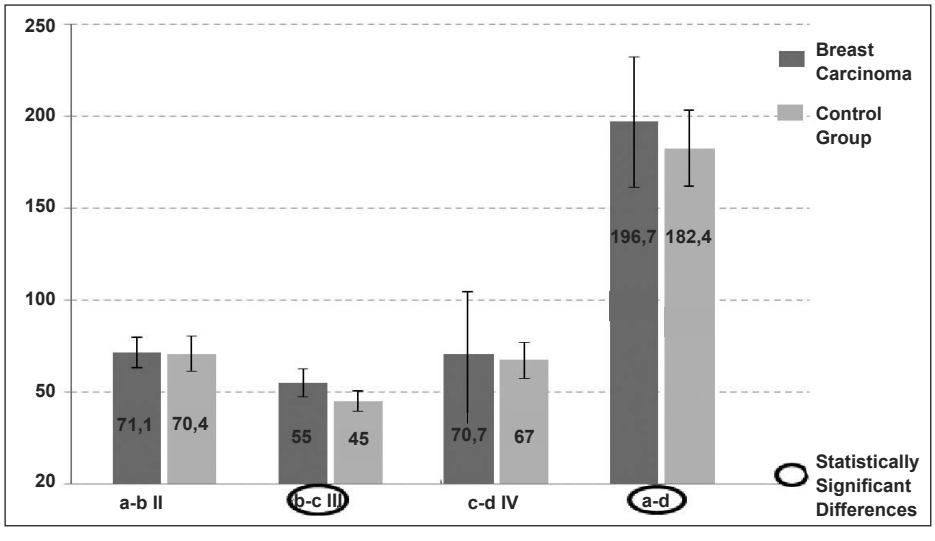

Fig. 4. Average values and standard deviations for palmar ridge count in breast carcinoma patients and control group on the right and left hand

Statistically significant differences were observed in the total ridge count in the a-d interdigital fields on both hands in cases with breast carcinoma compared to healthy controls ($p<0.001$).

Bilateral differences in the ridge count in specific fields and the total ridge count were significantly strongly manifested in the patients group compared to the control group. Right hands showed higher b-c ridge count, while a-b ridge count had almost equal values for both hands. B-c ridge count was higher on the both hands and reached statistically significant difference **(Fig. 5)** ($p<0.001$) respectively.

The overall dermatoglyphic assessment of the patients could be interpreted as an expression of caryotype abnormalities, similar to the chromosomal aberrations that are accompanied by certain dermatoglyphic changes [1, 20]. Data from literature shows a-b ridge count higher values in breast carcinoma women in comparison to the control group [11, 17]. The results of our study did not demonstrate statistically significant differences between the patients group and the controls in the a-b interdigital field. The differences in the values of palmar ridge count in breast carcinoma women could be attributed to dysontogenetic effects which interfere before the time of the formation of the papillary patterns in b-c interdigital field.

Each peristatic factor inducing oedema of the cells such as infectious or inflammatory process could be the basis of the increase of the palmar ridge count [6, 18]. Changes in the dermatoglyphic status of the breast carcinoma patients could possibly be an expression of the excessive effect of genetic and exogenous factors. Higher values of palmar ridge count could be taken as an indication of a disruption of the genetic control in the formation of papillary patterns in women with breast carcinoma or for some breaches in the homeostasis of their organisms.

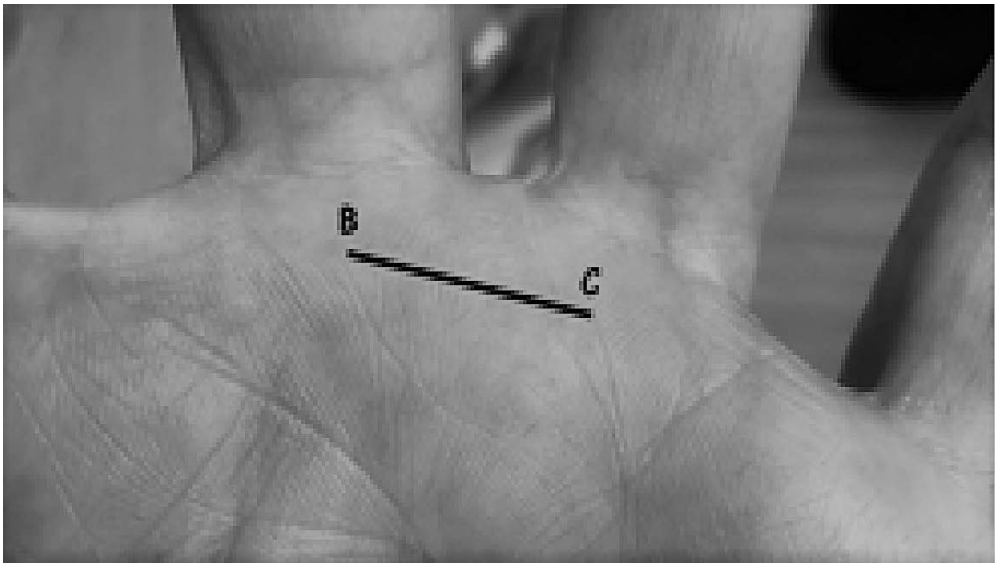

Fig. 5. b-c ridge count triradii

Conclusion

The use of dermatoglyphics is rather, unique approach at low cost for identifying predisposition for malignancy. This relatively noninvasive anatomical technique could reasonably be used for screening breast cancer on selected non-symptomatic women as part of definitive risk assessment strategy and for guiding future research. Palmar dermatoglyphics may have a future role in identifying women at increased risk with breast cancer.

References

1. **Ahmed-Popova, F., S. Sivkov, P. Nonchev, V. Akabaliev.** Palmar dermatoglyphic patterns in the thenar and the hypothenar areas in schizophrenic patients and control subjects. - *Bulgarian medicine,* **3,** 2013, 17-24.
2. **Babler, J. W.** Embryologic development of epidermal ridges and their configurations. - *In: Dermatoglyphics* - Science in transition. (Edited by: CC P, RM G, BA S), New York, Birth Defects, Wiley-Liss., 1991, 95-112.
3. **Balgir, R. S.** Congenital oral clefts and dermatoglyphics. Isr., - *J. Med Sci.,* **20,** 1984, 622-624.
4. **Cummins, H., C. Midlo.** Finger prints palms and soles. - *In: An introduction in dermatoglyphics.* Blakinston, Philadelphia, New York, Reprinted Dower, 1961, 319.
5. **Galton, F.** Fingerprint directories. London, Macmimillan, 1892, reprinted, New York, 1965.
6. **Holt, S.** The Genetics of dermal ridges. Springfield, Charles C. Tomas Illinois, 1968, 19.
7. **Karev, G. B.** Normal dermatoglyphic status of Bulgarians in Northeast Bulgaria. PhD dis, Varna, 1979, 216.
8. **Karev, G. B.** Anthropological, clinical and genetic aspects of dermatoglyphics and functional asymmetry. PhD dis, Sofia, 2006, 260.
9. **Karev, G. B.** Finger dermatoglyphics and their asymmetry in Bulgarian right-, mixed- and left-handers. - *Anthropol Anz,.* 2008, **66** (3):281-293.
10. **Karev, G. B.** Three palmar dermatoglyphic traits and their asymmetry in Bulgarian right-, mixed- and left-handers. - *Anthropol Anz.,* 2011, **68** (3):291-307.
11. **Maslarski, I. I.** Description of qualitative dermatoglyphic traits in twins. - *Comptes rendus de l' academie Bulgare des sciences,* **68.10,** 2015, 1241-1246.
12. **McGrath, J., R. Murray.** Risk factors for Schizophrenia: from conception to birth. - *In: Schizophrenia 2 nd ed.* (Edited by: SR H, DR W). Victoria, Black well Science Ltd., 1995, 187-205.
13. **Moore, K., T. V. Persaud.** The developing human. Saunders Publications: 7 th ed. 2004, 492-3.
14. **Purvis-Smitth, S. G.** Finger and palm printing technigue for clinician. - *J. Med Aust.,* **2,** 1969, 189.
15. **Raizada, A., V. Johri, T. Ramnath, D. Chowdhary, R. Garg.** Cross-sectional study on the palmar dermatoglyphics in relation to carcinoma breast patients. - *J. Clin. Diagn. Res.,* **7,** 2013, 609-612.
16. **Sakorafas, H., A. Tsiotou.** Genetic predisposition to breast cancer. A surgical perspective. - *Br. J. Surg.,* **87,** 2000, 149-162.
17. **Sivkov, S., V. Akabaliev, N. Kaleva.** Comparative dermatoglyphic study of schizophrenic patients: Evidence of the neurodevelopmental model of schizophrenia. - *Folia Medica,* **51,** 2009, 25-30.
18. **Sukanta, S., L. Danuta, C. David, J. Welham, O. El-Saadi, F. Lourdes et al.** Directional and fluctuating asymmetry in finger and a-b ridge counts in psychosis: A case-control study. - *BMJ Psych.,* **3,** 2003, 1-15.
19. **Toncheva., D, D. I. Gavrilov.** Contemporary standards for evaluation and treatment of family predispositions to breast and ovary carcinoma. At: Fourth National Conference, Varna, 10- 12.10.2013. Clinical behavior in breast carcinoma. Scientific book More 2013. Texts' for continuing (postgraduate) medical education. Editor Kalev. D. Varna, 10-12.10.2013, Art Treiser, 2013, 25-31.20.

20. **Tornjova-Randelova., S., D. Paskova-Topalova, J. Jordanov.** Dermatoglyphics in anthropology and medicine. Sofia, Academic Publishing house "Marin Drinov", 2011, 176.
21. **Tornjova-Randelova S., P. Borissova, D. Paskova-Topalova.** Quantitative characterization of finger and palm dermatoglyphics in Bulgarians. - *Anthropol Anz.,* **66,** 2008, 295-315.
22. **van Os, J., P. Woodruff, L. Fananas, F. Ahmed, N. Shuriquie, R. Howard, et al.** Association between cerebral structural abnormalities and dermatoglyphic ridge counts in schizophrenia. - *Comp Psychiatry,* **41,** 2000, 380-384.

Institute of Experimental Morphology, Pathology and Anthropology with Museum
Bulgarian Anatomical Society

Acta morphologica et anthropologica, 25 (1-2)
Sofia ● 2018

Review Articles

Transradial Approach for Heart Catheterization

Iva N. Dimitrova[1], Georgi Kotov[2], Alexandar Iliev[2], Boycho Landzhov[2]*

[1] *Department of Cardiology, University Hospital "St. Ekaterina", Medical University, Sofia, Bulgaria*
[2] *Department of Anatomy, Histology and Embryology, Medical University, Sofia, Bulgaria*

* Corresponding author e-mail: dimytrova@yahoo.com

Over the last decade, the transradial approach has become the preferred method for heart catheterization during diagnostic and therapeutic procedures. Compared to the more traditional transfemoral approach, it has significant advantages, including easier hemostasis, lower vascular complications (such as bleeding, thrombosis, fistulas and pseudoaneurysm), reduced hospital stay and improved healthcare costs. Nevertheless, it still poses significant challenges, such as smaller diameter and limitations on catheter size, longer procedure times, longer learning curve and variability of the artery. Several studies, however, point out that transradial approach failures and procedure times depend on the experience of the operator and are no different than those for the transfemoral approach once operators become proficient enough.

Key words: radial artery, transradial approach, heart catheterization

Introduction

The transradial approach (TRA) for heart catheterization was successfully utilised for the first time in 1989 by Dr. Lucien Campeau, who performed a percutaneous diagnostic coronary angiography using the TRA [7]. Later on, in 1993, Dr. Ferdinand Kiemeneij reported a successful percutaneous coronary intervention (PCI) using the TRA [17]. Initially, the method was established as an alternative to the more frequent transfemoral approach (TFA) and as recently as 2008 was performed in only 1.3% of the coronary interventions in the United States [21]. Over the last decade, however, the TRA has become the preferred method for heart catheterization, especially in Europe and Asia [3, 11]. The right radial artery has been used in almost 90% of the cases [3]. Preference for the TRA stems from the fewer complications, which are due to the radial artery's unique anatomy [9]. Furthermore, according to literature data, TRA significantly decreases vascular complications and the duration of hospital stay and optimises healthcare costs more than TFA [2, 3, 9, 16]. Despite all these advantages, TRA can also

present difficulties during heart catheterization, most often caused by a variant radial artery [9]. Other disadvantages include the relatively high incidence of catheterization failure and limitations of catheter size [5, 16].

The aim of the present manuscript was to briefly review the normal anatomy and variants of the radial artery and their significance for TRA, as well as to outline the advantages and disadvantages of the procedure.

Normal anatomy and variants of the radial artery

The radial artery is the smaller of the two terminal branches of the brachial artery. It arises from the brachial artery in the cubital fossa and traverses through the lateral aspect of the forearm. Further distally, it enters the palm and anastomoses with the deep branch of the ulnar artery. The proximal portion of the artery courses underneath the brachioradialis muscle; its middle part lies adjacent to the superficial branch of the radial nerve. The distal third of the radial artery is positioned superficially, between the tendons of the brachioradialis and flexor carpi radialis muscle [18].

Fig. 1. Angiographic photo of radial loop-proximal portion (arrowhead)

Burzotta et al. authored a classification of the anatomical variants of the radial artery: 1) high origin of the radial artery; 2) radioulnar loops with superficial brachioradial artery; 3) radial artery loop **(Fig. 1);** 4) double radial artery and 5) high origin with double radial artery [6]. Jelev and Surchev divided radial artery variations into two types – "high-arm" and "low arm" [15]. The former included variations in the origin and/or course of the radial artery, which do not alter the "usual" access site in the wrist. These variations do not impede the insertion of the transradial catheter [15]. The "low-arm" variations included hypoplasia of the radial artery and/or atypical wrist access. These variants may render the TRA impossible (in cases of aplasia of the artery) or extremely difficult (in cases of hypoplastic arterial segments). The same authors reported that cardiac catheterization may be impeded by the following aberrant variants of the radial artery: tortuosities of the artery, a radial artery loop, a radio-ulnar loop or a course behind the biceps brachii tendon [15]. Anatomical variations, although not pathological in nature, can cause diagnostic and therapeutic difficulties, which is why they should always be have in mind by both surgeons and internists [10-12, 24].

Advantages and limitations of the TRA

One of the main advantages of the TRA is the anatomical position of the radial artery. In the distal third of the forearm, it is positioned superficially, which allows for easy hemostasis through mechanical compression with a pressure device or a bandage, thus evading complications such as haematoma, thrombosis, pseudoaneurysm, arterio-

venous fistulas and compartment syndrome [1, 4, 9, 19]. Furthermore, the double blood irrigation of the hand constitutes a mechanism for prevention of hand ischemia in cases of radial artery thrombosis, even though it is rare in patients after TRA catheterization [4, 9]. One meta-analysis of randomised trials reported the following advantages of the TRA: absence of major nerves or veins near the artery; no need for postprocedural bed rest, which allows for immediate ambulation, better comfort for the patient and early discharge, which in turn improves the quality of life and reduces hospital stay and hospitalisation costs [1]. These data have been supported by later studies [2, 3, 9, 16]. In comparison to the TFA, the TRA reduces the risk of vascular and bleeding complications by 78% and the need for transfusion by 80% [14]. The two criteria where TFA was rated as superior to TRA were technical results (accounting for success of the procedure) and procedure times [14]. Nevertheless, several studies point out that in truth, TRA failures and procedure times depend on the experience of the operator and are no different than those for TFA once operators become proficient enough [1, 13, 14].

The meta-analysis of Agostoni et al. indicated several reasons for a procedural failure [1]. An inability to successfully puncture the radial artery can be a result of insufficient operator skill, vessel tortuosity or persistent arterial spasm. Difficulties in rotating and manipulating the catheter may lead to failure to cannulate the coronary ostia. Moreover, an interventional procedure - either TRA or TFA - could also fail because of inadequate catheter support or an inability to track the device in the correct place [1]. Gaining access to the radial artery may present more technical challenges and is generally more time-consuming than gaining femoral access [1, 23]. TRA has historically been associated with greater radiation exposure to the operator. However, it can be mitigated through proper placement of the patient's arm at their side rather than abducted 90° - as well as with better experience and proficiency [14]. Another disadvantage may be the limitation on catheter size - i.e. inability to perform coronary procedures requiring an 8F catheter or larger [1, 23].

Fig. 2. Angiographic photo of radial loop-middle portion (arrowhead)

The reported failure rates of TRA vary between 1-5% [8]. Most often, they are the result of inability for radial puncture, arterial spasm or anatomical variants **(Fig. 2)**. The reported variations of the arteries of the upper limb vary between 4-18.5% [4, 20, 22]. Usually, these variations are not considered a reason for procedure inability. It is more likely, however, that a radial artery with a smaller diameter, a remnant radial artery or a slender radial artery may present difficulties during TRA heart catheterization [9]. The radial artery's diameter varies between 2.69±0.40 mm in males and 2.43±0.38 mm in females [5]. An attempt to pass through an artery with a smaller diameter may be uncomfortable or even painful for the patient and may lead to a spasm and risk of artery perforation [9]. An avulsion of the radial artery has also been described [25].

Conclusion

The TRA for heart catheterization is an excellent alternative to the classical TFA, which minimises local vascular complications, improves patient comfort and quality of life, significantly shortens the hospital stay and optimises healthcare costs. Despite these advantages, the TRA requires a longer learning curve and is still associated with some specific challenges, such as variability of the radial artery, higher failure rate and longer procedure times.

References

1. **Agostoni, P., G. G. Biondi-Zoccai, M. L. de Benedictis, S. Rigattieri, M. Turri, M. Anselmi, C. Vassanelli, P. Zardini, Y. Louvard, M. Hamon.** Radial versus femoral approach for percutaneous coronary diagnostic and interventional procedures; Systematic overview and meta-analysis of randomized trials. - *J. Am. Coll. Cardiol.,* **44**(2), 2004, 349-356.
2. **Bertrand, O. F., P. Bélisle, D. Joyal, O. Costerousse, S. V. Rao, S. S. Jolly, D. Meerkin, L. Joseph.** Comparison of transradial and femoral approaches for percutaneous coronary interventions: a systematic review and hierarchical Bayesian meta-analysis. - *Am. Heart J.,* **163,** 2012, 632-648.
3. **Bertrand, O. F., S. V. Rao, S. Pancholy, S. S. Jolly, J. Rodés-Cabau, E. Larose, O. Costerousse, M. Hamon, T. Mann.** Transradial approach for coronary angiography and interventions: results of the first international transradial practice survey. - *JACC Cardiovasc. Interv.,* **3**(10), 2010, 1022-1031.
4. **Bhatt, D. L.** Cardiovascular Intervention: A Companion to Braunwald's Heart Disease. - *Elsevier,* 2016, 36–48.
5. **Brzezinski, M., T. Luisetti, M. J. London.** Radial artery cannulation: a comprehensive review of recent anatomic and physiologic investigations. - *Anesth. Analg.,* **109**(6), 2009, 1763-1781.
6. **Burzotta, F., C. Trani, M. de Vita, F. Crea.** A new operative classification of both anatomic vascular variants and physiopathologic conditions affecting transradial cardiovascular procedures. - *Int. J. Cardiol.,* **145,** 2010, 120-122.
7. **Campeau, L.** Percutaneous radial artery approach for coronary angiography. – *Cathet. Cardiovasc. Diagn.,* **16**(1), 1989, 3-7.
8. **Dimitrova, I., D. Trendafilova, A. Iliev, B. Landzhov.** Transradial catheterization failure due to high-bifurcating hypoplastic radial artery: case report. - *Acta Morphol. Anthropol.,* **24**(3-4), 2017, 86-88.
9. **Dimitrova, I., D. Trendafilova, A. Iliev, P. Simeonov, G. Kotov, B. Lanzdhov.** Radial artery variations and their influence on transradial approach during coronary angiography. - *Compt. Rend. Acad. Bulg. Sci.,* 2018. (in press).
10. **Georgiev, G. P.** Significance of anatomical variations for clinical practice. - *Int. J. Anat. Var.,* **10**(3), 2017, 43-44.
11. **Georgiev, G. P., I. Dimitrova.** Radial artery variations in interventional cardiology. - *Int. J. Anat. Var.,* **10**(4), 2017, 101-102.
12. **Georgiev, G. P., I. Dimitrova, L. Jelev, D. Marinova.** A case with aberrant origin of the brachial and antebrachial arteries and some remarks on the terminology of the upper limb variant arteries. - *J. Biomed. Clin. Res.,* **2**(1), 2009, 172-173.
13. **Goldberg, S. L., R. Renslo, R. Sinow, W. J. French.** Learning curve in the use of the radial artery as vascular access in the performance of percutaneous transluminal coronary angioplasty. - *Cathet. Cardiovasc. Diagn.,* **44**(2), 1998, 147-152.
14. **Helfrich, C. D., T. T. Tsai, S. V. Rao, J. M. Lemon, E. C. Eugenio, M. I. Vidovich, A. R. Shroff, B. S. Speiser, C. L. Bryson.** Perceptions of advantages and barriers to radial-access percutaneous coronary intervention in VA cardiac catheterization laboratories. - *Cardiovasc. Revasc. Med.,* **15**(6-7), 2014, 329-333.
15. **Jelev, L., L. Surchev.** Radial artery coursing behind the biceps brachii tendon: significance for the transradial catheterization and a clinically oriented classification of the radial artery variations. - *Cardiovasc. Intervent. Radiol.,* **31,** 2008, 1008-1012.

16. **Jolly, S. S., S. Yusuf, J. Cairns, K. Niemelä, D. Xavier, P. Widimsky, A. Budaj, M. Niemelä, V. Valentin, B.S. Lewis, A. Avezum, P. G. Steg, S. V. Rao, P. Gao, R. Afzal, C. D. Joyner, S. Chrolavicius, S. R. Mehta.** Radial versus femoral access for coronary angiography and intervention in patients with acute coronary syndromes (RIVAL): a randomised, parallel group, multicentre trial. - *Lancet.,* **377,** 2011, 1409-1420.
17. **Kiemeneij, F., G. J. Laarman.** Percutaneous transradial artery approach for coronary stent implantation. - *Cathet. Cardiovasc. Diagn.,* **30**(2), 1993, 173-178.
18. **Nasr, A. Y.** The radial artery and its variations: anatomical study and clinical implications. - *Folia Morphol. (Warsz),* **71**(4), 2012, 252-262.
19. **Norgaz, T., S. Gorgulu, S. Dagdelen.** Arterial anatomic variations and its influence on transradial coronary procedural outcome. - *J. Interv. Cardiol.,* **25**(4), 2012, 418-424.
20. **Ostojić, Z., J. Bulum, A. Ernst, M. Strozzi, K. Marić-Bešić.** Frequency of radial artery anatomic variations in patients undergoing transradial heart catheterization. - *Acta Clin. Croat.,* **54**(1), 2015, 65-72.
21. **Rao, S. V., F. S. Ou, T. Y. Wang, M. T. Roe, R. Brindis, J. S. Rumsfeld, E. D. Peterson.** Trends in the prevalence and outcomes of radial and femoral approaches to percutaneous coronary intervention: a report from the National Cardiovascular Data Registry. - *JACC Cardiovasc. Interv.,* **1**(4), 2008, 379-386.
22. **Rodríguez-Niedenführ, M., T. Vázquez, L. Nearn, B. Ferreira, I. Parkin, J. R. Sañudo.** Variations of the arterial pattern in the upper limb revisited: a morphological and statistical study, with a review of the literature. - *J. Anat.,* **199,** 2001, 547-566.
23. **Sallam, M., H. Al-Hadi, S. Rathinasekar, S. Chandy.** Comparative Study of the Radial and Femoral Artery Approaches for Diagnostic Coronary Angiography. - *Sultan Qaboos Univ. Med. J.,* **9**(3), 2009, 272-278.
24. **Stanchev, S., A. Iliev, G. P. Georgiev, L. Malinova, B. Landzhov.** A case of bilateral variations in the arterial branching in the upper limb and clinical implications. - *CP Case,* **1**(1), 2017, 006.
25. **Vasanth Kumar, A., A. Anirudh Kumar, V. Sameeraja, P. Mruthyunjaya Kumar.** Avulsion of radial artery during coronary angiogram - A case report. - *IHJ Cardiovasc. Case Rep.,* **1**, 2017, 80-82.

Institute of Experimental Morphology, Pathology and Anthropology with Museum
Bulgarian Anatomical Society

Acta morphologica et anthropologica, 25 (1-2)
Sofia ● 2018

Electron Microscopy Studies on the Ultrastructure of the Myocardium in Spontaneously Hypertensive Rats

Alexandar Iliev[1], Georgi Kotov[1], Iva Dimitrova[2], Boycho Landzhov[1]*

[1] *Department of Anatomy, Histology and Embryology, Medical University, Sofia, Bulgaria*
[2] *Department of Cardiology, University Hospital "St. Ekaterina", Medical University, Sofia, Bulgaria*

* Corresponding author e-mail: dralexiliev@abv.bg

A number of morphological studies on the ultrastructure of the myocardium show that myocardial hypertrophy is associated with hypertrophy of the individual cardiomyocytes, as well as an increase in their number (hyperplasia), hyperplasia of the cellular organelles, alterations in cell nuclei and interstitial proliferation. The various subcellular components increase or decrease disproportionally, i.e. can be regulated individually and different patterns may be formed depending on the factor initiating cardiac hypertrophy. Electron microscopy studies of the left ventricle of spontaneously hypertensive rats at the age of 1 month do not show significant differences between them and normotensive control animals. Adult (6-month old) spontaneously hypertensive rats, however, exhibit significant differences, including a higher number of nucleoli, fragmentation of mitochondrial cristae, increase in the myofibril/mitochondria volume ratio, proliferation of rough endoplasmic reticulum and rearrangement of the myofribrils, among others. With the progress of hypertension, the myocardial ultrastructure exhibits signs of hypertrophy, as well as initial degeneration.

Key words: myocardium, electron microscopy, ultrastructure, spontaneously hypertensive rat (SHR)

Introduction

The hypertrophy of the cardiac muscle represents perhaps the most important adaptive mechanism of the heart in response to increased workload [11]. A number of morphological studies on the ultrastructure of the hypertrophied myocardium have been done on both human subjects and experimental animal models [3, 11-16]. These studies showed that myocardial hypertrophy was associated with hypertrophy of the individual cardiomyocytes, as well as an increase in their number (hyperplasia), hyperplasia of the cellular organelles, alterations in cell nuclei and interstitial proliferation [11, 12]. Lund and Tomanek reported an increase in myofibril/cell-volume and a decrease in mitochondria/myofibril-volume ratios in spontaneously hypertensive rats (SHR) [15]. They also noted the presence of double intercalated discs and hypolemmal zones with abundant sarcoplasm rich in small mitochondria, Golgi complexes and free filaments. Several studies have also reported a decrease in the capillary density of the hypertrophied myocardium [9, 15]. Goldstein et al. studied the ultrastructural features of the hypertrophied left ventri-

cle in rabbits [4]. They discovered that the ultrastructure of the mitochondria was normal but their respiratory activity was increased. Furthermore, they observed an abundance of ribosomes and granular endoplasmic reticulum, widening of the Z bands and distortions of the intercalated discs, which were all interpreted as signs of increased protein synthesis. This and other studies concluded that the various subcellular components increase or decrease disproportionally, i.e. can be regulated individually and different patterns may be formed depending on the factor initiating cardiac hypertrophy [1, 4, 11].

Over the course of development of hypertrophy, the myocardium undergoes three distinct stages of changes. The first stage is characterised by an increase in protein synthesis and energy production with preserved cardiac function [16]. A stable state of cardiac hyperfunction exists in the second stage [16]. The third stage is associated with gradual exhaustion of the heart's protein synthesising apparatus, damage of the myofibrils, insufficient renewal of the mitochondria and eventually cellular atrophy [16]. Spontaneously hypertensive rats (SHR) are often used as a reliable model of hypertension in humans, which allows researchers to study the morphological basis and exact mechanisms through which hypertension leads to cardiac hypertrophy [8, 10, 12, 15].

Electron microscopy findings in the cardiomyocytes of young SHR (1-month-old)

Electron microscopy studies of the left ventricle of SHR at this early age do not show significant differences between SHR and control animals of the Wistar strain [12]. Our studies on 1 month old SHR revealed the presence of one or more nuclei, mostly centrally located. The nuclear membrane was clearly visualised and was mostly smooth, with very few convolutions **(Fig. 1)**. In line with the increased protein synthesis and growth of the cardiomyocytes associated with this period of the postnatal development, we noted the presence of finely dispersed chromatin and multiple nucleoli in a large number of nuclei. Mitochondria were arranged in one or more rows between the nuclei and the myofibrils and were most numerous in the central sarcoplasmic spaces and the subsarcolemmal sarcoplasm **(Fig. 2)**. Cury et al. reported the presence of various shapes of mitochondria: round (with approximately equal major and minor diameter); elongated (with major diameter significantly longer than the minor diameter) and mitochondria with irregular shape [2]. Palmer et al. divided the mitochondria into subsarcolemmal and interfibrillar based on their location [17]. Transmission electron microscopy (TEM)

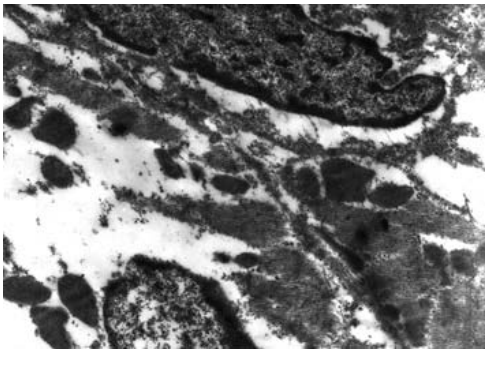

Fig. 1. Electron micrograph of the nucleus of a cardiomyocyte in a 1-month-old spontaneously hypertensive rat (SHR). Magnification x 7000

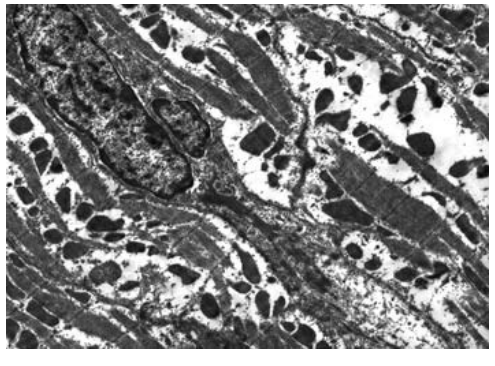

Fig. 2. Electron micrograph showing rows of mitochondria in a cardiomyocyte in a 1-month-old spontaneously hypertensive rat (SHR). Magnification x 4300

also makes it possible to visualise mitochondrial cristae which can be either lamelliform or tubular [7]. Riva et al. discovered that the cristae in subsarcolemmal mitochondria are lamelliform, while those in interfibrilar mitochondria tend to be tubular [18]. Goto et al. studied the ultrastructural characteristics of the sarcoplasmic reticulum and the abundance of caveolae in several groups of SHR and compared them with control animals [5]. These authors found that in young (5-week-old) animals the findings were consistent with the normal structure observed in the control group. In our studies on the ultrastructure of the myocardium of SHR, we also observed and described the structure and specific orientation of the myofibrils. They exhibited clearly visible cross-striations, with notable Z, I, A and M bands and were oriented along the long axis of the cardiomyocyte **(Fig. 3)**. As described by previous studies [11, 12], at this early age, the sarcomeres exhibit various stages of maturation. In less mature cardiac muscle cells, the thin and thick filaments could be arranged more loosely, with characteristic accumulation of glycogen granules between them [12]. Furthermore, these authors report that less mature and poorly organised sarcomeres tend to be located in the subsarcolemmal zone, in close proximity to abundant elements of rough endoplasmic reticulum, which is consistent with the process of myofribrillogenesis.

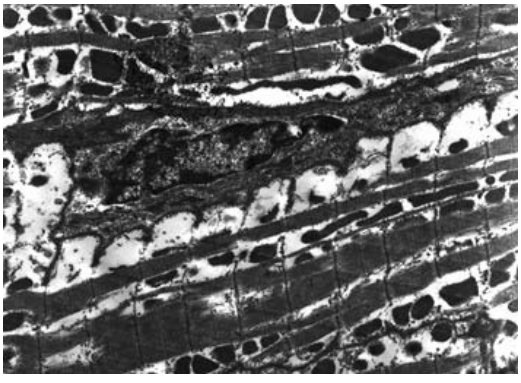

Fig. 3. Electron micrograph showing arrangement of the sarcomeres in a cardiomyocyte in a 1-month-old spontaneously hypertensive rat (SHR). Magnification x 4300

Electron microscopy findings in the cardiomyocytes of adult SHR (6-month-old)

In adult (6-month-old) animals, cardiac hypertrophy initiated by the elevated blood pressure reaches its full development. As shown by our previous studies, this process is related to increase in the thickness of the free wall and cross-sectional area of the cardiomyocytes and their nuclei, as well as accumulation of collagen fibres in the subendocardial and interstitial zone [8, 10]. The electron microscopic study of the subcellular structures revealed marked changes from normotensive control animals and the group of young SHR. Kawamura et al. reported that this stage of hypertrophy is associated with heterogeneous changes in the contractile elements, the mitochondria and the sarcoplasmic reticulum, which suggests heterogeneous malfunctions in later stages of cardiac hypertrophy [12]. In our studies, we noted that the nuclei of hypertrophied cells had a bigger number of nucleoli and their membranes were highly convoluted **(Fig. 4)**. These findings confirm the data of Maron et al. on human hearts [16] and can be interpreted as enhanced transcription in line with the increased protein synthesis in hypertrophied cells. The ultrastructural organisation showed signs of intracellular oedema. We noted that the mitochondria appeared swollen and there was evidence of fragmentation of the cristae in some of them **(Fig. 5)**. Similar results were obtained by Kawamura et al., who also noted disproportional changes in the volumes of the myofibrils and the mitochondria, resulting in a significant increase in the myofibril/mitochondria volume ratio [12]. Goto et al. reported an abnormal rearrangement of the caveolae leading to formation of caveolar conglomerates distributed in bands with variable width, parallel to the long axis of the myocardium in adult animals with significant hypertension [5]. They also

observed a higher density of the rough sarcoplasmic reticulum and fragmentation of the mitochondrial cristae [5]. The organisation of the myofibrils also appears to be altered in adult SHR. Upon comparison with the age-matched control animals and young SHR, we noted that myofibrils in 6-month-old SHR had a much more chaotic distribution, with more prominent Z-bands **(Fig. 6)**. Similar findings were reported by other authors [11, 14]. An interesting finding was described by Kawamura et al. who observed that myofibrils from adjacent cells were fixed in different stages of contraction [12]. Myofibrils on one side of the intercalated disc showed pronounced contraction, while on the other side, myofibrils were less markedly contracted. A possible explanation could be dissynchronous contraction in hypertrophied cells of adult animals. The same study found the intercalated discs in older animals tend to be longer and much more convoluted [12]. Legato et al. reported that pressure overloaded hearts contain smaller yet more numerous mitochondria [14]. They also noted the presence of double intercalated discs. Another prominent feature of cardiomyocytes from hypertensive animals was the presence of polyribosomes aligned along the long axes of thick filaments, which could be explained by the increased protein synthesis [14]. Fragments of myofilaments, rough endoplasmic reticulum and polyribosomes were also described under the sarcolemma and in close proximity to the intercalated disc and interpreted as areas of sarcomerogenesis [14].

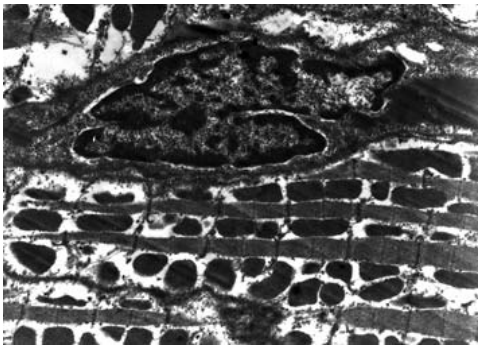

Fig. 4. Electron micrograph of the nucleus of a cardiomyocyte in a 6-month-old spontaneously hypertensive rat (SHR). Magnification x 7000

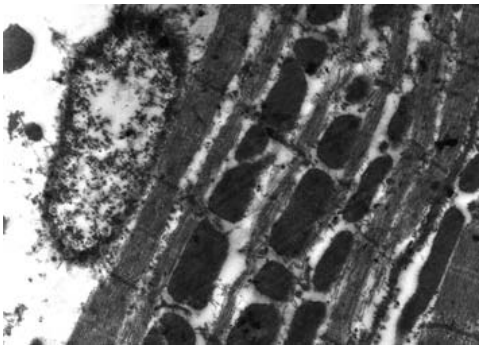

Fig. 5. Electron micrograph showing mitochondria with signs of degeneration in a cardiomyocyte in a 6-month-old spontaneously hypertensive rat (SHR). Magnification x 12 000

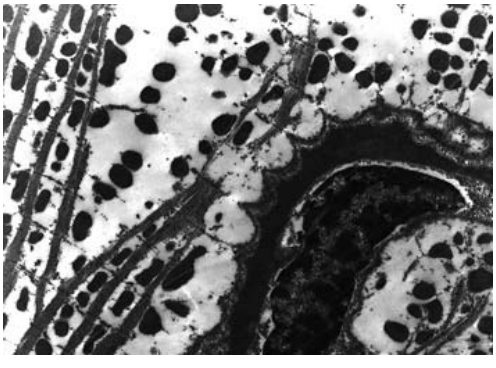

Fig. 6. Electron micrograph showing arrangement of the sarcomeres in a cardiomyocyte in a 6-month-old spontaneously hypertensive rat (SHR). Magnification x 4300

Conclusion

While the ultrastructural organisation in young SHR is mostly consistent to findings in normotensive control animals, adult SHR exhibit marked alterations. Changes in the various subcellular elements are heterogenous but it can be concluded that at the age of 6 months, the myocardial ultrastructure is consistent with the process of hypertrophy and intensive protein synthesis, while also beginning to exhibit signs of initial degeneration.

References

1. **Colgan, J. A., M. L. Lazarus, H. G. Sachs.** Post-natal development of the normal and cardiomyopathic Syrian hamster heart: a quantitative electron microscopic study. - *J. Mol. Cell. Cardiol.,* **10**(1), 1978, 43-54.
2. **Cury, D. P., F. J. Dias, M. C. Sosthenes, C. A. Dos Santos Haemmerle, K. Ogawa, M. C. da Silva, J. P. Mardegan Issa, M. M. Iyomasa, I. S. Watanabe.** Morphometric, quantitative, and three-dimensional analysis of the heart muscle fibers of old rats: transmission electron microscopy and high-resolution scanning electron microscopy methods. - *Microsc. Res. Tech.,* **76**(2), 2013, 184-195.
3. **Forbes, M. S., E. E. van Niel, S. I. Purdy-Ramos.** The atrial myocardial cells of mouse heart: a structural and stereological study. - *J. Struct. Biol.,* **103**(3), 1990, 266-279.
4. **Goldstein, M. A., L. A. Sordahl, A. Schwartz.** Ultrastructural analysis of left ventricular hypertrophy in rabbits. - *J. Mol. Cell. Cardiol.,* **6**(3), 1974, 265-273.
5. **Goto, Y., H. Yoshikane, M. Honda, S. Morioka, Y. Yamori, K. Moriyama.** Three-dimensional observation on sarcoplasmic reticulum and caveolae in myocardium of spontaneously hypertensive rats. - *J. Submicrosc. Cytol. Pathol.,* **22**(4), 1990, 535-542.
6. **Hibbs, R. G., V. J. Ferrans.** An ultrastructural and histochemical study of rat atrial myocardium. - *Am. J. Anat.,* **124**(3), 1969, 251-270.
7. **Hoppel, C. L., B. Tandler, H. Fujioka, A. Riva.** Dynamic organization of mitochondria in human heart and in myocardial disease. - *Int. J. Biochem. Cell Biology,* **41**(10), 2009, 1949-1956.
8. **Iliev, A. A., G. N. Kotov, I. N. Dimitrova, B. V. Landzhov.** Evaluation of structural myocardial changes during chronic hypertensive states in rats. - *J. Cardiol. Cardiovasc. Sciences,* **2**(1), 2018, 1-9.
9. **Iliev, A., G. Kotov, B. Landzhov, L. Jelev, I. Dimitrova, L. Malinova, D. Hinova-Palova.** A comparative analysis of capillary density in the myocardium of normotensive and spontaneously hypertensive rats. - *Acta Morphol. Anthropol.,* **24**(1-2), 2017, 19-25.
10. **Iliev, A. A., G. N. Kotov, B. V. Landzhov, L. S. Jelev, V. K. Kirkov, D. V. Hinova-Palova.** A comparative morphometric study of the myocardium during the postnatal development in normotensive and spontaneously hypertensive rats. - *Folia Morphol. (Warsz),* 2018, DOI: 10.5603/FM.a2017.0094. (in press)
11. **Imamura, K.** Ultrastructural aspect of left ventricular hypertrophy in spontaneously hypertensive rats: a qualitative and quantitative study. - *Jpn. Circ. J.,* **42**(8), 1978, 979-1002.
12. **Kawamura, K., C. Kashii, K. Imamura.** Ultrastructural changes in hypertrophied myocardium of spontaneously hypertensive rats. - *Jpn. Circ. J.,* **40**(10), 1976, 1119-1145.
13. **Kimpara, T., M. Okabe, H. Nishimura, T. Hayashi, K. Imamura, K. Kawamura.** Ultrastructural changes during myocardial hypertrophy and its regression: long-term effects of nifedipine in adult spontaneously hypertensive rats. - *Heart Vessels,* **12**(3), 1997, 143-151.
14. **Legato, M. J., L. A. Mulieri, N. R. Alpert.** The ultrastructure of myocardial hypertrophy: why does the compensated heart fail? - *Eur. Heart. J.,* **5**(Suppl F), 1984, 251-269.
15. **Lund, D. D., R. J. Tomanek.** Myocardial morphology in spontaneously hypertensive and aortic-constricted rats. - *Am. J. Anat.,* **152**(2), 1978, 141-151.
16. **Maron, B. J., V. J. Ferrans, W. C. Roberts.** Ultrastructural features of degenerated cardiac muscle cells in patients with cardiac hypertrophy. - *Am. J. Pathol.,* **79**(3), 1975, 387-434.
17. **Palmer, J. W., B. Tandler, C. L. Hoppel.** Biochemical properties of subsarcolemmal and interfibrillar mitochondria isolated from rat cardiac muscle. - *J. Biol. Chem.,* **252**(23), 1977, 8731-8739.
18. **Riva, A., B. Tandler, F. Loffredo, E. Vazquez, C. Hoppel.** Structural differences in two biochemically defined populations of cardiac mitochondria. - *Am. J. Physiol. Heart Circ. Physiol.,* **289**(2), 2005, H868-H872.

Institute of Experimental Morphology, Pathology and Anthropology with Museum
Bulgarian Anatomical Society

Acta morphologica et anthropologica, 25 (1-2)
Sofia ● 2018

Impact of Autoimmunity on Oogenesis and Ovarian Morphology

Maya Markova[*]*, Stefka Delimitreva, Anton Kolarov, Ralitsa Zhivkova*

Department of Biology, Medical Faculty, Medical University, Sofia, Bulgaria

* Corresponding author e-mail:mayamarkov@gmail.com

Compromised tolerance to ovarian components can lead to autoimmune oophoritis. Histological examination of affected ovaries reveals a mononuclear infiltrate, in many cases initially restricted to the follicular theca and sometimes associated with polycystic appearance. Autoimmune oophoritis interferes with follicle maturation and eventually diminishes the number of growing follicles, with a corresponding impact on fertility and hormonal secretion. In severe cases, all follicles advanced beyond the primordial stage are destroyed, leading to premature ovarian insufficiency (failure). Among known autoantigens, most important are the components of zona pellucida and of steroidogenic cells. Autoimmune ovarian disease is often associated with Addison's disease. In some cases, it is a manifestation of autoimmune polyendocrine syndrome. Little is known at present about the effects of systemic autoimmune diseases on the ovary, but data from patients and animal models show decreased ovarian reserve.

Key words: autoimmunity, oophoritis, premature ovarian failure, oocyte, fertility

Autoimmune diseases result from loss of normal immune tolerance to self-antigens. Due to the involvement of multiple complex regulatory mechanisms in their etiology and development, they are difficult to diagnose and especially to treat. This review addresses the effects of autoimmune diseases on oogenesis and overall ovarian morphology, which in recent years have been revealed as much more diverse and profound than previously estimated.

Impact of anti-ovarian and other organ-specific autoimmune responses

When discussing the influence of autoimmunity on oogenesis and overall ovarian function, autoimmune responses against ovarian components should be considered first. Autoantibodies against various ovarian antigens are frequently found in sera of women with unexplained infertility, though it is unclear in what proportion of cases they are a causative factor [2].The phenotype of the positive women varies from asymptomatic (autoantibodies detected in sera of fertile controls) to varying degrees of autoimmune ovarian disease. This disease is manifested as autoimmune oophoritis and is characterized by mononuclear inflammatory cell infiltrate in the theca layer of growing follicles, with early follicles without lymphocytic infiltration [17]. At a later stage, the granulosa

layer can also be invaded, resulting in destruction of growing follicles. Even primordial follicles are eventually either damaged by the lymphocytes and inflammatory cells infiltrating the ovary, or recruited and exhausted. In its extreme form, autoimmune ovarian disease leads to complete abolition of ovarian function and premature ovarian insufficiency (failure), defined as amenorrhea before age 40 [19].

In a comprehensive study of 357 patients with premature ovarian failure, 14.3% showed signs of autoimmunity, though its pathogenetic significance could not be established [1].Reliable diagnosis of autoimmune oophoritis requires ovarian biopsy, which is performed rarely because of the difficult access to the ovaries and the very limited importance of this diagnosis for the management of the condition [19]. While the role of autoimmunity as a causal factor in ovarian insufficiency is often difficult to estimate in patients, it has been inequivocally established in animal models. For certain mouse hybrids – (C57B1/6Cr x A/JCr)F1 (B6A) and (C3H/HeMs x 129/J)F1 (C31), creating and maintaining immune tolerance to antigens of growing ovarian follicles is problematic and requires the presence of a functional thymus. Neonatal thymectomy of the hybrid females leads to autoimmune oophoritis with rapid loss of oocytes and follicles at early adulthood, which in 60% of animals is complete by the age of 3 months. At a later age (12 months), the dysgenic ovaries show a tendency to develop trabecular tumors [14, 18].

Among the range of anti-ovarian autoantibodies, those directed against zona pellucida glycoproteins have been studied in most detail. Zona pellucida is a highly resistant formation of extracellular matrix that provides support for the oocyte and at the same time allows its communication with surrounding granulosa cells that form thin transzonal projections [15]. Given the significance of the zona for the maturing oocyte and the zygote, it is not surprising that immune responses targeting this structure jeopardize oogenesis and fertilization. In women treated for infertility by assisted reproduction techniques, negative correlation has been reported between serum positivity for anti-zona pellucida antibodies and success of the procedure [8]. Immunization of female BALB/c mice with murine zona pellucida glycoprotein ZP3 causes autoimmune oophoritis. The resulting autoantibodies penetrate into growing follicles, bind to the zona and eventually lead to inflammatory infiltration and destruction of the follicle [11]. Contraceptive vaccines based on zona pellucida components have been discussed for a long time, but have not yet found application in veterinary practice; the oophoritis they cause makes them unsuitable for humans [10]. In addition to zona zellucida glycoproteins, aldehyde dehydrogenase ALDH1A1 and selenium-binding protein SBP1 have been revealed as ovarian autoantigens associated with autoimmune ovarian disease in a subset of infertile patients [3].

Apart from the above mentioned ovary-specific reactions, the autoimmune response can target steroidogenic cells in general and affect the adrenal cortex besides the ovary, leading to autoimmune Addison's disease. More than half of the patients with autoimmune ovarian insufficiency have also adrenal autoimmunity [17], while over 6% of women with Addison's disease have also premature ovarian insufficiency [4]. In some women with adrenal autoimmunity, the ovarian morphology does not correspond to "classical" insufficiency with diminished number of follicles, but is characterized instead by numerous ovarian cysts. These patients have lean complexion and low testosterone levels, which distinguishes their condition from typical polycystic ovary syndrome [7]. Most women with such atypical polycystic ovaries are in their 30s. A parallel could be drawn between their condition and that of adolescents with autoimmune polyendocrine syndrome. These young women present with antibodies to steroidogenic cells, autoimmune oophoritis with cystic ovaries and a lymphocytic infiltrate in the steroidogenic theca [20]. It can be concluded that the course of the autoimmune process is highly variable, leading to a spectrum of severity and a wide range of age at diagnosis.

In this respect, it is noteworthy that polycystic ovary syndrome tends to be associated with another organ-specific autoimmune endocrine disorder, Hashimoto's thyroiditis [9]. The polycystic morphology can be explained with the initial restriction of the autoimmune response to the theca cells, while granulosa cells are preserved for a certain period [20]. The sequence of autoimmune ovarian disease is illustrated in **Fig. 1**.

Little is known about the effects of non-organ-specific (systemic) autoimmunity on the ovary. Women with systemic lupus erythematosus are often presumed to have normal fertility. However, measurements of anti-Müllerian hormone in these patients show lowered levels, indicating decreased ovarian reserve [13]. A proportion of women with lupus have amenorrhea associated with autoantibodies to corpus luteum [21]. It is possible that the impact of systemic autoimmunity on patients' ovaries is eclipsed by the more severe involvement of other organs (primarily the kidneys) and the gonadotoxic effect of cyclophosphamide treatment, which alone can cause premature ovarian insufficiency [12]. Therefore, animal models could provide useful information. The MRL/MpJ (MRL/+) mice that are genetically prone to systemic autoimmunity have a decreased number of ovarian follicles (including primordial follicles) and corpora lutea by the age of 3 months, compared to C57BL/6 mice [16]. Systemic autoimmunity can also be induced in animals without genetic predisposition by suitable treatments, e.g. zymosan [5, 6]. Research on such models will help to elucidate the effects of non-organ-specific autoimmune diseases on the ovary, with respect to oogenesis as well as endocrine function.

Acknowledgements: This work was supported by Grant no. DN 13/6-15.12.2017 of the National Science Fund of the Bulgarian Ministry of Education and Science.

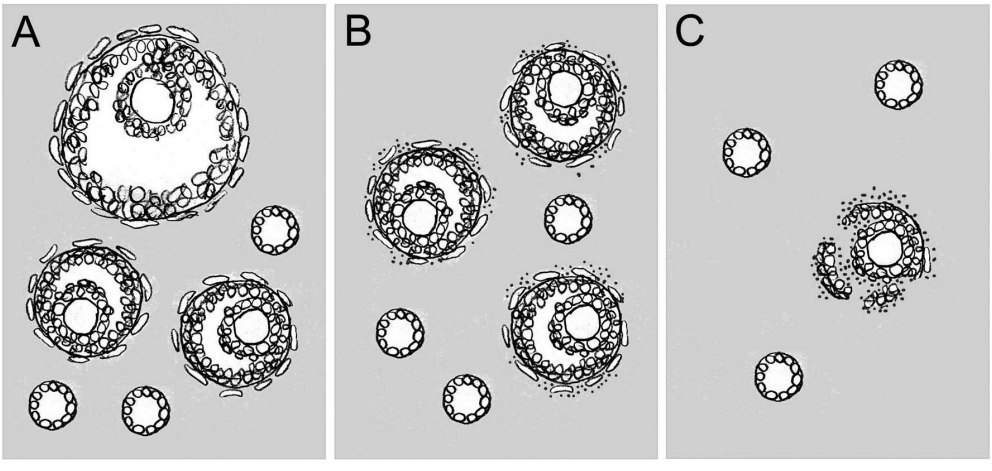

Fig. 1. Schematic drawings of progressive stages of autoimmune ovarian disease. A. Normal ovary, containing primordial, growing and preovulatory follicles. B. Oophoritis with theca infiltration (dots) hindering hormonal secretion, follicle growth and ovulation. In anti-zona pellucida response this stage may be skipped, while in anti-steroidogenic cell response it can be prolonged and lead to polycystic morphology. C. Penetration of the infiltrate into the granulosa and complete destruction of growing follicles. In a final stage (not shown), even primordial follicles are lost due to autoimmune targeting or excessive recruitment.

References

1. **Bachelot, A., A. Rouxel, N. Massin, J. Dulon, C. Courtillot, C. Matuchansky, Y. Badachi, A. Fortin, B. Paniel, F. Lecuru, M. A. Lefrère-Belda, E. Constancis, E. Thibault, G. Meduri, A. Guiochon-Mantel, M. Misrahi, F. Kuttenn, P. Touraine; POF-GIS Study Group.** Phenotyping and genetic studies of 357 consecutive patients presenting with premature ovarian failure. - *Eur. J. Endocrinol.,* **161,** 2009, 179-187.
2. **Delimitreva, S. M., R. S. Zhivkova, I. V. Chakarova, V. P. Hadzhinesheva, V. V. Lazarov, D. K. Dimitrova-Dikanarova.** Reaction of sera from infertile female patients with fractionated phylogenetically conserved ovarian antigens measured by ELISA: a pilot study. - *JBCR (Pleven),* **10,** 2017, 37-39.
3. **Edassery, S. L., S. V. Shatavi, J. P. Kunkel, C. Hauer, C. Brucker, K. Penumatsa, Y. Yu, J. A. Dias, J. L. Luborsky.** Autoantigens in ovarian autoimmunity associated with unexplained infertility and premature ovarian failure. - *Fertil. Steril.,* **94,** 2010, 2636-2641.
4. **Erichsen, M. M., K. Lovas, B. Skinningsrud, A. B. Wolff, D. E. Undlien, J. Svartberg, K. J. Fougner, T. J. Berg, J. Bollerslev, B. Mella, J. A. Carlson, H. Erlich, E. S. Husebye.** Clinical, immunological, and genetic features of autoimmune primary adrenal insufficiency: observations from a Norwegian registry. - *J. Clin. Endocrinol. Metab.,* **94,** 2009, 4882-4890.
5. **Ganova, P., V. Gyurkovska, N. Ivanovska.** Osteoclast formation is delayed in the absence of functional complement activity in a model of rheumatoid arthritis. - *In: Osteoclasts: Cell Biology, Functions and Related Diseases* (Ed. C. Reeves), New York, Nova Science Publishers, 2015, 19-40.
6. **Ganova, P., V. Gyurkovska, L. Belenska-Todorova, N. Ivanovska.** Functional complement activity is decisive for the development of chronic synovitis, osteophyte formation and processes of cell senescence in zymosan-induced arthritis. - *Immunol. Lett.,* **190,** 2017, 213-220.
7. **Gleicher, N., V. A. Kushnir, S. K. Darmon, Q. Wang, L. Zhang, D. F. Albertini, D. H. Barad.** New PCOS-like phenotype in older infertile women of likely autoimmune adrenal etiology with high AMH but low androgens. - *J. Steroid Biochem. Mol. Biol.,* **167,** 2017, 144-152.
8. **Ivanova, M., T. Djarkova, M. Mollova, M. Petrov, T. Tikhomirova, F. Dakhno.** Zona pellucida autoantibodies in women undergoing ART. - *Folia Biol (Praha),* **45,** 1999, 59-62.
9. **Lazarov, V. V., N. L. Trifonova, D. K. Dimitrova-Dikanarova.** Antibodies against immunologically sequestered antigens in patients with polycystic ovary syndrome (PCOS). - *Akush.Ginekol. (Sofiia),* **55,** 2016, 35-39.
10. **Lekhwani, S., N. Vaswani, V. S. Ghalaut, V. Shanker, R. Singh.** Immunocontraceptives: How far from reality? - *Adv. Biomed. Res.* **3,** 2014, 247.
11. **Lloyd, M. L., J. M. Papadimitriou, S. O'Leary, S. A. Robertson, G. R. Shellam.** Immunoglobulin to zona pellucida 3 mediates ovarian damage and infertility after contraceptive vaccination in mice. - *J. Autoimmun.,* **35,** 2010, 77-85.
12. **Marder, W., S. Fisseha, M. A. Ganser, E. C. Somers.** Ovarian damage during chemotherapy in autoimmune diseases: Broad health implications beyond fertility. - *Clin. Med. Insights Reprod. Health,* **6,** 2012, 9-18.
13. **Martins, N. F. E., M. I. Seixas, J. P. Pereira, M. M. Costa, J. E. Fonseca.** Anti-müllerian hormone and ovarian reserve in systemic lupus erythematosus. - *Clin. Rheumatol.,* **36,** 2017, 2853-2854.
14. **Michael, S. D., L. De Angelo, A. Kaikis-Astaras.** Plasma protein and hormone profiles associated with autoimmune oophoritis and ovarian tumorigenesis in neonatally thymectomized mice. - *Autoimmunity,* **6,** 1990, 1-12.
15. **Nikolova, V., R. Zhivkova, M. Markova, T. Topouzova-Hristova, A. Mitkova, S. Delimitreva.** Characterization of mouse oocytes and oocyte-cumulus complexes extracted for nuclear matrix and intermediate filaments (NM-IF). - *Acta Morphol. Anthropol.,* **19,** 2012, 149-152.
16. **Otani, Y., O. Ichii, S. Otsuka-Kanazawa, M. Chihara, T. Nakamura, Y. Kon.** MRL/MpJ-Fas(lpr) mice show abnormalities in ovarian function and morphology with the progression of autoimmune disease. - *Autoimmunity,* **48,** 2015, 402-411.
17. **Silva, C. A., L. Y. Yamakami, N. E. Aikawa, D. B. Araujo, J. F. Carvalho, E. Bonfá.** Autoimmune primary ovarian insufficiency. - *Autoimmun. Rev.,* **13,** 2014, 427-430.
18. **Taguchi, O., Y. Nishizuka, T. Sakakura, A. Kojima.** Autoimmune oophoritis in thymectomized mice: detection of circulating antibodies against oocytes. - *Clin. Exp. Immunol.,* **40,** 1980, 540-553.

19. **Warren, B. D., W. K. Kinsey, L. K. McGinnis, L. K. Christenson, S. Jasti, A. M. Stevens, B. K. Petroff, M. G. Petroff.** Ovarian autoimmune disease: clinical concepts and animal models. - *Cell Mol. Immunol.,* **11,** 2014, 510-521.
20. **Welt, C.K.** Autoimmune oophoritis in the adolescent. - *Ann. N Y Acad. Sci.,* **1135,** 2008, 118-122.
21. **Zhivkova, R., M. Markova, V. Hadzhinesheva, I. Chakarova, V. Nikolova, S. Delimitreva.** Factors of reproductive failure in women with lupus erythematosus. - *Akush.Ginekol. (Sofiia),* **55,** 2016, 20-23.

Institute of Experimental Morphology, Pathology and Anthropology with Museum
Bulgarian Anatomical Society

Acta morphologica et anthropologica, 25 (1-2)
Sofia ● 2018

Impact of Cadmium on Male Fertility

Ekaterina Pavlova[*]*, Nina Atanassova*

Institute of Experimental Morphology, Pathology and Anthropology with Museum, Bulgarian Academy of Sciences, Sofia, Bulgaria

* Corresponding author e-mail: e_bankova@yahoo.com

Cadmium (Cd) is a heavy metal and a major environmental pollutant. The general population is exposed to Cd mainly via drinking water and food products. It accumulates and is proved to cause severe damage to a variety of organs such as lung, brain, testis, kidney, liver, blood system and bone. Cd exerts direct cytotoxicity within the testis, mainly targeting two specific cell populations, the Sertoli cells and the Leydig cells, with consequent impairment of spermatogenesis and endocrine function. Cd induced oxidative stress in somatic and germ cells, mainly mediated by mimicry and interference with essential ions, beyond apoptosis occurring in germ cells. After Cd treatment disturbance of the hypothalamus-pituitary-gonadal axis is also reported.

Key words: cadmium, testis, fertility

Cadmium, in its pure form, is a soft silver-white metal, which is present in the earth crust in association with multiple different metals. Cd is indeed extracted as a secondary product, during the processing of different metals, such as zinc (Zn), lead (Pb), or copper (Cu). The presence of Cd and Cd compounds in the environment is a consequence of both natural and anthropic processes. Natural sources of Cd include volcanic activity, weathering consumption of rocks, sea aerosols, forest fires and mobilization from soils and landfills. As a derivative of anthropic activities, Cd and Cd compounds, such as Cd-chloride ($CdCl_2$), Cd-acetate and Cd-carbonate, derive from batteries, pigments, plastic stabilizers, pesticides and fertilizers, and photovoltaic devices, as well as from rubber processing, galvanization process, fossil combustion and waste incineration [6]. For the majority of animal species tested, the absorption of Cd can range from 0.5% to 3.0%, while in humans from 3.0% to 8.0% of the dose administered [20]. Factors influencing the uptake are chemical components of the diet, the body's nutritional status, age and gender proportionally to dosage used and time exposure to Cd [44]. Independently from the dietary Cd uptake, women seem to be more prone to Cd-related health effects, suggesting that a gender difference might exist in the susceptibility to Cd toxicity or in the body burden of Cd, probably because of differences in Cd absorption [13]. Indeed, the gastrointestinal absorption of dietary Cd is influenced by dietary intake of essential nutrients, including iron (Fe), Zn and selenium (Se) [6]. Cd concentration in blood is a marker of both recent and cumulative exposure, whereas urinary concentration mainly mirrors cumulative exposure [6, 13]. Among environmentally exposed population, to-

bacco smokers are the most exposed subjects, since tobacco leaves accumulate large amounts of Cd, making tobacco smoke the main source of Cd in smokers [6]. Non-smokers are exposed to Cd by dietary intake of contaminated food (particularly cereals and grains, leafy vegetables, potatoes and offal) and contaminated water, and vegetarians intake of Cd from food is almost double, compared to non vegetarians [13]. The occupational exposure occurs almost exclusively by inhalation of Cd-polluted fumes or dust and by ingestion through dust-contaminated hands. Workers in the metal refinery industry that release Cd have been shown to suffer from impaired health, such as damaged lungs, diarrhoea, stomach pains and severe vomiting, bone fracture, reproductive failure and possibly even infertility, damage to the central nervous system, psychological disorder, possibly DNA damage or cancer development [47].

It has been suggested that Cd is involved in carcinogenesis in multiple organs including kidney, prostate, liver and pancreas [4]. In fact, the International Agency for Research on Cancer (IARC) [18] classified Cd as a known human carcinogen in 1993 and Cd is ranked the 7th toxicant in the Priority List of Hazardous Substances of the Agency for Toxic Substances and Disease Registry [5, 49]. International and governmental agencies have made efforts to control and lower the Cd exposure to the general public in recent years. Nevertheless, Cd has a long biological half-life (20–40 years in humans) and it accumulates in the body over a considerable period of time. It accumulates and is proved to cause severe damage to a variety of organs such as lung, brain, testis, kidney, liver, blood system and bone [44, 55]. After absorption Cd is transported by blood and stored in organs rich in metallothionein (heart, intestine, kidney, liver, lung, pancreas, spleen and stomach), which exhibits high binding affinity for Cd [53].

Data showed that Cd affects the male reproductive system from embryonic stages to adulthood, and has adverse effects on gonadal development [52]. In mouse embryos, administration of Cd caused reduced genital ridge size and retarded migration of primordial germ cells into the genital ridges, resulting in attenuated populations of germ cells, aberrant maturation of gametes and subfertility [1, 51]. Cd has been demonstrated to affect spermatogenesis and/or semen quality and endocrine function, by different pathogenetic mechanisms. Cd severely affects testis structure, by damaging vascular endothelium and blood-testis barrier (BTB) integrity, and by inducing inflammation and apoptosis within the testis [24, 25]. Moreover, Cd exerts direct cytotoxicity within the testis, mainly targeting two specific cell populations, the Sertoli cells and the Leydig cells. It induced oxidative stress in somatic and germ cells, mainly mediated by mimicry and interference with essential ions, beyond apoptosis occurring in germ cells **(Fig. 1)** [13]. The interference with selected signaling pathways and the interference with the epigenetic regulation of genes involved in the regulation of the reproductive function, have been hypothesized as additional mechanisms of Cd-induced reprotoxicity, but have not been specifically investigated. Lastly, disturbance of the hypothalamus-pituitary-gonadal axis is also reported after Cd treatment.

Cadmium induces oxidative stress damage by decreasing the biological activities of some antioxidants, such as superoxide dismutase and glutathione peroxidase [23, 40, 45] with significant reductions in testicular function and androgen secretion [33]. Oxidative stress induced by Cd was associated with production of reactive oxygen species comprising mainly superoxide radical anion, hydrogen peroxide and hydroxyl radical. Oxidative stress is a common factor in about half of the infertile men, illustrating the importance of Cd [33]. It either leads to oxidative damage or activates signal transduction pathways to initiate defense responses [38]. Exposure to Cd is associated with elevated lipid peroxidation in many organs, inclusive the testis [33]. In birds, Cd affects various structures and metabolic processes, such as nucleic acids, carbohydrates, energy metabolism, protein synthesis and enzyme systems and serum testosterone levels [11].

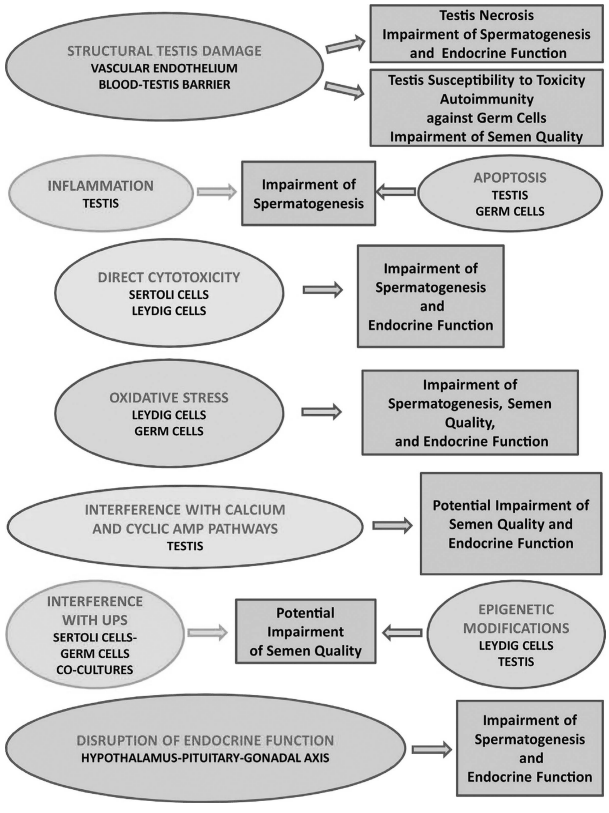

Fig. 1. Schematic overview of the proposed pathogenetic mechanisms of Cd-induced reprotoxicity by de Angelis et al. [2017]

Based on variability of testicular damage, several pathological mechanisms of Cd- induced testicular toxicity have been proposed. In mammals, among the most frequent mechanisms proposed were morphologic alterations and dysfunction in blood vessels [33]. Cadmium causes specific injury to the internal spermatic artery, its testicular and epididymal branches and the pampiniform plexus. It was suggested that Cd in almost all species with scrotal testis, acts principally on the blood vessels of the testis and epididymis, making them more permeable [46], which in turn determines fluid leakage into testis interstitium, followed by edema, hemorrhage, inflammation, hypoxia and, consequently, necrosis of the testis [3]. It was shown that Cd produced this effect by causing the breakdown of the junctions between endothelial cells of testicular capillaries and venules [39]. In particular, Cd was shown to induce alterations in the expression and function of the calcium-dependent cell adhesion molecule as vascular endothelial cadherin (VE-cadherin) at the cell–cell contacts, and a reorganization of the actin cytoskeleton [26, 42]. Cadmium induces a form of programmed necrosis in endothelial cells through disintegration of lysosomes followed by proteolysis, lipidolysis and digestion of nucleic acids resulting in the deterioration of physiological functions [33]. A specific metal ion transporter, ZIP8, has been identified as an enhancer of Cd uptake by vascular endothelial cells in the testis of mice, and its expression has been found to be associated to sensitivity to Cd-induced testis injury [12]. Thus reinforcing

the hypothesis that this transporter might be implicated in the differential susceptibility of animals to Cd toxic effects on vascular endothelial cells. The results of these studies suggest that vascular endothelium damage resulting in necrosis within the testis, may ultimately affect spermatogenesis and testis endocrine function [13].

Vascular smooth muscle cells (VSMC) can perform both contractile and synthetic functions, which are characterised by changes in morphology, proliferation and migration rates, and the expression of different marker proteins [33, 43]. VSMC are involved in physiological functions and pathological changes taking place in the vascular wall. In general, VSMC are sensitive to Cd cytotoxicity without any species-related differences, mainly due to a higher accumulation of the metal within cells [22]. Cadmium blocks the binding of androgen to the receptor but did not alter its affinity, suggesting that the metal is an inhibitor of hormone binding and may play a role in regulating testicular function and male fertility [33, 35].

As opposed to vascular mediated toxicity, it has been postulated that Cd exerts its effects via the physical and chemical properties of the Cd^{+2} ion, namely its similarities to calcium and zinc. As such, Cd is likely to substitute calcium or zinc in crucial physiological processes that are mediated by these ions, resulting in the activation and/or inhibition of several signaling pathways [48]. Zinc has a relationship with many enzymes in the body and can prevent cell damage through activation of the antioxidant defense system [33]. Decreased utilization of zinc by spermatogenic cells due to competitive action of Cd may cause disturbance in sperm developing process [2]. Several experimental studies in animals showed that Cd migh interfere with Se at multiple levels. Se is an essential element with pivotal functions in the maintenance of male reproduction, by influencing structure of the testis, spermatogenesis, semen quality and, ultimately, fertility [13].

An experimental *in vivo* study in animals showed that Cd exposure induced testis inflammation. Cd-loaded rats developed signs of testis inflammation, with significantly increased expression of inflammation markers, including inducible nitricoxide synthase, cyclooxygenase-2, tumor necrosis factor-α, nuclear factor-kB, and heme oxygenase-1, in testis homogenates [15]. Cd-induced testis inflammation resulted in widespread necrosis and vacuolization of the seminiferous epithelium cells, together with interstitial tissue edema and hemorrhage. These pathological changes were associated to an impairment of spermatogenesis [13, 15].

Sertoli cells show the major structural and functional alterations after Cd exposure, even at doses that do not result in visible damage within the testis [13]. Sertoli cells play crucial roles in supporting the self-renewal and differentiation of spermatogonial stem cells into mature sperm [27]. *In vitro* studies suggest that the Sertoli cell is the most vulnerable target of cadmium chloride and they are more sensitive than Leydig cells to Cd- induced damage [33]. The morphological changes in Sertoli cells after Cd exposure are associated with the induction of apoptosis [57]. Cadmium may selectively compromise the development and maintenance of the inter-Sertoli cell tight junctions (TJ), without affecting their secretory activity or the cell number and viability. In mouse, rat and cock Sertoli cells treated with Cd assumed chromatin condensation, nuclear cleaved into dense bodies, lamellar slight endoplasmic reticulum expansion, swelling mitochondria, and pathological vacuoles [7, 8, 31, 33].

The blood-testis-barrier (BTB) is a unique structure, formed by the tight junctions between adjacent Sertoli cells, which bisects the seminiferous epithelium into the basal and the apical/adluminal compartments, by segregating meiotic and post-meiotic germ cells behind the barrier in the apical compartment. Therefore BTB prevents not only the passage of cytotoxic agents from the blood into the seminiferous tubules, but also the passage of antigenic products of germ cell maturation into the circulation, which

might generate autoimmunity against germ cells [9, 13]. Although BTB is not a static ultrastructure, but undergoes massive remodeling during spermatogenesis in order to permit the transit of spermatocytes (preleptotene spermatocytes) [9, 13]. A damage of the BTB is associated with germ cells loss and reduced total sperm count, which determine subfertility or infertility conditions. Cadmium has been shown to dose- dependently affect BTB integrity, by inhibiting the establishment or inducing the disruption of the TJ between rat Sertoli cells *in vitro*, through a down regulation of occludin, a TJ integral membrane protein [10]. Setchell and Waites [46] demonstrated that the BTB is more vulnerable to Cd toxicity than the microvessels in adult rat testes, since the damage to the BTB occurred prior to the microvessels found in the interstitium. In addition, a single low dose of Cd at 1 mg/kg b.w. disrupted TJ associated microfilaments in rat Sertoli cells and also induced spermiation failure without visible vascular lesion in the testes [48]. Other studies have shown that E-cadherin is one of the primary targets of Cd toxicity in epithelial cells, since Cd interacts with the putative calcium-binding motif in E-cadherin, causing a disruption of the cadherin-based cell adhesion. But since E-cadherin coexists with tight junction-proteins (e.g., occludin, claudins, JAM-A) at the BTB, Cd would have immediate access to E-cadherin, making the testis more susceptible to Cd toxicity. Moreover, testosterone counteracted the Cd disruptive effects, possibly by inducing the expression of TJ integral membrane proteins such as occludin. Therefore, testosterone plays a crucial role in the regulation of Sertoli cells TJ-permeability barrier [10], which is consistent with data that androgen promotes the BTB integrity and cell adhesion function in the testis [36, 54]. These observations also illustrate that androgen (or a manipulation of the androgen receptor in Sertoli cells) can be a potential target candidate to manage Cd-induced testicular toxicity.

The studies focused on the correlation between exposure to Cd at environmental concentrations and semen quality are controversial. Several studies found a significant negative correlation between Cd concentration and semen parameters, whereas some studies failed to demonstrate a clear correlation between Cd exposure and semen quality [13]. Many studies in man and in various species of mammals showed that Cd induces various changes in testicular histopathology. A marked reduction of seminiferous tubular diameter after the high dose of Cd, along with the conspicuous decrease of the tubular volume density was reported [14, 33]. Repeated injections of low doses of Cd also impair spermatogenesis. Microscopical changes were observed in the germinal epithelium like necrosis, irreversible degeneration of germ cells and progressive sloughing from the basement membrane [33]. All testicular germ cell populations can be affected by Cd. This includes a decrease in number of spermatogonia and spermatocytes, aberrant morphology in all developing stages, release of immature cells into the lumen [4, 34, 41 58] and failure in spermiation [17]. Elongated and round spermatids, as well as spermatocytes were found in the tubule lumen in > 98% of tubules [37]. Spermatocytes displayed morphological characteristics of apoptosis, including chromatin condensation, cell shrinkage and apoptotic body formation in fowl [31, 33]. Besides sperm concentration, sperm motility is also severely affected by Cd. Sperm motility is recognized to be more sensitive to this trace element, as reduced sperm motility has been observed at a dose far below the dose affecting sperm production. However, it is concluded that Cd accumulation in germinal cells and Cd effects on sperm count and sperm motility are dose- and time dependent [1]. Data by Ige et al. [19] demonstrated that pre-treatment of rat model with Allium cepa extract prevented $CdSO_4$-induced reproductive toxicity by improving sperm quality and enhancing testicular lipid peroxidation status.

In male rodents, it is well established that Cd significantly alters the circulating levels of several hormones (e.g., testosterone, LH, FSH, Inhibin-B) [28, 32]. Previous

studies have shown that Cd impairs the testosterone production in isolated Leydig cells without affecting their viability [30, 56], demonstrating that steroidogenic disruption in Leydig cells is likely to be an initial target of Cd toxicity as an endocrine modulator. Cd can also modify hormone levels by affecting the hypothalamic-pituitary-testicular axis in different aspects, not only via its effects on Leydig cells. It was also shown that, in the testis of mice and rats, Cd affects the expression of steroidogenesis enzymes, such as StAR, cholesterol C20-22 desmolase, 17 β-hydroxylase, 17 β-hydroxysteroid dehydrogenase [21], and suppresses the expression of LH receptor [16, 28]. A large number of studies documented that Cd mimics the function of steroid hormones; therefore, this "metallohormone" has been proposed as endocrine disruptor interfering with endogenous endocrine system. It has been shown that Cd can directly bind to estrogen receptor and androgen receptor, and that Cd exerts strong estrogenic-like and androgenic-like actions, both *in vivo* and *in vitro* [13]. Estrogenic effects of Cd are mediated by the high affinity binding to the ligand-binding domain of estrogen receptor [50], the receptor isoform that drives the mitogenic actions of E_2 in target organs. Cd has been shown to prevent androgens from binding to their receptor, and to mimic the actions of androgens on cell growth and gene expression *in vitro* [35]. Moreover, *in vivo* studies in castrated rats demonstrated that low doses of Cd dose-dependently increased the weight of the prostate gland and of the seminal vesicles and this effect was blocked by an antiandrogen, thus suggesting that Cd actions are mediated by androgen receptor [13, 35]. All of these Cd effects on the endocrine system involved not only direct effects on target organs and cells, but also impairment of the circadian release of noradrenaline, with subsequent changes in GnRH secretion from the hypothalamus, in LH and prolactin secretion from the pituitary, and in testosterone circulating concentrations, in male rats [28, 29]. In summary, the results of these studies suggest that disruption of the hypothalamus-pituitary-gonadal axis may mediate the toxic effect of Cd on spermatogenesis and endocrine function of the testis [13].

Conclusions

Despite the heterogeneity of study designs in animal models and epidemiological studies in man, the data in literature strongly determine cadmium as reprotoxic element. Cadmium directly affect selected cell populations of the testis, which include direct cytotoxicity and functional impairment of Sertoli and Leydig cells, induced oxidative stress in both somatic and germ cells. It affects germ cell populations leading to reduced semen density and quality. Cadmium treatment causes a direct disturbance of the hypothalamus-pituitary-gonadal axis, which might impair spermatogenesis and endocrine function of the testis.

References:

1. **Alaee, S., A. Talaiekhozani, S. Rezaei, K. Alaee, E. Yousefian.** Cadmium and male infertility. - *J. Infertil. Reprod. Biol.,* **2**(2), 2014, 62-69.
2. **Amara, S., H. Abdelmelek, C. Garrel, P. Guiraud, T. Douki, J. L. Ravanat, A. Favier, M. Sakly, K. Ben Rhouma.** Preventive effect of zinc against cadmium-induced oxidative stress in the rat testis. - *J. Reprod. Dev.,* **54,** 2008, 129-134.
3. **Aoki, A., A. P. Hoffer.** Reexamination of the lesions in rat testis caused by cadmium. - *Biol. Reprod.,* **18** (4), 1978, 579–591.
4. **Aoyagi, T., H. Ishikawa, K. Miyaji, K. Hayakawa, M. Hata.** Cadmium-induced testicular damage in a rat model of subchronic intoxication. - *Reprod. Med. Biol.,* **12,** 2002, 59-63.

5. **ATSDR.** The 2007 CERCLA Priority List of Hazardous Substances. Agency for Toxic Substances and Disease Registry, U.S. Department of Health and Human Services, Atlanta, GA, 2007.
6. **ATSDR.** Toxicological profile for cadmium. *In: Toxicological Profiles, Agency for Toxic Substances and Disease Registry,* 2012.
7. **Bekheet, S. H. M.** Cadmium chloride rapidly alters both BTB tight junction proteins and germ cells in young rat testes. - *Egypt. Acad. J. Biolog. Sci.,* **2,** 2010, 59-74.
8. **Bizarro, P., S. Acevedo, G. Nino-Cabrera, P. Mussali-Galante, F. Pasos, M. R. Avila-Costa, T. I. Fortoul.** Ultrastructural modifications in the mitochondrion of mouse Sertoli cells after inhalation of lead, cadmium or lead-cadmium mixture. - *Reprod. Toxicol.,* **17,** 2003, 561-566.
9. **Cheng, C. Y., D. D. Mruk.** The blood-testis barrier and its implications for male contraception. – *Pharmacol. Rev.,* **64**(1), 2012, 16-64.
10. **Chung, N. P., C. Y. Cheng.** Is cadmium chloride-induced inter-sertoli tight junction permeability barrier disruption a suitable in vitro model to study the events of junction disassembly during spermatogenesis in the rat testis? - *Endocrinology,* **142**(5), 2001, 1878-1888.
11. **Cinar, M.** Cadmium and effects at biological system. – *Veterinarium,* **14,** 2003, 79-84.
12. **Dalton,T. P., L. He, B. Wang, M. L. Miller, L. Jin, K. F. Stringer, X. Chang, C. S. Baxter, D. W. Nebert.** Identification of mouse SLC39A8 as the transporter responsible for cadmium-induced toxicity in the testis. - *Proc. Natl. Acad. Sci.U. S. A.,* **102**(9), 2005, 3401-3406.
13. **De Angelis, C., M. Galdiero, C. Pivonello, C. Salzano, D. Gianfrilli, P. Piscitelli, A. Lenzi, A. Colao, R. Pivonello.** The Environment and Male Reproduction: the Effect of Cadmium Exposure on Reproductive System and Semen Quality and its Implication in Fertility. - *Reprod. Toxicol.,* **73,** 2017, 105-127
14. **De Souza Predes, F., M. A. Diamante, H. Dolder.** Testis response to low doses of cadmium in Wistar rats. - *Int. J. Exp. Pathol.,* **91,** 2010, 125-131.
15. **Fouad, A. A., W. H. Albuali, I. Jresat.** Simvastatin treatment ameliorates injury of rat testes induced by cadmium toxicity. - *Biol. Trace Elem. Res.,* **153**(1–3), 2013, 269-278.
16. **Gunnarsson, D., G. Nordberg, G., Selstam.** Differential effects of cadmium on the gene expression of seven-transmembrane-spanning receptors and GAPDH in the rat testis. – *Toxicol. Lett.,* **168,** 2007, 51-57.
17. **Hew, K. W., W. A. Ericson, M. J. Welsh.** A single low cadmium dose causes failure of spermiation in the rat. - *Toxicol. Appl. Pharmacol.,* **121,** 1993, 15-21.
18. **IARC**, IARC monographs vol. 100C. - *In: Evaluation of carcinogenic risks to humans,* International Agency for Research on Cancer, Lyon, France, 2012.
19. **Ige, S. F., S. B. Olaleye, R. E. Akhigbe, T. A. Akanbi, O. A. Oyekunle, U. A. Udoh.** Testicular toxicity and sperm quality following cadmium exposure in rats: Ameliorative potentials of Allium cepa. - *J. Hum. Reprod. Sci.,* **5**(1), 2012, 37-42.
20. **Järup, L., M. Berglund, C. G. Elinder, G. Nordberg, M. Vahter.** Health effects of cadmium exposure. A review of the literature and a risk estimate. - *Scand. J. Work Environ. Health,* **24**(1), 1998, 1-51.
21. **Ji, Y. L., H. Wang, P. Liu, X. F. Zhao, Y. Zhang, Q. Wang, H. Zhang, C. Zhang, Z. H. Duan, C. Meng, D. X. Xu.** Effects of maternal cadmium exposure during late pregnant period on testicular steroidogenesis in male offspring. - *Toxicol. Lett.,* **205**(1), 2011, 69-78.
22. **Kaji, T., C. Yamamoto, S. Miyajima, M. Suzuki, Y. Fujiwara, M. Sakamoto, F. Koizumi.** Vascular smooth muscle cells in culture are highly sensitive to cadmium cytotoxicity without species related differences: comparison with Chang liver cells. - *Biol. Pharm. Bull.,* **18,** 1995, 1392-1395.
23. **Kara, H., A. Cevik, V. Konar, A. Dayangac, M. Yilmaz.** Protective effects of antioxidants against cadmium-induced oxidative damage in rat testes. - *Biol. Trace. Elem. Res.,* **120,** 2007, 205-239.
24. **Kishimoto, T., T. Oguri, S. Yamabe, M. Tada.** Effect of cadmium injury on growth and migration of cultured human vascular endothelial cells. - *Hum. Cell,* **9,** 1996, 43-48.
25. **Kishimoto, T., Y. Fukuzawa, M. Abe, M. Isobe, M. Hashimoto, M. Tada.** Cadmium injury of cultured human vascular endothelial cells. - *Hum. Cell,* **4,** 1991, 329-334.
26. **Kolluru, G. K., K. P. Tamilarasan, P. Geetha, N. Durgha, S. Chatterjee.** Cadmium induced endothelial dysfunction: consequence of defective migratory pattern of endothelial cells in association with poor nitric oxide availability under cadmium challenge. - *Cell Biol. Int.,* **30,** 2006, 427-438.

27. **Kubota, H., M. Avarbock, R. Brinster.** Growth factors essential for selfrenewal and expansion of mouse spermatogonial stem cells. - *Proc. Natl. Acad. Sci. U. S. A.,* **101,** 2004, 16489-16494.
28. **Lafuente, A., A. Gonzalez-Carracedo, A. Romero, P. Cano, A. I. Esquifino.** Cadmium exposure differentially modifies the circadian patterns of norepinephrine at the median eminence and plasma LH, FSH and testosterone levels. - *Toxicol. Lett.,* **146,** 2004, 175-182.
29. **Lafuente, A., P. Cano, A. Esquifino.** Are cadmium effects on plasma gonadotropins, prolactin, ACTH, GH and TSH levels, dose-dependent? - *BioMetals,* **16,** 2003, 243-250.
30. **Laskey, J. W., P. V. Phelps.** Effect of cadmium and other metal cations on in vitro Leydig cell testosterone production. - *Toxicol. Appl. Pharmacol.,* **108,** 1991, 296-306.
31. **Li, J. L., R. Gao, S. Li, J. T. Wang, Z. X. Tang, S. W. Xu.** Testicular toxicity induced by dietary cadmium in cocks and ameliorative effect by selenium. - *Biometals,* **23,** 2010, 695-705.
32. **Luca, D., C. Lilli, C. Bellucci, F. Mancuso, M. Calvitti, I. Arato, G. Falabella, S. Giovagnoli, M. C. Aglietti, A. Lumare, G. Muzi, R. Calafiore, M. Bodo.** Toxicity of cadmium on Sertoli cell functional competence: an in vitro study, - *J. Biol. Regul. Homeost. Agents,* **27**(3), 2013, 805-816.
33. **Marettov, E., M. Maretta, J. Legáth.** Toxic effects of cadmium on testis of birds and mammals: a review. - *Animal reproduction science,* **155,** 2015, 1-10.
34. **Marettová, E., M. Maretta, J. Legáth.** Changes in the peritubular tissue of rat testis after cadmium treatment. - *Biol. Trace Elem. Res.,* **134,** 2010, 288-295.
35. **Martin, M. B., H. J. Voeller, E.P. Gelmann, J. Lu, E. G. Stoica, E. J. Hebert, R. Reiter, B. Singh, M. Danielsen, E. Pentecost, A. Stoica.** Role of cadmium in the regulation of AR gene expression and activity. - *Endocrinology,* **143**(1), 2002, 263-275.
36. **Meng, J., R. Holdcraft, J. Shima, M. Giswold, R. Braun.** Androgens regulate the permeability of the blood–testis barrier. - *Proc. Natl. Acad. Sci. U. S. A.,* **102,** 2005, 16696-16700.
37. **Mruk, D. D., C. Y. Cheng.** Environmental contaminants. Is male reproductive health at risk? - *Spermatogenesis,* **1,** 2011, 1-8.
38. **Nair, A. R., O. de Gheselle, K. Smeets, E. van Kerkhove, A. Cuypers.** Cadmium-induced pathologies: where is the oxidative balance lost (or not)? – *Int. J. Mol. Sci.,* **14,** 2013, 6116-6143.
39. **Niewenhuis, R. J., C. Dimitriu, W. C. Prozialeck.** Ultrastructural characterization of the early changes in intercellular junctions in response to cadmium (Cd2+) exposure in LLCPK1 cells. - *Toxicol. Appl. Pharmacol.,* **142,** 1997, 1-12.
40. **Patra, R. C., A. K. Rautray, D. Swarup.** Oxidative stress in lead and cadmium toxicity and its amelioration. - *Vet. Med. Int.,* 2011, http://dx.doi.org/10.4061/2011/457327.
41. **Pavlova, E., J. Ivanova, D. Dimova, Y. Gluhcheva, N. Atanassova.** Alterations in adult mouse testis after subacute intoxication with cadmium and monensin detoxication. - *Eur. Chem. Bull.,* **1**(11), 2012, 463-465.
42. **Prozialeck, W. C., J. Edwards, J. M. Woods.** The vascular endothelium as a target of cadmium toxicity. - *Life Sci.,* **79,** 2006, 1493-1506.
43. **Rensen, S. S. M., P. van Doevendans, G. Eys.** Regulation and characteristics of vascular smooth muscle cell phenotypic diversity. - *Neth. Heart J.,* **15,** 2007, 100-108.
44. **Sarkar, A., G. Ravindran, V. Krishnamurthy.** A brief review on the effect of cadmium toxicity: from cellular to organ level. - *Int. J. Biotech. Res.,* **3,** 2013, 17-36.
45. **Sen Gupta, R., J. Kim, C. Gomes, S. Oh, J. Park, W. B. Im, J. Y. Seong, R. S. Ahn, H. B. Kwon, J. Soh.** Effect of ascorbic acid supplementation on testicular steroidogenesis and germ cell death in cadmium-treatedmale rats. - *Mol. Cell Endocrinol.,* **221,** 2004, 57-66.
46. **Setchell, B. P., G. M. H. Waites.** Changes in the permeability of the testicular capillaries and of the "blood–testis barrier" after injection of cadmium chloride in the rat. – *J. Endocrinol.,* **47,** 1970, 81-86.
47. **Singh, P., S. Chaudhary, A. Patni, V. Sankhla.** Effect of cadmium chloride induced genotoxicity in bone marrow chromosomes of swiss albino mice and subsequent protective effects of Emblica officinalis and vitamin C. - *J. Herb. Med. Toxicol.,* **1**(2), 2007, 67-71.
48. **Siu, E. R. , E. W. Wong, D. D. Mruk, K. L. Sze, C. S. Porto, C. Y. Cheng.** An occludin-focal adhesion kinase protein complex at the blood-testis barrier: a study using the cadmium model. - *Endocrinology,* **150**(7), 2009, 3336–3344.
49. **Siu, E. R., D. D. Mruk, C. S. Porto, C. Y. Cheng.** Cadmium-induced testicular injury. - *Toxicol. appl. pharmacol.,* **238**(3), 2009, 240-249.

50. **Stoica, A., B. S. Katzenellenbogen, M. B. Martin.** Activation of estrogen receptor-alpha by the heavy metal cadmium. - *Mol. Endocrinol.,* **14**(4), 2000, 545-553.
51. **Tam, P., W. Liu.** Gonadal development and fertility of mice treated prenatally with cadmium during the early organogenesis stages. - *Teratology,* **32**(3), 1985, 453-462.
52. **Thompson, J., J. Bannigan.** Cadmium: toxic effects on the reproductive system and the embryo. - *Reprod. Toxicol.,* **25**(3), 2008, 304-315.
53. **Waalkes, M. P., C. D. Klaassen.** Concentration of metallothionein in major organs of rats after administration of various metals. - *Fundam.Appl. Toxicol.,* **5,** 1985, 473-477.
54. **Wang, R., S. Yeh, L. Chen, H. Lin, C. Zhang, J. Ni, C. Wu, P. A. di Sant'Agnese, M. de Mesy-Bentley, C. Tzeng, C. Chang.** Androgen receptor in Sertoli cell is essential for germ cell nursery and junctional complex formation in mouse testes. - *Endocrinology,* **147,** 2006, 5624-5633.
55. **World Health Organization. Regional Office for Europe.** Air quality guidelines. World Health Organization. Regional office for Europe, Copenhagen, Denmark, 2000.
56. **Yang, J. M., M. Arnush, Q. Y. Chen, X. D. Wu, B. Pang, X. Z. Jiang.** Cadmium induced damage to primary cultures of rat Leydig cells. - *Reprod. Toxicol.,* **17,** 2003, 553-560.
57. **Yu, X., S. Hong, E. M. Faustman.** Cadmium-induced activation of stress signaling pathways: disruption of ubiquitin-dependent protein degradation and apoptosis in primary rat Sertoli cell-gonocyte cocultures. - *Toxicol. Sci.,* **104,** 2008, 385-396.
58. **Zhou, T., X. Jia, R. E. Chapin, R. R. Maronpot, M. W. Harris, J. Liu, M. P. Waalkes, E. M. Eddy.** Cadmium at a nontoxic dose alters gene expression in mouse testes. - *Toxicol. Lett.,* **154,** 2004, 191-200.

Institute of Experimental Morphology, Pathology and Anthropology with Museum
Bulgarian Anatomical Society

Acta morphologica et anthropologica, 25 (1-2)
Sofia ● 2018

Preserving the Pontiff: an Account of the Body Preservation Methods Used by the Roman Catholic Church

Nikola Tomov[*]

Department of Anatomy, Faculty of Medicine, Trakia University, Stara Zagora, Bulgaria

* Corresponding author e-mail: tomovmd@gmail.com

Incorruptibility in an important topic in the major Christian denominations. If a body or its parts do not undergo the normal process of decay, it is sometimes considered a sign of sanctity, attributed to divine intervention. Even though body preservation and incorruptibility are seen as distinct, bodily remains of saints are objects of veneration.

Historically, many of the bodies of deceased Roman popes were artificially preserved, buried in conditions enhancing the probability of natural preservation, or both. These circumstances have created a number of bodily relics of popes, subsequently canonized as saints, even without claims for incorruptibility.

The present report summarizes some of the recorded methods used for preservation of the bodies of the Roman popes.

Key words: body preservation, embalming, pope, relics

Introduction

In the past, the lack of decay of a dead body has often been seen as miraculous. Finding a body which defies the natural course of decomposition was unexplainable and was attributed to a divine intervention. Some individuals were canonized as saints mainly because their body were found in a more or less preserved state, and were called Incorruptible [8].

The importance of relics was explained by Thomas Aquinas in his Summa Theologica: "In memory of [the saints], we ought to honor any relics in a fitting manner, principally their bodies, which were temples of the Holy Spirit dwelling and operating in them, and destined to be likened to the body of Christ by the glory of the Resurrection" [1]. The saints are viewed as intermediaries between this world and God, being liminal beings. They dwell both in this life as well in the afterlife, and are present in their physical bodies trough the Holy Spirit, as St. John Damascene says, "For death is rather the sleep of the saints than their death" [6].

The bodies of holy individuals are both temples of the Holy Spirit and "saving fountains which in many ways pour out benefactions" [6]. The preserved body becomes a sacramental icon, which preserves its human nature, while in the same time acts as a mediator of the divine [16].

Historically faithful have chosen to preserve the bodies of prominent individuals considered holy during their lifetime [10]. In this fashion laymen could remain in touch with the saint and ask for prayer intercession before God. The Pope is the most important figure in the Catholic church, being infallible and holding the seat of the Prince of Apostles St. Peter. Despite the controversies a Pope might be associated with, he is the Vicar Dei and occupies a special place between the laymen and God, similar to the one of a saint. Therefore, the desire to preserve a dead pope's body can be reasoned, both with practical, as well with spiritual reasons. The present report gives an insight on some of the practices used by the Catholic church for preservation of popes' bodies.

Historical Methods of Body Preservation

The following is a list of some of the methods, historically employed for the preservation of the dead Pontiff. It is based on literary sources, such as the works of the 14th century physician Guy de Chauliac, who performed embalmings of popes, and even developed separate protocols for lean and for adipose bodies. Those methods were quite successful, and allowed a body to be viewed for up to eight days, without decay [16].

Washing and shaving

Immediately following the last rites, the body of the deceased Pope was washed with warm water, and his beard and head were shaved [8]. This may have resulted in the most superficial layer of the skin being scraped off, making the skin more susceptible to further treatment.

Treatment of the skin

The first recorded account of treatment of the body originates from Pascal II's burial in 1118 [12]. The description (being "covered in balsam") is similar to one of impregnation [16]. More details regarding the preparation include that the body was rubbed with heated wine, containing aromatic herbs. It was rubbed vigorously before being anointed for the last time with balsam [8].

Removal of internal organs

Emptying of body cavities was not unknown to medieval embalmers. This provoked pope Boniface VIII in 1299 to issue his bull Detestande feritatis, which prevented division and disembowelment of the body for the sake preservation or remote burial [3]. However, evidence exists, that the body of the dead pope might have been incised [11] in order to release fluid and/or gas from the abdominal cavity [17].

It seems that this bull and the taboo for evisceration were soon forgotten. It is known that between 1590 and 1914 the papal praecorida (a term for vital organs, i.e. heart and intestines) were removed and buried separately in the church of Santi Vincenzo e Anastasio a Trevi. Most probably this was done as a part of a more elaborate embalming procedure, involving some of the other methods described. In the 20th century, this practice halted. John Paul II, however (who explicitly opposed his embalming) had a part of his intestines, removed during surgery following his assassination attempt in 1981 placed in the same church [15].

Cleansing of the intestines

Because of the taboo on evisceration, methods for removal of the bacteria-infested intestinal contents were developed. They included an enema with a decocotion of bitter apple and red borax to expel fecal matter, which was followed by another one, containing, among others, vinegar, rose oil, alum, aloe, myrrh, acacia, and nutmeg [17].

Sealing of the orifices

It is known that the anus, mouth, ears, and nostrils of the late pontiff were stuffed with cotton, wax, incense, and myrrh, aloe, and nutmeg, if available [8]. This was done mainly out of practical reasons, to stop putrid fluids from flowing out during the viewing of the body [16], but the conserving properties of the herbs and resins used should not be ignored.

Dressing

Since the Pope has to be buried in his liturgical vestments, his body is to be dressed in multiple layers of clothing, including trousers, shirt, hose, and tunic, followed by the belt and cincture, fanon, stole, short tunic, maniple, dalmatic, gloves, and pallium [8, 16]. The cloth of the garments can act as an absorbent for any fluids that might flow out of the body during purification. The innermost layers of cloth can also stick to the surface of the body, especially when there is treatment of the latter with balsam and resins [8, 12]. Upon drying out, the resin-soaked fabric can preserve at least the shape of the body.

Treatment with lime

Instead of being embalmed, it is known that Clement VI's body (died in 1352) was rubbed with lime to prevent quick decomposition during the transport to his burial place [16]. This method is in fact dehydration of the body, a prerequisite for long-term preservation, used since ancient times [19]

Site of burial

The first popes were buried near the tomb of St. Peter. Even though their tombs were described as "simple", they included a coffin a marble, brick, or terra-cotta, which more or less insulated the body from the elements. More recent burials included elaborate sarcophagi, made of marble or other stone [15]. They also provide a sealed environment, away from moisture and extreme temperature changes.

Contemporary Methods of Body Preservations

Treatment of the body

The 20th century records contain more detailed descriptions of the fate of the dead pope's body. Pius X was buried underneath St. Peter's basilica in 1914, and was not treated, as per his explicit wishes (9). His relics were subsequently recovered, declared incorrupt, and he was canonized as a saint of the Catholic church. The preservation of his body might have been a result of the conditions it was laid in (see below). When the body was removed from the tomb, in order to preserve it in the condition it was found, it was treated with a chemical solution. However, as it was claimed, this treatment re-

sulted in the skin turning brown. Pius X's remains are now covered in a bronze mask and vestments, covering this discoloration, with the current condition of the body being unknown [10, 14].

The embalming of Pius XII's remains (1958) created a significant controversy, due to the failed attempt to preserve the body using a process involving herbs and aetheric oils, following what was claimed to be an ancient tradition. The preservation was extremely unsuccessful, leaving the body of the pope decomposing and putrefying in front of the shocked faithful [18].

Pope John XXIII (died in 1963) was preserved using what we can call a modern method. The Italian anatomist Gennaro Goglia perfused the body with 10 liters of embalming fluid [2], reportedly containing ethyl alcohol, formalin, sodium sulphate and potassium nitrate [4]. In 2001, his body was recovered in an extremely good condition. To prevent subsequent deterioration, it was treated with solutions containing formalin, alcohols, camphor, nitrobenzene, turpentine, benzoic acid, and mercury bichloride, before it was displayed in a glass coffin [13]. The face was however hidden with a wax mask, despite it may not have been needed [4].

Subsequent popes of the 20th century (Paul VI and John Paul I) were also treated to a different degree with preserving fluids [10, 14]. After the botched embalming of Pius XII, the papal morticians most likely turned to formulas similar to the traditional modern mix of fixatives used for John XXIII as well. John Paul II was reportedly not embalmed, but only "prepared", without further details of the procedure being known [20]. Speculations exist, that this preparation might have involved rubbing the skin with a fixative [13]. Fixation of the skin might aid in preserving the appearance of the body, even if the soft tissues have decayed.

Site of burial

Since the 16th century, the body of the pope was first laid in a cypress coffin. The cypress coffin is in turns placed in a metal one, which is soldered shut. The two coffins are put in an elm one, which is nailed with golden nails, before being carried to its final resting place in an elaborate tomb, or a niche [15]. The triple coffin placed in a sarcophagus is a significant insulation of the dead body, keeping oxygen and moisture out, thus creating a microenvironment not dependent on external conditions.

Even the case of burial in "simple ground", as it was requested by Paul VI in 1978 [21] the set of coffins was laid to rest not in soil, but rather in the rammed rubble in the Vatican grottoes below St. Peter's Basilica [22]. Keeping the body away from water and heat can trigger a natural mummification process, with little or no help in terms of treatment.

Discussion and Conclusions

The methods, described above, surely served a very practical purpose – to preserve a dead body for the time of viewing [17]. However, the treated body, if given the right conditions, may not decay, but be rather preserved over time. This can explain the existence of a number of body relics, which can be viewed as incorrupt by the faithful, even though no such claim from church officials exists.

The death of a pope is a major and rather rare event. Therefore, the accounts of it are often quite detailed, and sometimes include a description of the treatment of the dead body. This is however not the case for the death of other individuals, having their bodies declared incorrupt long time after their passing. It is possible that some of those bodies were subjected to treatments, similar to the ones used for the pope's body, which

were poorly documented. It is nowadays known through forensic analysis, that embalmment was a common practice for the elite in the Middle ages, and that the procedures were more or less standardized [5]. Therefore, the popes were not an exception, but were rather treated with the most modern and advanced procedures of their time. In the same time, other preserved relics might have been treated using similar widespread methods. A scientific analysis of such relics is needed in order to confirm or exclude this hypothesis.

References

1. **Aquinas, T.** Summa Theologica. Benziger Bros, New York, 1947.
2. **Bobbio, A.** The "miracle" of Pope John. Christian Family, 2001 [in Italian] Available at http://www.stpauls.it/fc01/0122fc/0122fc32.htm.
3. **Brown, E. A.** Death and the human body in the later Middle Ages: the legislation of Boniface VIII on the division of the corpse. - *Viator,* **12,** 1981.
4. **Carroll, R.** Pope welcomes embalmed predecessor on a saintly mission. The Guardian, 04.06.2001. Available at https://www.theguardian.com/world/2001/jun/04/catholicism.religion
5. **Charlier, P., J. Poupon, G. F. Jeannel, D. Favier, S. M. Popescu, A. Augias, I. Huynh-Charlier, L. Laquay, O. Boudouma, C. Dorion-Peyronnet.** The embalming of John of Lancaster, first Duke of Bedford (1435 AD): A forensic analysis. - *Medicine, Science and the Law,* **56**(2), 2015, 107-115
6. **Chase, F. H.** Saint John of Damascus: Writings. Catholic University of America Press, Washington, 1958.
7. **Cruz, J. C.** The Incorruptibles: A Study of the incorruption of the bodies of various Catholic Saints and Beati, TAN Books, Charlotte, 1977.
8. **Dykmans, M.** Papal ceremonial form from the end of the Middle Ages to the Renaissance. Bruxelles-Rome, Institut historique Belge de Rome, 1977. [in French]
9. **Guruge, A.** The Next Pope. WOWNH LLC, New Hampshire, 2010.
10. **Jeremiah, K.** Christian mummification: an interpretative history of the preservation of saints, martyrs and others. McFarland & Company, Jefferson, 2012.
11. **Lindberg, D. C.** Science in the Middle Ages. Chicago, University of Chicago Press, 1978.
12. **Paravicini-Bagliani, A.** The Pope's Body. Chicago, University of Chicago Press, 1978.
13. **Potenza, T.** Vatican's secret, and deadly, project to mummify saints. New York Post, 22.03.2014. Available at https://nypost.com/2014/03/22/making-of-a-saint-the-vaticans-quest-to-preserve-its-leaders/.
14. **Quigley, C.** Modern Mummies: The Preservation of the Human Body in the Twentieth Century. McFarland & Company, Jefferson, 2006.
15. **Reardon, W. J.** The deaths of the popes: Comprehensive accounts, including funerals, burial places and epitaphs. McFarland & Company, Jefferson, 2004.
16. **Rollo-Koster, J.** Death of Clergymen: Popes and Cardinals' Death Rituals - *In: Death in Medieval Europe: Death Scripted and Death Choreographed* (ed. J. Rollo-Koster). New York, Routledge, 2017.
17. **Rollo-Koster, J.** The People of Curial Avignon: A Critical Edition of the Liber Divisionis and the Matriculae of Notre Dame la Majour, Edwin Mellen Press, Cincinnati, 2009, 91, 139, 165, 330-331.
18. **Schlott, R.** Papst Pius XII. Der bizarre Tod des Stellvertreters. Spiegel Online, 08.10.2008, Available at http://www.spiegel.de/einestages/papst-pius-xii-der-bizarre-tod-des-stellvertreters-a-947942.html.
19. **Sivrev, D., M. Miklosova, A. Georgieva, N. Dimitrov.** Modern day plastination techniques – successor of ancient embalmment methods. *Trakia Journal of Sciences,* **3**(3), 2005, 48-51.
20. **Smoltczyk, A.** The Death of John Paul II: The Papal Embalmer. Spiegel online, 06.04.2005. Available at http://www.spiegel.de/international/the-death-of-john-paul-ii-the-papal-embalmer-a-349892.html
21. **The Testament of Paul VI.** Available at https://w2.vatican.va/content/paul-vi/en/speeches/1978/august/documents/hf_p-vi_spe_19780810_testamento-paolo-vi.html
22. **Walsh, J. E.** The Bones of St. Peter. Doubleday, New York, 1982.

Institute of Experimental Morphology, Pathology and Anthropology with Museum
Bulgarian Anatomical Society

Acta morphologica et anthropologica, 25 (1-2)
Sofia ● 2018

Wax Embedding as a Method for Preservation of Body Relics Used by the Orthodox Church

Nikola Tomov[1], Januarius (Yanko) Dzhangozov[2, 3]*

1 Department of Anatomy, Faculty of Medicine, Trakia University, Stara Zagora, Bulgaria
2 Archimandrite, Bulgarian Orthodox Church – Patriarchate of Bulgaria
3 Department of Historical and Practical Theology, Faculty of Orthodox Theology, St. Cyril and St. Methodius University, Veliko Tarnovo, Bulgaria

* Corresponding author email: tomovmd@gmail.com

Body relics of saints are important objects of veneration in the Orthodox Church. Regardless if they are considered incorrupt, practical reasons dictate that they should be protected from external influence, which may lead to their damage or destruction. This is especially true in cases when small fragments from a body are displayed to the faithful in a reliquary. The practice of the Orthodox Church has adopted the placement of such fragments in blocks of pure wax or wax-containing mixture. Per se this constitutes an impregnation, the last stage of a mummification/plastination process, following after dehydration and fixation. Herein we analyze the practice of wax embedding as a final step of preservation, known since antiquity, and remaining principally unchanged due to its efficacy.

Keywords: embedding, wax, relics, body preservation

Introduction

Holy relics occupy a special place in Christian ritual. Ever since the birth of the Church remains of martyrs and saints were venerated by the faithful, and valued more than treasures, as documented in the writings of St John Damscene [2]. Since the Second council of Nicaea (787 AD) relics were no longer just objects of veneration, but also a necessity for consecrating an altar to celebrate the Eucharist on [6].

The growing number of churches and the requirement to use a piece of the relics of a saint for the altar table gave rise to a practice of preservation of such relics by embedding them in a wax medium. This method has been widespread ever since, and is used for preservation of various relics in altars and reliquaries.

The use of wax embedding

Relics in altars

Canon VII of the Second council of Nicaea requires that a relic of a martyr be built in any altar table used for consecration of the Eucharist [6]. Whole bodies, regardless of their state of preservation, have been subsequently divided into pieces and distributed throughout the Christian world. The sacred texts call for the relic used for concecration to be enclosed in the altar table itself [5]. Usually, a mixture of beeswax and other ingredients would be used for that. This mixture is called wax-mastic, ceromasticum, or, in the Slavic tradition, voskomastik. Apart from wax and mastic, this cement-like substance includes myrrh, aloes, frankincense, rose oil, and perhaps marble dust, which are boiled together before being poured over the relics. Wax-mastic is used not only for sealing of relics, but historically also as glue, fixing the top of the altar table to its stipes [4].

Although relics would normally be built in the altar table itself, pieces of cloth with relics sewn in them are also used. Those cloth pieces are called Antimensia (from the Greek: ἀντιμήνσιον, „instead of the table"). The Eucharist is then celebrated on top of the antimension, which itself contains a relic, embedded in a small piece of wax. The procedure of relic embedding is similar to the one used in altar consecration and involves pouring of hot wax (or wax-mastic, fragrant gum, oil) over them [4, 6].

Relics in reliquaries

Pieces of relics are not used exclusively in the altars. Many of them are available for veneration of the faithful in reliquaries. Particles of various sizes are enclosed in boxes and containers, often adorned with precious materials. Commonly the relic pieces, small enough to be lost or being prone to disintegration, are pressed in small disks of wax or wax-mastic. Examples of relics kept in this fashion can be seen in thousand churches, as we show on **Fig. 1** and **2.** Often no additional protection is placed on top of the wax disks.

Wax-mastic is particularly useful for preparation of relics for display. According to the proportion of the ingredients, it should remain flexible and adhesive, easily workable with the heat of the hands [4]. The soft texture allows the relic to be pressed easily in the small disk. Furthermore, wax-mastic should have constant properties in different ambient temperatures. It is supposed not to melt in the heat of the summer or to crack with the cold of the winter [4].

Fig. 1. Wooden box reliquary with relics of multiple saints, kept at the Monastery of the Seven Altars, Bulgaria. Relic pieces of different size, shape, and condition are seen, but all are preserved by embedding in wax disks, without further protection.

Fig. 2. Bronze reliquary with relics of St. Charalambos (left), Sts. Cosmas and Damian (middle) and St. Simeon of Samokov (right), kept at Gigintsi Monastery, Bulgaria. The relic pieces are embedded in wax, and placed in slots in the bronze inlay, without being covered.

Discussion and conclusions

The century-long practice of the Church to keep relics inside containers or pieces, filled with wax and/or other resinous media, is a fine example of impregnation. Impregnation, or the soaking of the tissue with different chemical compounds, is the final stage of the process of mummification [8]. Together with impregnation, the aetheric oils and plant resins, included in the recipe for wax-mastic, might also act as fixatives. Combined, those two properties of the embedding medium grant that the tissue piece can remain unchanged over a long period of time, as it is shown uncountable times. Although it was previously noted, that enclosing relics in wax or wax-mastic serves the purpose to protect them from turning into dust and being lost [1, 3], herein we originally interpret this practice as a form of intentional preservation.

The essence of the process of wax embedding is no different from the one of the final stage of mummification or modern day plastination. The steps are closely followed: fixation and dehydration (in the single stage of desiccation), followed by impregnation with a polymer. Despite that the materials used slightly differ, the process is just one of the many variants of a well-known protocol for preservation of biological tissues [7].

References

1. **Butler, A. J.** The ancient Coptic churches of Egypt. Clarendon press, Oxford, 1884.
2. **Chase, F. H.** Saint John of Damascus: Writings. Catholic University of America Press, Washington, 1958.
3. **Goar, J.** Euchologion sive Rituale Graecorum. Akademische Druck- und Verlagsanstalt, Graz, 1960.
4. **Izzo, J. M.** The antimension in the liturgical and canonical tradition of the Byzantine and Latin churches: an inter-ritual inter-confessional study. Pontificum Athenaeum Antonianum, Rome, 1975.
5. **Krasnopevkov-Rumovsky, V.** Novaya skirzhal, ili Obyasnenie o tserkvi, o liturgii i o vseh sluzhbah i utvaryah tserkovnih. Pochayiv Lavra, Pochayiv, 2013. [in Russian]
6. **Percival, H. R.** The Seven ecumenical councils of the undivided church: their canons and dogmatic decrees, together with the canons of all the local synods which have received ecumenical acceptance. James Parker and Company, Oxford, 1900.
7. **Sivrev, D., A. Georgieva, N. Dimitrov.** From mummification to plastination. - *Acta morphologica et anthropologica,* 10, 2005, 288-290.
8. **Sivrev, D., M. Miklosova, A. Georgieva, N. Dimitrov**. Modern day plastination techniques – *successor of ancient embalmment methods. Trakia Journal of Sciences,* **3**(3), 2005, 48-51.

Guidelines for Authors

Acta morphologica et anthropologica is an open access peer review journal and publishes original articles, short communications, reviews, letters to the Editors. The aim of the journal is to provide a forum for cytological, histological, anatomical and anthropological research community in life sciences, including cell biology, immunobiology, pathology, neurobiology, environmental and toxicological research, reproductive biology, pharmacology, physical development and medical anthropology, paleoanthropology, anatomy, paleoanatomy, etc.

Contact details and submission

Manuscripts should be in English with total length not exceeding 10 standard pages, line-spacing 1.5, justified with 2.5 cm margins. The authors are advised to use Times New Roman, 12 pt throughout the text. Pages should be numbered at the bottom right corner of the page. Manuscript submission is electronic only. The manuscripts should be sent to**: iempam@bas.bg.**

All correspondence, including notification for Editor's decision, requests for revision, is sent by e-mail. After acceptance of the manuscript a hard copy should be sent to Editorial Office address:

Institute of Experimental Morphology, Pathology and Anthropology with Museum
Bulgarian Academy of Sciences
Editorial Office of Acta Morphologica et Anthropologica
Acad. Georgi Bonchev Str., Bl. 25
1113 Sofia, Bulgaria

Article structure

The article should be arranged under the following headings: Introduction, Materials and Methods, Results, Discussion, Conclusion, Acknowledgements and References.

Title page - includes:

- **Title** – concise and informative;
- **Author**(s)' **names and affiliations** - indicate the given name(s) and family name(s) of all authors. Present the authors' affiliation addresses below the names. Indicate all affiliations with a lower-case superscript after the author's name and in front of the appropriate address. Provide the full postal address information for each affiliation, including the country name.
- **Corresponding author** - clearly indicate who will handle the correspondence for refereeing, publication and post-publication. An e-mail should be provided.
- **Abstract** - state briefly the aim of the work, the principal results and major conclusions and should not exceed 150 words. References and uncommon, or non-standard abbreviations should be avoided.
- **Key words** - provide up to 5 key words. Avoid general, plural and multiple concepts. The key words will be used for indexing purposes.

Introduction - state the objectives of the work and provide an adequate background, avoiding a detailed literature survey or summary of the results.

Materials and Methods - provide sufficient detail to allow the work to be reproduced. Methods already published should be indicated as a reference: only relevant modifications should be described.

Results - results should be clear and concise.

Discussion - should explore the significance of the results in the work, not repeat them. A combined *Results and Discussion* section is often appropriate. Avoid extensive citation and discussion of published literature.

Conclusions - the main conclusions of the study should be presented in a short section.

Acknowledgements - list here those individuals who provided help during the research and the funding sources.

Units - please use the International System of Units (SI).

Math formulae - please submit math equations as editable text, not as images.

Electronic artwork - number the tables and illustrations according to their sequence in the text. Provide captions for them on a separate page at the end of the manuscript. The proper place of each figure in the text should be indicated in the left margin of the corresponding page. **All illustrations (photos, graphs and diagrams)** should be referred to as "figures" and given in abbreviation "Fig.", and numbered in Arabic numerals in order of its mentioning in the manuscript. They should be provided in grayscale as JPEG or TIFF format, minimum 300 dpi. The illustrations should be submitted as separate files.

References - they should be listed in alphabetical order, indicated in the text by giving the corresponding numbers in parentheses. The "References" should be typed on a separate sheet. The names of authors should be arranged alphabetically according to family names. In the reference list titles of works, published in languages with non-Latin alphabet, should be translated, original language must be indicated at the end of reference (e.g., [in Bulgarian]). Articles should include the name(s) of author(s), followed by the full title of the article or book cited, the standard abbreviation of the journal (according to British Union Catalogue), the volume number, the year of publication and the pages cited, for books - the city of publication and publisher. In case of more than one author, the initials of the second, third, etc. authors precede their family names.

For articles: **Davidoff, M. S., R. Middendorff, G. Enikolopov, D. Riethmacher, A. F. Holstein, D. Muller**. Progenitor cells of the testosterone-producing Leydig cells revealed. - *J. Cell Biol.,***167**, 2004, 935-944.

Book article or chapter: **Rodriguez, C. M., J. L. Kirby, B. T. Hinton. The development** of the epididymis**.** - *In: The Epididymis - from molecules to clinical practice* (Eds. B. Robaire, B. T. Hinton), New York, Kluwer Academic Plenum Publisher, 2002, 251-269.

Electronic books: **Gray, H.** *Anatomy of the human body* (Ed. W.H.Lewis), 20th edition, NY, 2000. Available at http://www.Bartleby.com.

PhD thesis: **Padberg, G**. Facioscapulohumeral diseases. *PhD thesis*, Leiden University, 1982, 130 p.

Website: National survey schoolchildren report. National Centre of Public Health and Analyses, 2014. Available at http://ncphp.government.bg/files

Page charges

Manuscript publication is free of charges.

Ethics in publishing

Before sending the manuscript the authors must make sure that it meets the Ethical guidelines for journal publication of Acta morphologica et anthropologica.

Human and animal rights

If the work involves the use of human subjects, the authors should ensure that work has been carried out in accordance with *The Code of Ethics of the World Medical Association* (Declaration of Helsinski). The authors should include a statement in the manuscript that informed consent was obtained for experimentation with human subjects. The privacy rights of human subjects must always be observed.

All animal experiments should comply with the *ARRIVE guidelines* and should be carried out in accordance with the U. K. Animals (Scientific procedures) Act, 1986 and the associated guidelines *EU Directive 2010/63/EU* for animal experiments, or the National Institutes of Health guide for the care and use of Laboratory animals (NIH Publications no. 8023, revised 1978) and the authors should clearly indicate in the manuscript that such guidelines have been followed.

Submission declaration

Submission of the manuscript implies that the work described has not been published previously, is not considered under publication elsewhere, that its publication is approved by all authors, and that if accepted, it will not be published elsewhere in the same form, in English or in any other language, including electronically, without the informed consent of the copyright-holder.

Contributors

The statement that all authors approve the final article should be included in the disclosure.

Copyright

Upon acceptance of an article, the authors will be asked to complete a "Journal Publishing Agreement". An e-mail will be sent to the corresponding author with the Journal Publishing Agreement Form or a link to the online version of this agreement.

Peer review

This journal operates a single blind review process. All contributions will be initially assessed by the Editor for suitability for the journal. All suitable papers are then sent to two independent expert reviewers to assess the scientific quality of the paper. The Editor is responsible for the final decision regarding acceptance or rejection of articles.

After acceptance

Proof correction

The corresponding author will receive proofs by e-mail in PDF format and will be requested to return it with any corrections within a week.

Offprints

The journal provides free access to all papers in each volume that can be downloaded from the following website: http://www.iempam.bas.bg/journals/acta.html.